รายงานการวิจัย

เรื่อง

การประยุกต์ใช้งาน Symbolic and Optimization Toolboxes ของโปรแกรม MATLAB ในการศึกษาเสถียรภาพแรงดันสถิตย์ในระบบไฟฟ้ากำลัง

Applications of MATLAB Symbolic and Optimization Toolboxes in the Study of Static Voltage Stability in Power Systems

โดย

ผศ.ดร. อาทิตย์ โสตรโยม

ได้รับทุนอุดหนุนการวิจัยจากมหาวิทยาลัยสยาม

การประยุกต์ใช้งาน Symbolic and Optimization Toolboxes ของโปรแกรม MATLAB ในการศึกษาเสถียรภาพแรงดันสถิตย์ในระบบไฟฟ้ากำลัง

Applications of MATLAB Symbolic and Optimization Toolboxes in the Study of Static Voltage Stability in Power Systems

โดย

ผศ.ดร. อาทิตย์ โสตรโยม

ได้รับทุนอุดหนุนการวิจัยจากมหาวิทยาลัยสยาม

Project Title Applications of MATLAB Symbolic and Optimization Toolboxes in the Study of Static Voltage Stability in Power Systems

Principal Investigator Dr. Arthit Sode-Yome

ABSTRACT

Modern electric power utilities are facing many challenges due to ever-increasing complexity in their operation and structure. In the recent years, one of the problems that receive wide attention is the voltage instability. With an open-access market, poorly scheduled generation for the competitive bidding is one of many reasons for voltage instability problem in the deregulated electricity environment. Thus, in order to relieve or at least minimize the system from the voltage instability problem, many electric utilities and researchers have devoted a great deal of efforts in system studies related to static voltage stability.

In static voltage stability study, Continuation Power Flow (CPF) and optimization methods are the main analysis techniques that are used to find voltage stability margin or loading margin (LM) of the system. Based on these techniques, utilities and researchers may require developing and devoting a great deal of effort to create a program. Adding to this, they may face a difficulty to ensure the correct answers.

The development of Flexible AC Transmission System (FACTS) devices in power transmission system has led to many applications of these controllers not only improve various stability issues but also provide operating flexibility to power systems. There are various types of FACTS devices available for this purpose, namely, Static Var Compensator (SVC), Static Synchronous Compensator (STATCOM), Thyristor-Controlled Series Capacitor (TCSC), Static Synchronous Series Compensator (SSSC) and Unified Power Flow Controller (UPFC). With the use of Flexible AC Transmission system (FACTS) to enhance static voltage stability, simulation effort may be increased.

Attention is drawn in this research to propose a new simulation approach for voltage stability study using Symbolic and Optimization toolboxes in MATLAB. The research simulates load flow, CPF and optimization technique in static voltage stability study. The proposed technique is applied to system with FACTS devices, namely SVC, STATCOM, TCSC, SSSC and UPFC. Moreover, simulation times are studied and compared in test systems. This may be useful for utilities to find voltage stability assessment of medium-size power systems without devoting a great deal of effort.

Keywords: Voltage Stability, FACTS devices, MATLAB, Symbolic toolbox, Optimization toolbox

Acknowledgements

Author would like to express his sincere appreciation, gratitude and indebtedness to Siam University for the financial support. Without the support from them, he think that he could not complete his research.

The author deeply acknowledges mentors, namely Dr. Nadarajah Mithulananthan and Prof. Dr. Kwang Y. Lee for their help, suggestion and valuable guidance to make this work more valuable to research.

Last but not least, the author would like to give most of the gratitude to his parents for making their son succeeded during the first part of his life. Good things are given to my past away father for his sacrifice.

Dr. Arthit Sode-Yome

Table of Contents

Table of Contents (Cont'd)

Table of Figures

Table of Tables

Chapter 1

Introduction

1.1 Introduction

Modern electric power utilities are facing many challenges due to ever-increasing complexity in their operation and structure. In the recent past, one of the problems that receive wide attention among utilities has been the voltage instability [1]-[3]. With the lack of new generation, transmission facilities and over exploitation of the existing facilities geared by increase in load demand make these types of problems are more likely to happen in the modern power systems.

In recent decades, several major voltage instability have been observed and reported in many countries such as France, Belgium, Sweden, Germany, Japan, the United States, etc [4],[5]. Voltage instability is the cause of voltage collapse, which results in wide spread power interruptions. Voltage instability due to the lack of ability to foresee the impact of contingencies is the main reason for the worst North American power interruption on August 14th, 2003. In this incident, reports indicate that approximately 50 million people were interrupted from the continuous supply of power for more than 15 hours [5]. Moreover, with an open-access market, poorly scheduled generation from the competitive bidding is one of many reasons for voltage instability problem in the deregulated electricity environment.

Voltage instability is the inability of the power system to transfer reactive power to the load due to exhaustion of the reactive power sources or enormous reactive power losses in the transmission system. It is mainly associated with reactive power imbalance. In voltage stability study, slowly developing changes in the power system occur that eventually lead to a shortage of reactive power and declining voltage. At the collapse point or maximum voltage stability margin, reactive power is out of use such that the voltage is sharply decreased and finally collapsed. The maximum load that can be supplied prior to the point at which the system reactive power is out of use is called static voltage stability margin or loading margin (LM) of the system. Voltage instability and collapse in practical power systems can be avoided by increasing the static voltage stability margin. This can be done by adjusting factors that principally contribute to it.

Major contributory factors to voltage instability are power system configuration, generation pattern, and load pattern [1]-[4],[6]-[11]. Power system network or topology can be modified to alleviate voltage instability by adding reactive power sources i.e. shunt capacitors or Flexible AC Transmission System (FACTS) devices at the appropriate location [14]-[21]. Impact of generation pattern and load pattern on static voltage stability can be found in references [22]-[30].

1.2 Research Motivation

Power /system network can be modified to enhance voltage stability margin by introducing FACTS devices in the transmission system. There are various types of FACTS devices available for this purpose, namely Static Var Compensator (SVC), Static Synchronous Compensator (STATCOM), Thyristor-Controlled Series Capacitor (TCSC), Static Synchronous Series Compensator (SSSC) and Unified Power Flow Controller

(UPFC) [14]. Each of these FACTS devices, however, has its own characteristics and limitations [11]. Appropriate models of these FACTS devices including AC and DC representation may be required to represent all the behaviors and limitations of the devices, especially when they are operated at the limits [11],[15],[16]. It would be useful to study and compare these five well-known FACTS devices, namely SVC, STATCOM, TCSC, SSSC and UPFC, with appropriate representation in the same test system.

In static voltage stability study, Continuation Power Flow (CPF) and optimization methods are the main analysis techniques that are used to find voltage stability margin or loading margin (LM) of the system [11],[13]. Based on these techniques, utilities and researchers may require developing and devoting a great deal of effort to create a program. Adding to this, they may face a difficulty to ensure the correct answers. Moreover, with the use of Flexible AC Transmission system (FACTS) to enhance static voltage stability, simulation effort may be increased.

According to above observation, attention is drawn in this research to propose a new simulation approach for voltage stability study using Symbolic and Optimization toolboxes in MATLAB. The research simulates load flow, CPF and optimization technique in static voltage stability study. The proposed technique is applied to system with FACTS devices. Moreover, simulation times are studied and compared in test systems. This may be useful for utilities or researchers to find voltage stability assessment of medium-size power systems without devoting a great deal of effort.

1.3 Research Objectives

The objectives of this research is to propose a new simulation approach for voltage stability study using Symbolic and Optimization toolboxes in MATLAB. The research simulates load flow, CPF and optimization technique in static voltage stability study in a simple way. The proposed technique is applied to system with the well-known FACTS devices, namely SVC, STATCOM, TCSC, SSSC and UPFC, in order to investigate the influence of FACTS controllers with AC-DC representation in static voltage-stability margin. This may be useful for utilities to find voltage stability assessment of medium-size power systems without devoting a great deal of effort.

1.4 Outline of Report

The report is structured as follows:

- Chapter 2 presents concepts and mathematical representation of power system for static voltage stability study with FACTS devices. Analysis tools and test systems used in this study are also presented.
- Chapter 3 presents the proposed simulation approach based on Symbolic and Optimization toolboxes in MATLAB
- Chapter 4 presents the simulation results for voltage stability assessment of the power systems including details representation of all well-known FACTS devices.
- Finally, Chapter 5 provides a summary, contribution and future work of the research.

Chapter 2

Literature Review, Modeling, Tools and Test Systems

2.1 Introduction

Voltage stability can be broadly classified based on time frame of simulation into two categories: static voltage stability and dynamic voltage stability. In dynamic consideration, the study includes dynamic effects of equipment such as transformer tap changers, induction motor, load, etc., whereas static study considers load variation as a slow process over long period of time [3],[4]. Most of the problem found in power system realizes voltage collapse as a static phenomenon [3],[4]. Static study involves only the solution of algebraic equations and therefore is computationally less extensive than dynamic analysis. It is appropriate for a bulk power system study, which involves enormous number of buses and generators [3]. Accordingly, the research conducted in this study is concentrated only in static voltage stability.

Mathematical models for static voltage stability study consist of load flow equation, singularity condition of load flow Jacobian and the equation for non-zero left eigenvectors. There are many analysis techniques and tools used for static voltage stability study. Moreover, if FACTS device with appropriate AC and DC representation is introduced in the power system, more equations are added in voltage stability study. This chapter presents static voltage stability study including overview, mathematics representation and analysis techniques. Mathematical representation of all FACTS devices in static voltage stability study is presented. Moreover, analysis tools and the test systems used throughout this study are also presented.

This chapter is organized as follows. Section 2.2 summarizes literature related to this project. Section 2.3 introduces static voltage stability. In Section 2.4, stability models and mathematical representation of all FACTS devices are summarized. These models are introduced in static voltage stability study. In Section 2.5, analysis tools that are used throughout the study are presented. Section 2.6 mentions, in brief, about the test systems including the 3-bus and the IEEE 14-bus test systems that has been used to test all the proposed methodology. Finally, a summary of the chapter is given in Section 2.7.

2.2 Literature Review

2.2.1 Static Voltage Stability

Concerns on voltage instability have come into attention to many utilities and researchers for several decades. Started in 1990, the energy function method has been proposed in [31], which defines a security measure to indicate vulnerability to voltage collapse. In 1993, another approach is presented in [7] based on singular value decomposition of load flow Jacobian matrix and matrices derived from the Jacobian matrix. Later, this method has been practically applied to large-scale power system in [1], which presents the development of systematic approach to voltage stability assessment of large-scale power systems using both static and dynamic techniques. In this study, modal analysis at the “nose point” of PV curve is used to identify the SVC location. In [8], the modal analysis method is further applied to AC-DC system with HVDC facility.

Continuation power flow method is proposed for the computation of voltage collapse points in large AC/DC power systems in [32] and [33]. Continuation power flow method yields voltage sensitivity information and time performance that justify its use as a production tool. It appears particularly promising when HVDC lines with controller limits are considered. Tangent vector method is proposed in [34] to identify the weakest bus, based on the largest tangent vector component as a function of load increase. The explicit advantage of this method is to provide less computational effort, since the tangent vector components are calculated as a predictor step in continuation power flow process. Later, in order to compare all available methods, reference [35] studies and discusses some voltage collapse indices, namely singular value decomposition, eigenvalue decomposition, reduced Jacobian determinant, test function and tangent vector. The results obtained confirm that the tangent vector is a more promising voltage security index [34],[35].

The establishment of novel method for the study of voltage stability is performed in the following literatures. Reference [36] proposes a new method of finding voltage stability limit in P-Q plane. Equations are required to generate the voltage stability boundary using the exact transmission line model. Likewise, reference [37] proposes a novel method of determining various stability margins of critical bus or area in a large power system using the boundary of voltage stability of critical bus in P-Q plane. In [38], the derivation of the simple analytical expression for S-V (MVA-voltage) and expression for maximum MVA, MW and MVAR limitation through the exact representation of line with ABCD parameter is succeeded. Another methodology based on local measurement on bus voltage and load current to estimate the proximity to voltage collapse is presented in [39]. In this methodology, the voltage collapse assumes to happen when apparent impedance equals thevenin impedance.

Based on the literatures reviewed above, it becomes evident that the conventional methods used to investigate the static voltage stability could be classified as test function, modal analysis, sensitivity, and tangent vector methods. These methods can effectively analyze the large-scale power system regarding to voltage stability and they could be considered as indicators to predict the distance to voltage collapse or loading margin in the study of voltage stability assessment. Beside the conventional methods, other methodology i.e. P-Q plane and $Z_{thevenin}$ techniques could be adapted for the voltage stability study. The novel method, however, has limitations when a practical size power system is considered. Compared with other conventional methods, tangent vector method based on Continuation Power Flow (CPF) process is considered as the most promising approach, since it is based on load flow calculation at various load increase or loading factor (LF). Moreover, CPF method can provide completed PV curves as well as voltages at various loading factors.

2.2.2 Network Improvement with FACTS Devices

FACTS devices have been used to increase voltage stability margin for the past several years. One of the early literatures proposed is reference [40] that describes the applications of FACTS to improve voltage and transient stabilities. These applications are shown to offer the potential for enhancing the system's stability margin. In [41], contributions are made on selection of SVC parameters such as controller gains, droop slopes, reference voltages and compensator ratings needed for voltage stability improvement. Reference [42] proposes transient stability models of STATCOM and SSSC, which are also suitable for voltage stability enhancement. Examination on the use of TCSC for stability improvement of power systems is also presented in [43]. Importantly, reference [44] describes the UPFC function in resolving voltage and thermal loading

concern in planning studies. With the help of UPFC, the new 138 kV line approaches the effectiveness of an uncompensated 345 kV line.

Appropriate models of FACTS including control and operating limits are necessary for the voltage stability study. In [15], detailed steady-state models with control of SVC and TCSC to study their effects on voltage collapse phenomena in power systems are presented. Further, reference [45] investigates modeling technique appropriate for representing the UPFC. For well-known FACTS devices, reference [16] presents transient stability and power flow models of SVC, STATCOM, TCSC, SSSC and UPFC suitable for voltage and angle stability studies.

Very scant research attention has been focused on appropriate models of FACTS devices in voltage stability study. More research attention should be placed on voltage stability with appropriate AC-DC model of all FACTS controllers so that the behaviors and limits of the devices can be captured and their impact on voltage stability can be studied. This could provide more accurate reflections of FACTS devices in the stressed system conditions, especially when the devices are operated at their limits.

Based on these available techniques, utilities and researchers may require developing and devoting a great deal of effort to create a program. Adding to this, they may face a difficulty to ensure the correct answers. Moreover, with the use of Flexible AC Transmission system (FACTS) with AC-DC representation, simulation effort may be increased.

2.3 Static Voltage Stability Study

2.3.1 Overview

Static voltage instability is mainly associated with reactive power imbalance. Reactive power support that the bus receives from the systems can limit loadability of that bus. If the reactive power support reaches the limit, the system will approach the maximum loading point or voltage collapse point due to high real and reactive power losses [1]-[4],[11]. Accordingly, the reactive power supports should be local and adequate in order to avoid problem associated with its transmission, especially in a stressful condition.

In static voltage stability, slowly developing changes in the power system occur that eventually lead to a shortage of reactive power and declining voltage. This phenomenon can be seen from the plot of the voltage at receiving end versus the power transferred. The plots are popularly referred to as P-V curve or “Nose” curve. As the power transfer increases, the voltage at the receiving end decreases. Eventually, the critical (nose) point, the point at which the system reactive power is out of use, is reached where any further increase in active power transfer will lead to very rapid decrease in voltage magnitude. Before reaching the critical point, the large voltage drop due to heavy reactive power losses can be observed. The maximum load that can be increased prior to the point at which the system reactive power is out of use is called static voltage stability margin or loading margin of the system. The only way to save the system from voltage collapse is to reduce the reactive power losses in the transmission system or to add additional reactive power prior to reaching the point of voltage collapse. This has to be carried out in the planning stage with several system-wide studies.

Under normal operating conditions, power system exhibits slow dynamics, with transient oscillations of small amplitude compared with the overall change observed in a

short time. Therefore, it is reasonable to assume a quasi-static condition. The typical quasi-steady-state description of a power system considered for static voltage stability analysis is given by the differential-algebraic equations (2.1) [3],[4].

$$\begin{aligned} \dot{x} &= f(x, y, \lambda) \\ 0 &= g(x, y, \lambda) \end{aligned} \tag{2.1}$$

or

$$\begin{bmatrix} \dot{x} \\ 0 \end{bmatrix} = F(x, y, \lambda) = F(z, \lambda) \tag{2.2}$$

where z corresponds to a vector of the system state and algebraic variables and λ is the loading factor representing the percent increase in load.

In static voltage analysis, the equilibrium point is considered. At equilibrium point, the equation (2.2) is simplified to $F(z_0, \lambda_0) = 0$. Hence, an equilibrium point (z_*, λ_*) where determinant of Jacobian, $dF(z_*, \lambda_*)/dz$, becomes zero is known as a singular bifurcation point. This equilibrium point in power system has been directly associated with voltage collapse point [3].

The power flow model is used to identify the voltage stability indices as the power flow equation yields adequate results, as singularities in related power flow Jacobian can be associated with actual singular bifurcation of the corresponding dynamical system. The power flow model used to obtain different voltage stability indices is represented by the typical load-flow vector nonlinear equation defined the active and reactive power mismatches at system buses, i.e.

$$F(u, \lambda) = \begin{bmatrix} \Delta P(u, \lambda) \\ \Delta Q(u, \lambda) \end{bmatrix} = 0 \tag{2.3}$$

where $F(u, \lambda)$ is a subset of $F(z, \lambda)$, with under quasi-static condition u typically representing V and δ, voltages and phase angles, respectively.

The system load change drives the system to collapse in the following way:

$$\begin{aligned} P_{D,i} &= P_{o,i}(1 + \lambda K_{P,i}) \\ Q_{D,i} &= Q_{o,i}(1 + \lambda K_{Q,i}) \end{aligned} \tag{2.4}$$

where $P_{o,i}$ and $Q_{o,i}$ represent the initial active and reactive loads at bus *i* and constants $K_{P,i}$ and $K_{Q,i}$ represent the active and reactive load increase direction of bus *i*, respectively.

In summary, for the voltage stability study, the power flow model is used, where the variations of constant active and reactive power loads are assumed to be the main parameters driving the system to collapse point.

2.3.2 Analysis Techniques

The purposes of analysis techniques are to identify system conditions causing voltage instability, to find loading margin of the system and to specify the parameters affecting the voltage stability of the system. In static voltage stability study, four analysis techniques are popularly used, namely, direct, modal analysis, continuation power flow and optimization technique methods.

Direct Method

Direct method uses power flow equations, singular conditions of power flow Jacobian and non-zero left eigenvectors to find the maximum loading point. These conditions are summarized in (2.5)

$$\begin{aligned} & F(z,\lambda) = 0 && \text{-> Power Flow Equation} \\ & \frac{dF(z,\lambda)^T}{dz} w = 0 && \text{-> Singularity Condition} \\ & \|w\| = 1 && \text{-> Non-zero Left Eigenvector} \end{aligned} \tag{2.5}$$

where w is the left eigenvector. Direct method consists in solving equation (2.5) for z, λ and w, to directly obtain the collapse point (z_*, λ_*). This method allows to directly determine the loading margin ($\Delta\lambda = \lambda_* - \lambda_o$) at any operating point defined by λ_o. An obvious disadvantage of this technique is the high computational cost, requiring good initial conditions. In addition, pertinent information between maximum loading margin λ and the base case λ_o is not available.

Modal Analysis Method

In standard power flow, the Jacobian (J) contains the first derivatives of the reactive power mismatch equation $Q(z,\lambda)$ with respect to the voltage magnitude *V*. Hence, linearizing the steady state equation $F(z,\lambda) = 0$ at the equilibrium point (z_0, λ_0),

$$\Delta F\left(z,\lambda\right)=J\Delta z \tag{2.6}$$

$$\begin{aligned}\begin{bmatrix}\Delta\hat{F}\left(\delta,V,\lambda\right)\\ \Delta Q\left(\delta,V,\lambda\right)\end{bmatrix}&=\begin{bmatrix}\dfrac{\partial\hat{F}\left(\delta_0,\lambda_0\right)}{\partial\delta} & \dfrac{\partial\hat{F}\left(\delta_0,\lambda_0\right)}{\partial V}\\ \dfrac{\partial Q\left(\delta_0,\lambda_0\right)}{\partial\delta} & \dfrac{\partial Q\left(\delta_0,\lambda_0\right)}{\partial V}\end{bmatrix}\begin{bmatrix}\Delta\delta\\ \Delta V\end{bmatrix}\\ &=\begin{bmatrix}J_1 & J_2\\ J_3 & J_4\end{bmatrix}\begin{bmatrix}\Delta\delta\\ \Delta V\end{bmatrix}\end{aligned} \tag{2.7}$$

where $\hat{F}\left(\delta,\lambda\right)$ represents the active power mismatch $P\left(\delta,\lambda\right)$[3].

The load flow Jacobian can be decomposed in such a way that

$$J=W\sum U^T \tag{2.8}$$

where *W* and *U* are the left and right eigenvector matrixes, respectively, and $\sum$ is the matrix of singular values. Since matrix J represents the partial derivatives of the active and reactive power equations as a function of the state variables, one has:

$$\begin{bmatrix}\Delta\delta\\ \Delta V\end{bmatrix}=U\sum{}^{-1}W^T\begin{bmatrix}\Delta P\\ \Delta Q\end{bmatrix} \tag{2.9}$$

If *U* and *W* hold the singular vectors, then $\sum$ holds the singular values. When the system Jacobian becomes singular, the state variables present large variations for small load disturbances. This can be used for voltage stability study. When the system becomes stressed, the next incremental changes of load cause the voltage to dramatically reduce. The reduction in voltage further causes the large change in phase angle difference, which finally results in system voltage collapse. At the collapse point, load flow study provides no solution. The singularity of system Jacobian can be used as an indicator to detect proximity of voltage instability. Moreover, right and left eigenvectors, which are the decomposition of Jacobian, can reveal information related to the weakest bus and weakest area of the system.

Continuation Power Flow Method

Continuation Power Flow (CPF) presents another way of determining proximity to voltage collapse point in power system. The method is an iterative method that can trace P-V curve of the system up to the maximum loading (“nose”) point without having

numerical problems. CPF overcomes some difficulties of successive power flow solution method, so they allow the user to trace the complete voltage profile by automatically changing the value of Loading Factor (LF or λ). It involves predictor and corrector steps to guarantee a well behaved numerical solution of the related equation. PV curves are currently in use at some utilities for determining proximity to collapse so that operator can take timely preventive measures to avoid voltage collapse.

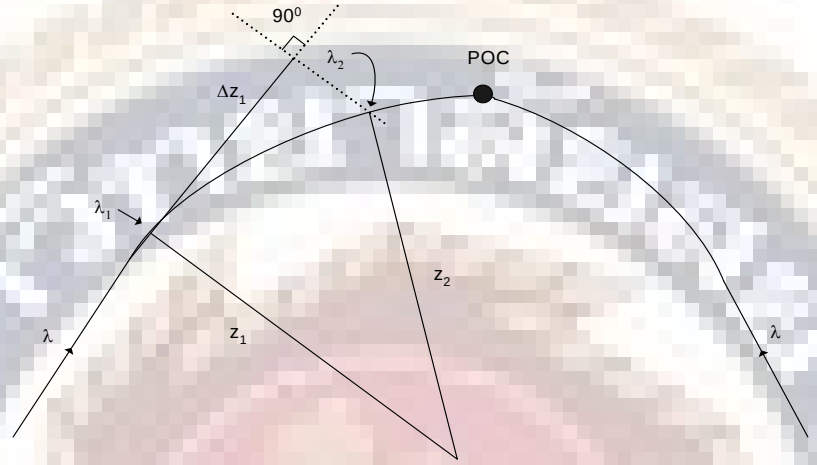

Figure 2.1: Continuation method geometry in state space and parameter space.

The CPF method uses the successive power flow solution to fully compute the voltage profiles up to collapse point to determine the loading margin. From Figure 2.1, assuming that the system is initially at the state (z_1, λ_1), the predictor generates an initial guess ($z_1+\Delta z_1$, $\lambda_1+\Delta\lambda_1$) which is then used in the corrector step to compute a new equilibrium point (z_2, λ_2) on the system profile. To obtain the actual value of z_2 and λ_2, one can use the perpendicular hyperplane to the tangent vector to find the desired point in the branch. Tangent vector which is a byproduct of the CPF process can also be used as an index to identify the weakest bus of the system. Mathematically, the CPF procedure can be summarized in two steps, namely predictor and corrector steps [3],[32]-[33]. A third step known as parameterization is introduced to avoid some convergence problem [3].

Predictor

The direction vector Δz_1 at the initial state (z_1, λ_1) on the system profile can be computed from the tangent vector to this trajectory at that point. At equilibrium point, the following relation can be applied:

$$\frac{dF}{d\lambda}(z_1,\lambda_1)=\frac{dF}{dz}(z_1,\lambda_1)\left.\frac{dz}{d\lambda}\right|_1+\left.\frac{\partial F}{\partial\lambda}\right|_1=0$$
$$\left.\frac{dF}{dz}\right|_1\left.\frac{dz}{d\lambda}\right|_1=-\left.\frac{\partial F}{\partial\lambda}\right|_1 \qquad (2.10)$$
$$\frac{dz}{d\lambda}=-\left[\frac{dF}{dz}\right]^{-1}\left.\frac{\partial F}{\partial\lambda}\right|_1$$

Thus, the direction vector and the parameter step come from the normalization of the tangent vector i.e.

$$\Delta\lambda_1=\frac{k}{\left\|\left.\frac{dz}{d\lambda}\right|_1\right\|} \qquad (2.11)$$

$$\Delta z_1=\Delta\lambda_1\left.\frac{dz}{d\lambda}\right|_1 \qquad (2.12)$$

where k is a scalar positive constant that controls the size of the predictor step. The normalization in equation (2.12) results in the reduction of the step size as the system approaches the collapse point, since the magnitude of the tangent vector increase as the system get closer to this point.

Corrector

Once the initial guess ($z_1+\Delta z_1$, $\lambda_1+\Delta\lambda_1$) is determined in the predictor step, the actual point (z_2, λ_2) on the system profile must be calculated by solving the following equations for z and λ from equations below.

$$F(z,\lambda)=0$$
$$\rho(z,\lambda)=0 \qquad (2.13)$$

where the first set of equations corresponds to the steady-state system equation and the second set of equations represents a condition that guarantees non-singularity at the bifurcation point.

Parameterization

Parameterization technique may be used to avoid difficulty when the equilibrium point is close to the collapse point, since the system Jacobian becomes ill-conditioned. A simple technique is local parameterization, which is carried out simply by interchanging the parameter λ with the system variable z that has the largest normalized entry in the tangent vector, so that λ becomes part of the equation variables and z becomes the new parameter p, i.e.

$$p = \max\left\{\left|\frac{\Delta z_i}{z_i}\right| \quad , \quad \left|\frac{\Delta\lambda}{\lambda}\right|\right\} \tag{2.14}$$

As power system approaches the bifurcation, p changes from λ to the system bus voltage (z) that is varying the most, and after a few iterations of the method it returns back to λ.

Optimization Technique Method

Static voltage stability study can be carried out by formulating the problem as an optimization problem [3]. Thus, distance to collapse can be maximized as follows:

Maximize

$$\lambda \tag{2.15}$$

subject to

$$F(z,\lambda) = 0 \tag{2.16}$$

This problem may be solved using Lagrangian

$$L(z,\lambda,w) = \lambda + w^T F(z,\lambda) \tag{2.17}$$

where w corresponds to the Lagrangian multipliers. Hence, necessary conditions to obtain a solution are

$$\frac{dL}{dw} = F(z,\lambda) = 0$$

$$\frac{dL}{dz} = \frac{dF(z,\lambda)}{dz}^{T} w = 0 \qquad (2.18)$$

$$\frac{dL}{d\lambda} = w^{T} \frac{\partial F(z,\lambda)}{\partial \lambda} + 1 = 0 .$$

These equations are basically the same as equation (2.5), with the exception of the third one, which quarantees a nonzero w. Other power system limits such as voltage and thermal limits can also be introduced in the optimization formulation as an inequality constraint in (2.16).

Among the existing technique, CPF method is the most promising approach, since it is based on power flow calculation. It can provide complete PV curves as well as voltages at every bus at various loading factors, which can be used as an indicator to detect the proximity to voltage collapse. Thus, CPF method is used as an analysis tool for voltage stability assessment throughout the study.

2.3.3 Voltage Stability Margin Enhancement

Voltage instability of the system can be avoided by increasing voltage stability margin. Voltage stability margin can be enhanced by various ways i.e. by adding reactive power sources, increasing generation at the appropriate locations or reducing reactive power losses throughout the system. Introducing FACTS devices at the appropriate location is an effective way to increase voltage stability margin by adding reactive power where it is needed the most. It can be also viewed as a way to reduce reactive power losses, as the power flow is changed to less congested lines. In the following section, models and mathematics representation of FACTS devices that are used in this study are presented.

2.4 FACTS devices

The development of Flexible AC Transmission System (FACTS) controllers in power transmission system have led to many applications of these controllers not only to improve the stability of the existing power network but also to provide operating flexibility to the power system. FACTS controllers, developed by Electric Power Research Institute (EPRI) and Westinghouse Electric Corporation (Westinghouse), help utilities meet both the growing demand for electric power and the emerging challenges of open transmission access. The new devices, coupled with better computer and communications technology, offer the potential for enhanced system voltage stability both during the steady state operation and especially following system disturbance.

FACTS devices have been defined by the IEEE as “alternating current transmission system incorporating power electronic-based and other static controllers to enhance controllability and increase power transfer capability” [3],[14]. From the above definition, two main objectives of such devices can be restated as follows:

- To increase the power transfer capability of the transmission networks
- To provide direct control of power flow over designated transmission routes.

With these objectives, the FACTS controllers may provide significant benefits in terms of greater flexibility and extended stability margin of the power system.

To accomplish the objectives, FACTS devices increase the power system performance by delivering or absorbing real and/or reactive power. Although FACTS devices can offer high-speed control for enhancing power system, one disadvantage of power electronic based controllers is their high cost per unit of rating compared to that of similar conventional equipment. Table 2.1 gives an idea about the cost of various FACTS controllers compared to that of shunt and series capacitors [14].

Table 2.1: Cost comparison of FACTS controllers

Shunt Controller	Cost (US $)
Shunt Capacitor	8/kVar
Series Capacitor	20/kVar
SVC	40/ kVar controlled portions
TCSC	40/ kVar controlled portions
STATCOM	50/ kVar
UPFC Series Portions	50/ kVar Through power
UPFC Shunt Portions	50/ kVar controlled

Although FACTS devices are much more expensive than capacitor, they provide smooth and rapid response to secure power system during normal and abnormal operations. Shunt capacitor, on the other hand, provides coarse response and can not control voltage at the connected bus. Moreover, reactive power delivered by shunt capacitor is proportional to the square of voltage magnitude. Accordingly, these FACTS controllers are used for the stability improvement, especially for voltage stability.

In static voltage stability study, FACTS devices can be introduced into the formulation by adding equations of FACTS devices in the power flow equation. Conventionally, only AC equations are used. However, it may not provide a practical solution in the DC sides. Thus, appropriate model with AC and DC equations of each FACTS devices are important.

There are many types of FACTS controllers available in power systems. They can be connected to a transmission line at any appropriate location in series, in shunt or in a combination of series and shunt. The SVC and STATCOM are connected in shunt, whereas TCSC and SSSC are connected in series. UPFC, on the other hand, is connected in series and shunt combination. Each of FACTS devices has its own characteristic and limitations depending on its properties. They are represented by different models and mathematics equations. In the following subsections, static models and mathematical representation of all FACTS devices are presented.

2.4.1 SVC

SVC is a shunt connected static Var generator/load whose output is adjusted to exchange capacitive or inductive current so as to maintain or control specific power system variables. SVC is similar to a synchronous compensator in that it is used to supply or absorb reactive power but without rotating part. It is also have the equivalent of automatic

voltage regulator system to set and maintain a target voltage level. The basic structure of SVC is shown in Figures 2.2.

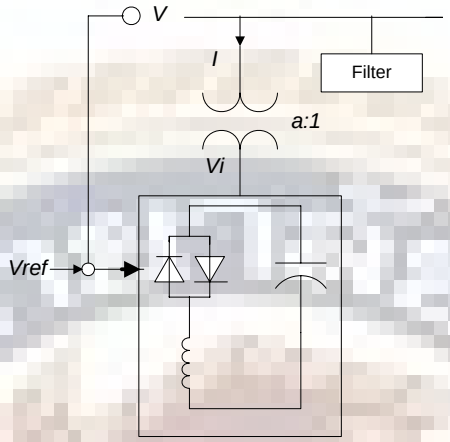

Figure 2.2: Basic structure of SVC.

SVC is composed of a controllable shunt reactor and shunt capacitor(s). Typically, the power system control variable controlled by SVC is the terminal bus voltage. Total susceptance (B_e) of SVC can be controlled by controlling the firing angle (α) of thyristors. Consequently, it represents the controller with variable impedance that is changed with the firing angle of Thyristor-Controlled Reactor (TCR).

During the normal operation, the total susceptance can be controlled according to the terminal voltage. However, at limits, minimum or maximum susceptance, SVC behaves like a fixed capacitor or an inductor. At point B_{max}, all thyristor switched capacitor are switched on, with SVC providing rated capacitive current at specified voltage. At point B_{min}, the thyristor-controlled reactor is fully switched on, and all thyristor switched capacitors are off to give inductive current at a defined voltage.

SVC can increase voltage stability of the system by immediately providing reactive power support when the system has voltage problems such as due to a trip of an important generator or transmission line, etc.

Appropriate model including appropriate representation of SVC can be incorporated in static voltage stability study by adding SVC equations in the power flow equations. The validated p.u. Differential-Algebraic Equations (DAEs) corresponding to this model are [15]-[16]:

$$\begin{bmatrix} \dot{x}_c \\ \dot{\alpha} \end{bmatrix} = f(x_c, \alpha, V, V_{ref}) \tag{2.19}$$

$$0 = \underbrace{\begin{bmatrix} B_e - \dfrac{2\alpha - \sin 2\alpha - \pi(2 - X_L / X_C)}{\pi X_L} \\ I - V_i B_e \\ Q - V_i^2 B_e \end{bmatrix}}_{g(\alpha, V, V_i, I, Q, B_e)} \tag{2.20}$$

where B_e is the total susceptance, α is firing angle of thyristor, X_L is inductance, X_C is capacitance, I is injected current, V_i is terminal voltage of SVC. Equation (2.20) can be introduced into the power flow equation in the CPF process. It represents limits not only on the firing angle α, but also on the current I, the control voltage V and the SVC voltage V_i as well as the reactive power Q.

2.4.2 STATCOM

STATCOM is based on a solid state synchronous voltage source that is analogous to an ideal synchronous machine except the rotating part. It generates a balanced set of sinusoidal voltages at the fundamental frequency with rapidly controllable amplitude and phase angle. As shown in Figure 2.3, STATCOM is the voltage-source converter, which converts a DC input voltage into AC output voltage in order to compensate the active and reactive needed by the system. The reference signal Q_{ref} and P_{ref} can control the amplitude V and phase angle β of output voltage, respectively.

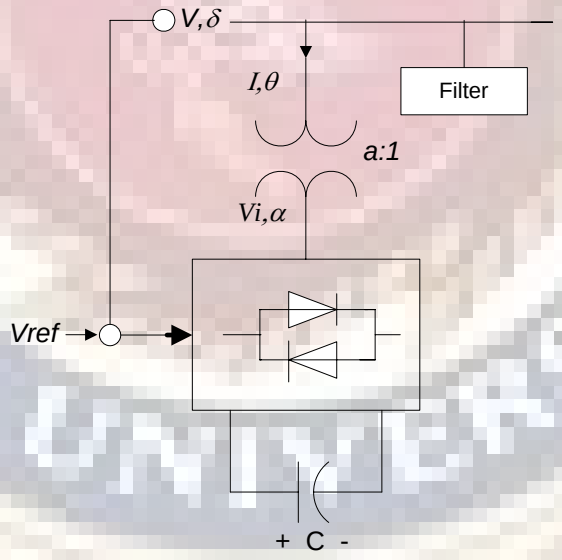

Figure 2.3: Basic structure of STATCOM.

Varying the amplitude of output voltage can control the reactive power exchange between STATCOM and the AC system. If the amplitude of the output voltage is increased above that of AC system voltage, STATCOM generates reactive power for the AC system. If the amplitude of the output voltage is decreased below that of the AC

system, STATCOM absorbs the reactive power. If the output voltage is equal to the AC system voltage, the reactive power exchange is zero.

The real power exchanges between STATCOM and the AC system can be controlled by altering the phase angles between the inverter output and the AC system voltages. STATCOM supplies real power to the AC system if the output voltage is made to lead the corresponding AC system voltage. Conversely, STATCOM absorbs real power from the AC system, if the output voltage is made to lag the AC system voltage.

The process of energy transfer from the AC to DC side and vice versa in a voltage source converter is direct, i.e., the net instantaneous power at the AC terminals must always be equal to the net instantaneous power at the DC terminals, if the losses in the circuit are neglected. If a DC capacitor is connected across the input terminals of the converter, the converter keeps the DC capacitor voltage at a required level. The real power can be stored by making the converter output voltage lag the AC system voltage, so that the converter absorbs a small amount of real power from the AC system to cover its internal losses and keep the capacitor voltage at desired levels. The real power injected can be accomplished by making converter output voltage lead the AC system voltage. The ability to supply real power depends on the size of DC capacitor and the real power losses due to switching. However, large amount of real power injected can be accomplished by using other types of energy storage.

The STATCOM can provide both capacitive and inductive compensation and is able to control output current over the rated maximum capacitive or inductive range independent of the AC system voltage. It can provide full capacitive output current at any practical system voltage when STATCOM is at the maximum limit. This is contrast to the SVC which can supply only diminishing output current with decreasing system voltage as determined by the designed maximum equivalent capacitive admittance. This type of controller is, therefore, more effective than the SVC in providing transmission voltage support and the expected stability improvements. In general, a reduction of more than 50 % in the physical size of installation can be expected when a STATCOM is compared to SVC. Also, for steady state reactive support, a STATCOM is capable of supporting higher loads than what would be possible with a SVC of comparable MVAr rating [11], [14].

There are two techniques for controlling the STATCOM. The first technique, referred to as phase control, is to control the phase shift α to control the STATCOM output voltage magnitude. The other technique referred to as Pulse Width Modulation (PWM) on the other hand allows for independent control of output voltage magnitude and phase shift; in this case, the DC voltage is controlled separately from the AC output voltage. The STATCOM increases voltage stability margin of the system by providing active and reactive power at the connected bus. Moreover, this device does not significantly alter the existing system impedance, which is an advantage over SVC.

In summary, STATCOM has better characteristics over SVC; when the system voltage drops enough to force the STATCOM output to ceiling, its maximum reactive power output will not affect by the voltage magnitude. Therefore, it exhibits constant current characteristics when the voltage is low under the limit. The steady state power exchange between the controller and the AC system is mostly reactive, as active power is only consumed to supply for the internal losses.

The p.u. DAEs corresponding to STATCOM controller are described as follows:

$$\begin{bmatrix} \dot{x}_c \\ \dot{\alpha} \\ \dot{m} \end{bmatrix} = f(X_c, \alpha, m, V, V_{dc}, V_{ref}, V_{dc,ref}) \tag{2.21}$$

$$\dot{V}_{dc} = \frac{VI}{CV_{dc}}\cos(\delta-\theta) - \frac{1}{R_c C}V_{dc} - \frac{R}{C}\frac{I^2}{V_{dc}} \tag{2.22}$$

$$0 = \underbrace{\begin{bmatrix} P - VI\cos(\delta-\theta) \\ Q - VI\sin(\delta-\theta) \\ P - V^2G + kV_{dc}VG\cos(\delta-\alpha) + kV_{dc}VB\sin(\delta-\alpha) \\ Q + V^2B - kV_{dc}VB\cos(\delta-\alpha) + kV_{dc}VG\sin(\delta-\alpha) \end{bmatrix}}_{g(\alpha,k,V,V_{dc},\delta,I,\theta,P,Q)} \tag{2.23}$$

where V_{dc} is DC voltage of voltage source inverter, m is modulation index, α is angle of internal synchronous source, R_c is internal DC losses due to switching, X_c is reactance of the capacitor, δ is angle of voltage and θ is angle of current.

The steady state model of STATCOM can be readily obtained from equations (2.21)-(2.23) as

$$0 = \begin{bmatrix} V - V_{ref} \pm X_{SL} I \\ V_{dc} - V_{dcref} \\ P - V_{dc}^2 / R_C - RI^2 \\ g(\alpha, k, V, V_{dc}, \delta, I, \theta, P, Q) \end{bmatrix} \tag{2.24}$$

Equation (2.24) includes AC and DC representation of STATCOM and it can be directly included in power flow program with the proper handling of limits, to analyze the static voltage stability of power system with STATCOM. If DC equations are introduced in the study, more practical solutions regarding to both AC and DC sides can be obtained.

2.4.3 TCSC

TCSC controllers use TCR in parallel with capacitor segments of series capacitor bank. The combination of TCR and capacitor allow the capacitive reactance to be smoothly controlled over a wide range and switched upon command to a condition where the bi-directional thyristor pairs conduct continuously and insert an inductive reactance into the line. The basic structure of the device is shown in Figures 2.4. The total susceptance of the line is controlled by controlling the firing angle of the thyristor.

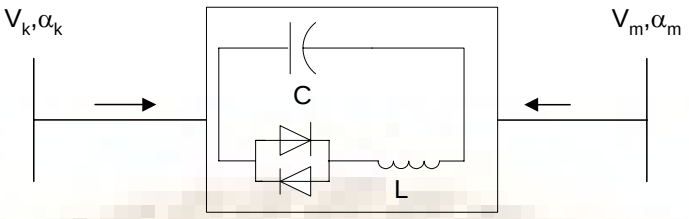

Figure 2.4: Basic structure of TCSC.

Suitable models to handle control limits and operation constraints are important. The p.u. DAEs corresponding to this device are shown as follows:

$$\begin{bmatrix} \dot{x}_c \\ \dot{\alpha} \end{bmatrix} = f(x_c, \alpha, V, V_{ref}) \tag{2.25}$$

$$0 = \underbrace{\begin{bmatrix} P + V_k V_m B_e \sin(\delta_k - \delta_m) \\ -V_k^2 B_e + V_k V_m B_e \cos(\delta_k - \delta_m) - Q_k \\ -V_m^2 B_e + V_k V_m B_e \cos(\delta_k - \delta_m) - Q_m \\ B_e - B_e(\alpha) \\ \sqrt{P^2 + Q_k^2} - IV_k \end{bmatrix}}_{g(\alpha, V_k, V_m, \delta_k, \delta_m, I, P, Q_k, Q_m, B_e)} \tag{2.26}$$

where *k* and *m* are buses where TCSC is connected in between,

$$\begin{aligned} B_e(\alpha) = {} & \pi\left(k_x^4 - 2k_x^2 + 1\right)\cos k_x(\pi - \alpha)/ \\ & \{X_C[\pi k_x^4 \cos k_x(\pi - \alpha) \\ & - \pi \cos k_x(\pi - \alpha) - 2k_x^4 \alpha \cos k_x(\pi - \alpha) \\ & + 2\alpha k_x^2 \cos k_x(\pi - \alpha) - k_x^4 \sin 2\alpha \cos k_x(\pi - \alpha) \\ & + k_x^2 \sin 2\alpha \cos k_x(\pi - \alpha) - 4k_x^3 \cos^2 \alpha \sin k_x(\pi - \alpha) \\ & - 4k_x^2 \cos \alpha \sin \alpha \cos k_x(\pi - \alpha)]\} \end{aligned} \tag{2.27}$$

and

$$k_x = \sqrt{\frac{X_C}{X_L}} \tag{2.28}$$

The steady state model of TCSC can be easily obtained from (2.25)-(2.28) as

$$0 = \begin{bmatrix} B_e - B_{e,ref} \\ g\left(\alpha, V_k, V_m, \delta_k, \delta_m, I, P, Q_k, Q_m, B_e\right) \end{bmatrix} \tag{2.29}$$

which can be directly introduced into the power flow formulation. From equation (2.29), the total susceptance of TCSC can be controlled at a specific value.

2.4.4 SSSC

SSSC is based on a solid-state synchronous voltage source employing an appropriate DC to AC inverter with gate turn-off thyristor, which can be used for series compensation of transmission lines. The SSSC is similar to the STATCOM as illustrated in Figure 2.5, as it is based on a DC capacitor fed VSI that generates a three-phase voltage at fundamental frequency, which is then injected in a transmission line through a transformer connected in series with the system.

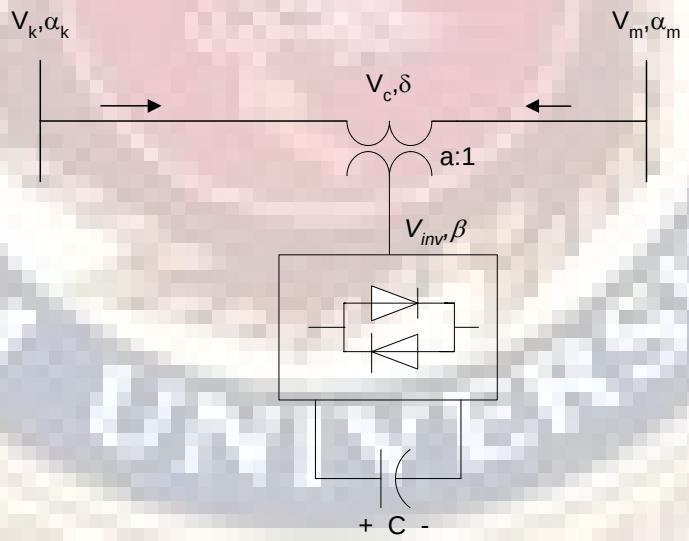

Figure 2.5: Basic structure of SSSC.

The main control objective of the SSSC is to directly control the current and indirectly the power, flowing through the line, by controlling the reactive power exchange between the SSSC and the AC system. The main advantage of this controller over a TCSC

is that it does not significantly affect the impedance of the transmission system and, therefore, there is no danger of having resonance problem.

The p.u. DAEs of SSSC including the control and operation limits can be elaborated as follows:

$$\begin{bmatrix} \dot{x}_c \\ \dot{\beta} \\ \dot{m} \end{bmatrix} = f(x_c, \beta, m, I, V_{dc}, I_{ref}, V_{dcref}) \tag{2.30}$$

$$\dot{V}_{dc} = \frac{VI}{CV_{dc}}\cos(\delta-\theta) - \frac{G_C}{C}V_{dc} - \frac{R}{C}\frac{I^2}{V_{dc}} \tag{2.31}$$

$$0 = \underbrace{\begin{bmatrix} P_k - V_k I\cos(\delta_k-\theta) \\ Q_k - V_k I\sin(\delta_k-\theta) \\ P_m - V_m I\cos(\delta_m-\theta) \\ Q_m - V_m I\sin(\delta_m-\theta) \\ P - P_k + P_m \\ Q - Q_k + Q_m \\ P - V^2G + kV_{dc}VG\cos(\delta-\beta) + kV_{dc}VB\sin(\delta-\beta) \\ Q + V^2B - kV_{dc}VB\cos(\delta-\beta) + kV_{dc}VG\sin(\delta-\beta) \end{bmatrix}}_{g(\beta,k,V_{dc},V_k,V_m,V,\delta_k,\delta_m,\delta,I,\theta,P_k,P_m,P,Q_k,Q_m,Q)} \tag{2.32}$$

where β is angle of internal voltage, δ is angle of AC voltage generated by SSSC, G_c is $1/R_c$.

To realize the models in power flow program, equations (2.30)-(2.32) are used as

$$0 = \begin{bmatrix} I - I_{ref} \\ V_{dc} - V_{dcref} \\ P - G_C V_{dc}^2 - RI^2 \\ g(\beta,k,V_{dc},V_k,V_m,V,\delta_k,\delta_m,\delta,I,\theta,P_k,P_m,P,Q_k,Q_m,Q) \end{bmatrix} \tag{2.33}$$

which can be incorporated directly into the power flow program. DC equations are included in the formulation to provide more practical solutions regarding to DC side.

2.4.5 UPFC

It is well known that UPFC is a versatile device for power flow control. The UPFC consists of two identical voltage-source inverters: one in shunt and the other one in series with the line; the general scheme is illustrated in Figure 2.6. Two inverters, namely shunt inverter and series inverter which operate via a common DC link with a DC storage capacitor, allow UPFC to independently control active and reactive power flows on the line as well as the bus voltage. Active power can freely flow in either direction between the AC terminals of the two inverters through the DC link. Although each inverter can generate or absorb reactive power at its own AC output terminal, they can not internally exchange reactive power through DC link. The VA rating of the injected voltage source is determined by the product of the maximum injected voltage and the maximum line current at which power flow is still provided.

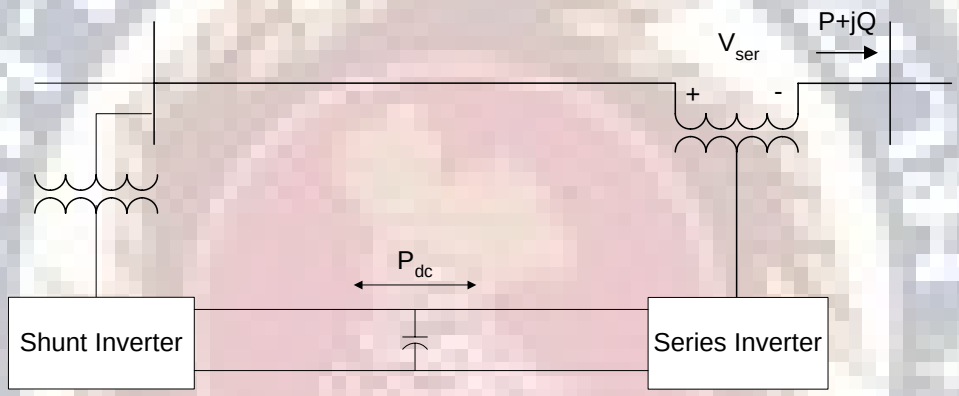

Figure 2.6: UPFC configuration.

The shunt inverter provides local bus voltage control when operated by itself as a STATCOM. When operated in conjunction with the series inverter, the shunt inverter has two functions: to control bus voltage by reactive power injection to the power system and to supply active power to the series inverter via the DC link for series flow control.

The series inverter, on the other hand, provides line power flow control by injecting an AC voltage with controllable magnitude and phase angle at the power frequency, in series with the line via an insertion transformer. This injected series voltage is, in effect, a synchronous series AC voltage source, which provides active series compensation for line voltage control and angle regulation through the transmission line current. The transmission line currents flow through this voltage sources resulting in active and reactive power exchange between the inverter and the AC system. The active power exchanged at the series AC terminal is converted by the inverter into DC power that appears at the DC link as positive or negative active power demand and transfer to the other converter located at the other side of the line.

It is obvious that the operation of UPFC is very important since it affects both the transmission line flow and voltage magnitude. Operation limit and control constraints of

UPFC are very crucial to realize the actual operation of the device. To realize that, the validated p.u. DAEs corresponding to this model can be derived as follows:

$$\begin{bmatrix} \dot{x}_c \\ \dot{\alpha} \\ \dot{\beta} \\ \dot{m}_{sh} \\ \dot{m}_{se} \end{bmatrix} = f(x_c, \alpha, \beta, m_{sh}, m_{se}, V_k, V_l, V_{dc}, \delta_k, \delta_l, P_{l,ref}, Q_{l,ref}, V_{k,ref}, V_{dc,ref}) \tag{2.34}$$

$$\dot{V}_{dc} = \frac{V_k I_{sh}}{C V_{dc}} \cos(\delta_k - \theta_{sh}) + \frac{V_m I_l}{C V_{dc}} \cos(\delta_m - \theta_l) - \frac{G_C}{C} V_{dc} - \frac{R_{sh}}{C} \frac{I_{sh}^2}{V_{dc}} - \frac{R_{se}}{C} \frac{I_l^2}{V_{dc}} \tag{2.35}$$

$$0 = \underbrace{\begin{bmatrix} P_{sh} - V_k I_{sh} \cos(\delta_k - \theta_{sh}) \\ Q_{sh} - V_k I_{sh} \sin(\delta_k - \theta_{sh}) \\ P_{sh} - V_k^2 G_{sh} + k_{sh} V_{dc} V_k G_{sh} \cos(\delta_k - \alpha) + k_{sh} V_{dc} V_k B_{sh} \sin(\delta_k - \alpha) \\ Q_{sh} + V_k^2 B_{sh} - k_{sh} V_{dc} V_k B_{sh} \cos(\delta_k - \alpha) + k_{sh} V_{dc} V_k G_{sh} \sin(\delta_k - \alpha) \end{bmatrix}}_{g_{sh}(\alpha, k_{sh}, V_k, V_{dc}, \delta_k, I_{sh}, \theta_{sh}, P_{sh}, Q_{sh})} \tag{2.36}$$

$$0 = \underbrace{\begin{bmatrix} P_k - P_{sh} - V_k I_l \cos(\delta_k - \theta_l) \\ Q_k - Q_{sh} - V_k I_l \sin(\delta_k - \theta_l) \\ P_l - V_m I_l \cos(\delta_m - \theta_l) \\ Q_l - V_m I_l \sin(\delta_m - \theta_l) \\ P_k - P_l - P_{sh} - P_{se} \\ Q_k - Q_l - Q_{sh} - Q_{se} \\ P_{se} - V^2 G_{se} + k_{se} V_{dc} V G_{se} \cos(\delta - \beta) + k_{se} V_{dc} V B_{se} \sin(\delta - \beta) \\ Q_{se} + V^2 B_{se} - k_{se} V_{dc} V B_{se} \cos(\delta - \beta) + k_{se} V_{dc} V G_{se} \sin(\delta - \beta) \end{bmatrix}}_{g_{se}(\beta, k_{se}, V_{dc}, V_k, V_l, V, \delta_k, \delta_l, \delta, I_l, \theta_l, P_k, P_l, P_{sh}, P_{se}, Q_k, Q_l, Q_{sh}, Q_{se})} \tag{2.37}$$

$$0 = \underbrace{\begin{bmatrix} I_k \cos(\theta_k) - I_{sh} \cos(\theta_{sh}) - I_l \cos(\theta_l) \\ I_k \sin(\theta_k) - I_{sh} \sin(\theta_{sh}) - I_l \sin(\theta_l) \\ P_k - V_k I_k \cos(\delta_k - \theta_k) \\ Q_k - V_k I_k \sin(\delta_k - \theta_k) \end{bmatrix}}_{g_{con}(V_k, \delta_k, I_k, I_{sh}, I_l, \theta_k, \theta_{sh}, \theta_l, P_k, Q_k)} \tag{2.38}$$

where *se, sh* represent series and shunt components, respectively and *l* represents the line used for current and power flow control.

The UPFC steady state model can be obtained by using the equations (2.34)-(2.38) as

$$0 = \begin{bmatrix} V_k - V_{k,ref} \\ V_{dc} - V_{dc,ref} \\ P_{se} - P_{se,ref} \\ Q_{se} - Q_{se,ref} \\ P_{sh} - P_{se} - G_C V_{dc}^2 - R_{sh} I_{sh}^2 - R_{se} I_l^2 \\ g_{sh}(\alpha, k_{sh}, V_k, V_{dc}, \delta_k, I_{sh}, \theta_{sh}, P_{sh}, Q_{sh}) \\ g_{se}(\beta, k_{se}, V_{dc}, V_k, V_l, V, \delta_k, \delta_l, \delta, I_l, \theta_l, P_k, P_l, P_{sh}, P_{se}, Q_k, Q_l, Q_{sh}, Q_{se}) \\ g_{con}(V_k, \delta_k, I_k, I_{sh}, I_l, \theta_k, \theta_{sh}, \theta_l, P_k, Q_k) \end{bmatrix} \tag{2.39}$$

which again can be incorporated into the power flow program.

The limits of UPFC can be divided into 2 limits: shunt compensation limits and series compensation limit. Shunt compensation limits are basically firing angle and V_{dc} limits, which can be handled in the same way as the case of STATCOM. Series compensation limit, however, involves the capacity of the series compensation, which incorporates the active and reactive power limits.

2.5 Analysis Tools

In this study, voltage stability with FACTS devices are studied and validated with the help of a program developed in MATLAB and standard CPF program, UWPFLOW. UWPLOW is a research tool that has been designed to calculate maximum loading margin of the power system associated with saddle-node and limit-induced bifurcation for given load and generation directions [59]. The program has detailed static models of various power system elements such as generators, loads, HVDC links, and various FACTS controllers, particularly SVC, STATCOM and TCSC devices under phase and PWM control schemes, representing control limits with accuracy of for all models. There are no models for SSSC and UPFC controllers available in UWPFLOW. Programs developed in MATLAB using m file and Symbolic/Optimization toolboxes are used to find the solution of voltage stability study with FACTS devices. The result developed in MATLB is compared with UWPFLOW for the case of SVC, STATCOM and TCSC.

2.6 Test Systems

The simple 3-bus test system and the modified IEEE 14-bus test systems [13] are used to validate the proposed approach. Single line diagrams of the 3-bus and modified IEEE 14-bus test systems are illustrated in Figs. 2.7 and 2.8, respectively. The modification from the original IEEE 14-bus test system is that generators located at buses 6 and 8 were changed from synchronous compensators to generators.

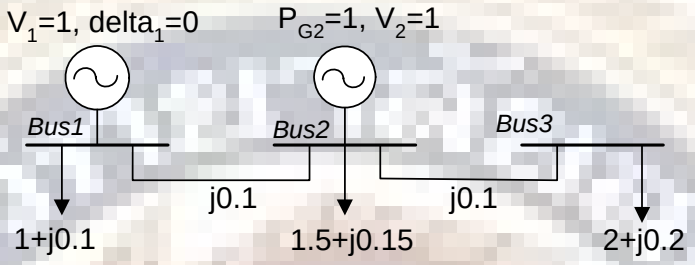

Figure 2.7: Single line diagram of the 3-bus system.

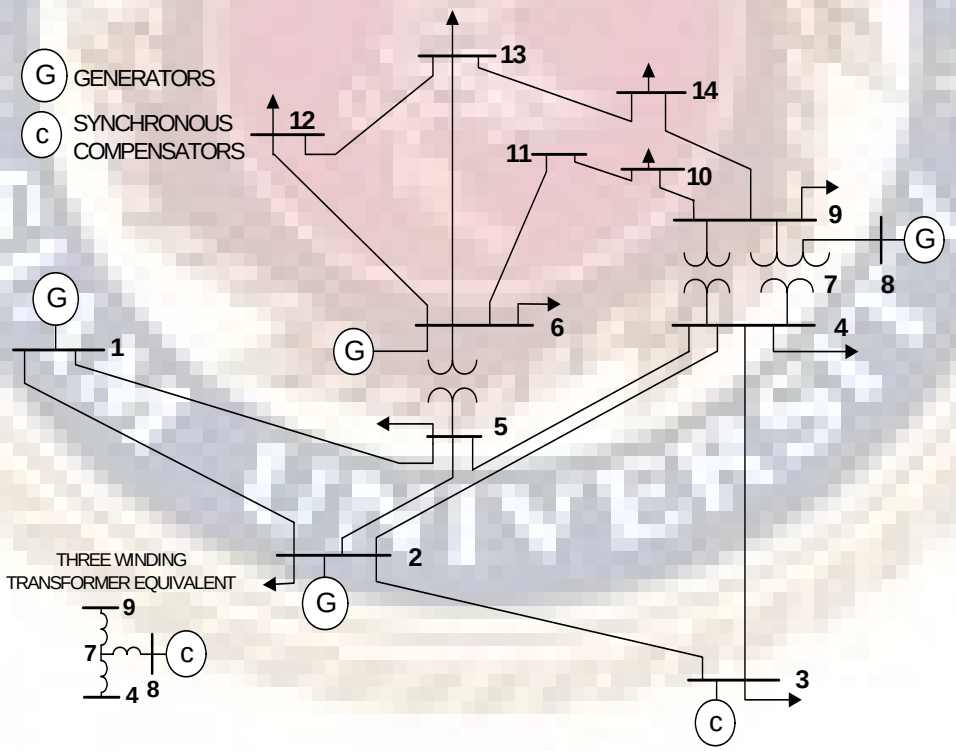

Figure 2.8: Single line diagram of the modified IEEE 14-bus system.

2.7 Summary

This chapter presents concepts and analysis techniques for voltage stability study in power systems. Various ways to enhance voltage stability margin including an introduction of FACTS devices are also presented in the chapter. Equations representing AC and DC parts of well-known FACTS devices are presented and they can be introduced directly into load flow equations in static voltage stability study. Analysis tools and test systems used throughout the study for voltage stability with FACTS devices are also presented.

Chapter 3

Voltage Stability Study Using Symbolic and Optimization Toolboxes

3.1 Introduction

The proposed approach is presented in this Chapter for load flow, CPF and optimization techniques. Load flow is proposed first. Then, the method is applied to the CPF and optimization process.

3.2 MATLAB Symbolic and Optimization Toolboxes

MATLAB (matrix laboratory) is a numerical computing environment and fourth-generation programming language. Although MATLAB is intended primarily for numerical computing, an optional toolbox, allowing access to symbolic computing capabilities. In MATLAB, there are plenty of toolboxes used for finding solution in particular areas such as optimization, fuzzy logic, neural networks, etc.

Optimization Toolbox provides widely used algorithms for standard and large-scale optimization. These algorithms solve constrained and unconstrained continuous and discrete problems. The toolbox includes functions for linear programming, quadratic programming, binary integer programming, nonlinear optimization, nonlinear least squares, systems of nonlinear equations, and multiobjective optimization. Optimization Toolbox provides widely used optimization algorithms for solving nonlinear programming problems. The toolbox includes solvers for unconstrained and constrained nonlinear optimization and solvers for least-squares optimization.

Symbolic Toolbox provides tools for solving and manipulating symbolic math expressions and performing variable-precision arithmetic. In addition to performing symbolic math operations, the toolbox provides variable-precision arithmetic functions for computations that require exact control over numeric accuracy.

Symbolic and Optimzation toolboxes are the main features of MATLAB used in this research. More details of these toolboxes can be found in reference [60].

3.3 Load Flow

Power flow or load flow consists of solving real and reactive power balance equations of all buses in power systems to obtain all state variables when control variables are specified. According to this, Symbolic toolbox in MATLAB can be used to create power flow equations when the system data and control variables are known. Then, a simple command called “lsqnonlin” in Optimization toolbox is used to find the solution for all state variables. The steps behind the proposed method can be summarized as shown in the Fig. 3.1.

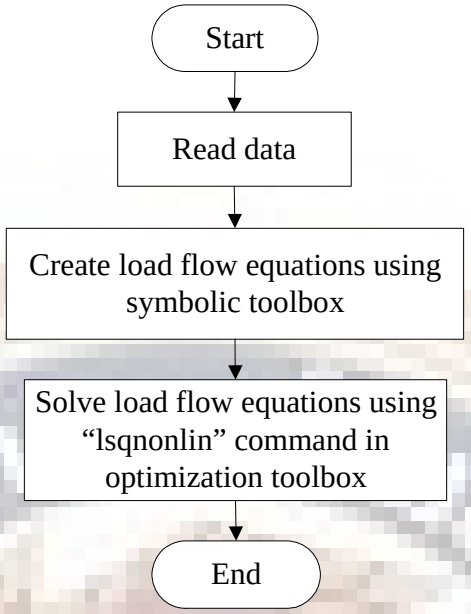

Figure 3.1: Load flow calculation using Symbolic and Optimization toolboxes.

From Fig. 3.1, system parameters are read from input data to create power balance equations using Symbolic toolbox. The solution is then found by using a single "lsqnonlin" command. It can be noticed that Jacobian is not required to compute in the formulation process since it is already embedded in Optimization toolbox. The solution is found in a simple way, as only one command is used.

3.4 Continuation Power Flow

Continuation Power Flow is basically a series of load flow calculation with predictor and corrector steps. The formation of CPF is complicated and it requires good programming skill. However, with the help of Symbolic and Optimization toolboxes, the formulation is much easier. Figure 3.2 illustrates steps behind the CPF process with Symbolic and Optimization toolboxes. From Fig. 3.2, the system data is read first, then Symbolic toolbox is introduced to create power flow equations. The power flow calculation is performed to find the load flow Jacobian for the following predictor step.

In the predictor step, state variables are predicted from the current status of load flow Jacobian to predict the bus angles and voltages at higher LF. In the corrector step, the actual value of state variables are computed from load flow equations and initial condition obtained from the predictor step. Prior to the collapse point, parameterization step is performed to avoid convergence difficulty of CPF process by switching state variable from LF to the voltage at the weakest bus, which is found from a bus having highest voltage decrease. The process is repeated until the PV curve is completed. For simplicity, in the research, parameterization is introduced after the last LF that allows load flow solution to converge.

3.5 Optimization Technique

Optimization technique can be solved with the help of Symbolic and Optimization toolboxes as well. Fig. 3.3 shows various steps of optimization technique including

reading input data, creating power flow equations, creating necessary conditions and solving necessary conditions for optimal solutions. From the proposed method, Lagrangian function and necessary conditions are automatically created by using Symbolic toolbox. The optimal solution is then found from the necessary conditions by using a single command, “lsqnonlin”.

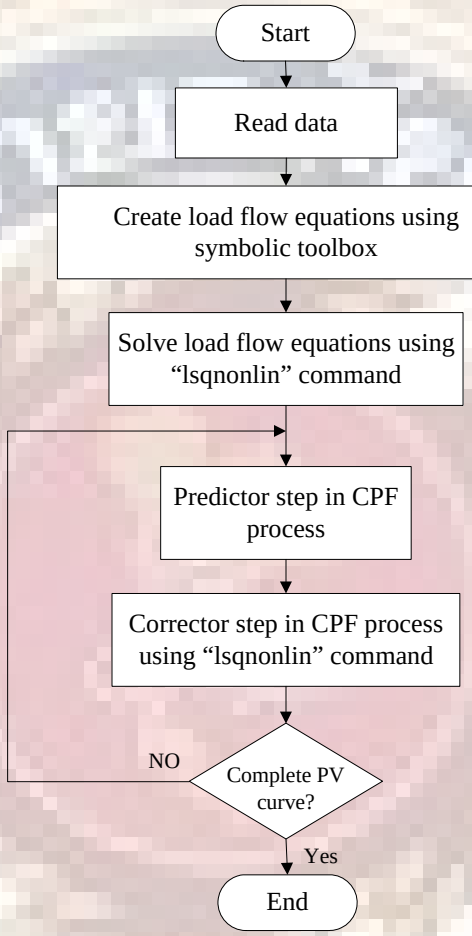

Figure 3.2: CPF using Symbolic and Optimization Toolboxes.

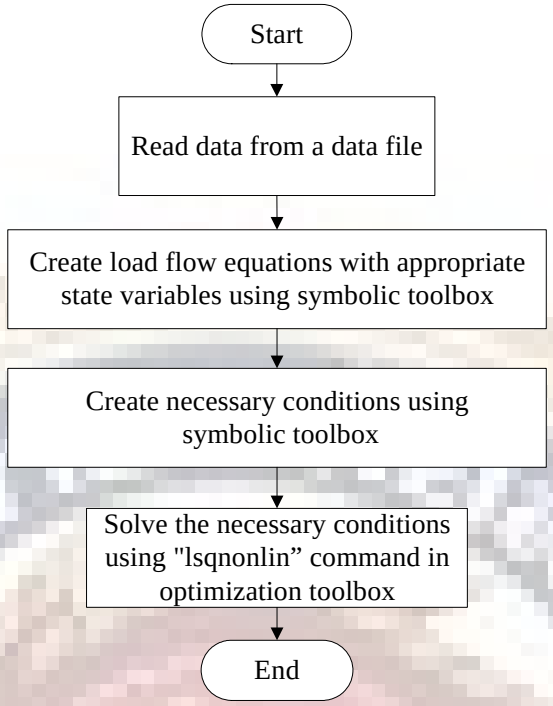

Figure 3.3: Optimization technique using Symbolic and Optimization Toolboxes.

FACTS devices are applied in the process by adding equations including AC and DC representation in load flow equation. The proposed simulation method is validated in the next Chapter in two test systems, namely the 3-bus test system and the modified IEEE 14-bus test system.

3.6 Summary

In this chapter, simulation approach based on Symbolic and Optimization toolboxes of MATLAB are proposed for load flow, CPF and Optimization method in static voltage stability study of the system including FACTS controllers. .

Chapter 4

Simulation Results

4.1 Introduction

The proposed simulation approach is simulated for load flow, CPF and Optimization techniques. Load flow is tested in the first step, as it is the first part of CPF process. Optimization method is tested in the last step in order to compare the result with that of CPF method. Finally, FACTS devices are applied in the modified IEEE 14-bus test systems.

4.2 Load Flow

4.2.1 The Three-bus Test System

In order to solve power flow equation in a simple way, state variables are selected to be equal to two times number of buses plus 1. The last state variable is LF, which is introduced in the load flow for CPF in the predictor step. In the three-bus test system, there are 7 state variables: 3 for bus angles, 3 for bus voltages and 1 for LF, which is zero for load flow. After reading the input data, Symbolic toolbox is introduced to create the following power flow equations:

$$\begin{aligned}
\delta_1 &= 0 \\
P_{G2} - (1+\lambda) P_{D2} - 10V_2V_1 \sin(\delta_2 - \delta_1) - 10V_2V_3 \sin(\delta_2 - \delta_3) &= 0 \\
-(1+\lambda) P_{D3} - 10V_3V_2 \sin(\delta_3 - \delta_2) &= 0 \\
V_1 &= 1 \\
V_2 &= 1 \\
-(1+\lambda) Q_{D3} + 10V_3V_2 \cos(\delta_3 - \delta_2) - 10V_3^2 &= 0 \\
\lambda &= 0
\end{aligned}$$

From the above equations, there are 7 equations with 7 state variables. State variables namely angle at bus 1, voltages at bus 1 and 2, and LF are control variables as they are specified. A single MATLAB command "lsqnonlin" is then used to obtain the solution in a simple way. The solution of load flow is therefore $x = [\delta_1, \delta_2, \delta_3, V_1, V_2, V_3, \lambda]^T$=[0.0000, -0.2527, -0.4632, 1.0000, 1.0000, 0.9570, 0.0000]^T.

4.2.2 The Modified IEEE 14-bus Test System

In the 14-bus test system, there are 28+1 state variables: 14 for bus angles, 14 for bus voltages and 1 for LF. There are 28 equations, which are created by using Symbolic toolbox. The solution is then found from the help of "lsqnonlin" command in Optimization toolbox. The solution of load flow is, therefore, [0.0000, -0.0437, -0.1563, -0.0988, -0.0808, -0.1017, -0.0876, -0.0307, -0.1188, -0.1201,-0.1127, 0.1159, -0.1172, -0.1343, 1.0600, 1.0750, 1.0612, 1.0600, 1.0603, 1.1246, 1.0956, 1.1312, 1.0813, 1.0816, 1.0993,

1.1084, 1.1015, 1.0727, 0.0000] ^{T} for state variables [δ_1,…, δ_{14}, V_1,…,V_{14}, λ] ^{T}. Load flow solution is used in CPF process, which is presented in the next Section.

4.3 Continuation Power Flow

4.3.1 The Three-bus Test System

Jacobian of the first load flow is used in the predictor step to predict state variables for the next LF. At the next LF and predicted state variables, the corrected state variables can be found in the corrector step. When the load flow solution is diverged at the collapse point, parameterization step is activated at the last converged LF.

PV curves of the test systems based on CPF with the help of Symbolic and Optimization toolboxes are shown in Fig. 4.1. From PV curve, LM of the system is 1.2625 p.u. Numerical results of all state variables during predictor, corrector and parameterization steps are tabulated in Tables 4.1 and 4.2. In this study, step sizes of LF in the predictor step and voltage in parameterization step are specified at 0.1 and 0.02 p.u., respectively. These values are important and they should be carefully selected.

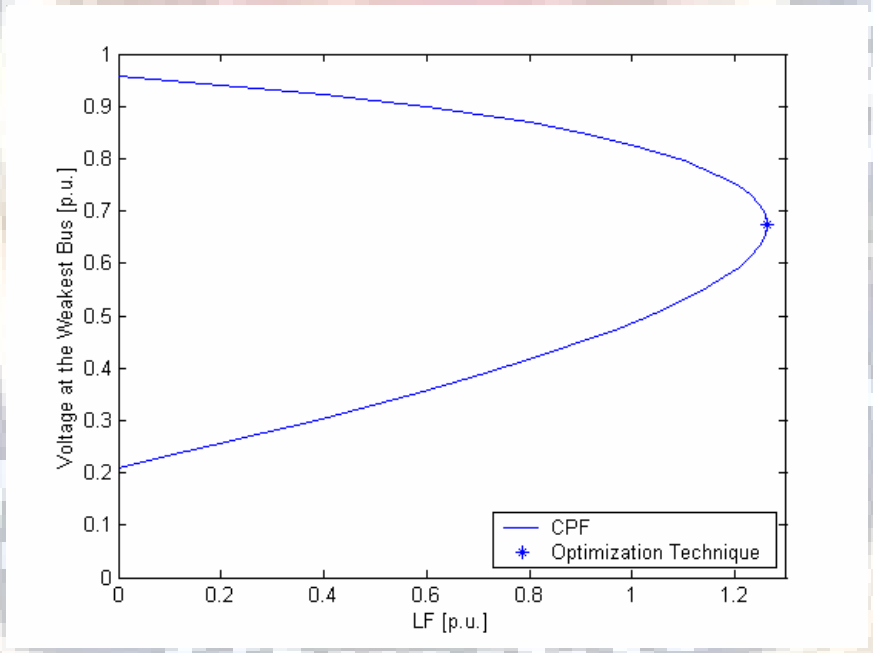

Figure. 4.1 PV curve of three bus test system.

Table 4.1 State Variables during Corrector and Parameterization Steps at some LFs of the Three-bus System

	Corrector Steps			Parameterization	
δ_1	0.0000	0.0000	0.0000	0.0000	0.0000
δ_2	-0.2527	-0.2890	-0.7342	-0.7478	-0.7571
δ_3	-0.4632	-0.5228	-1.3580	-1.4012	-1.4392
V_1	1.0000	1.0000	1.0000	1.0000	1.0000
V_2	1.0000	1.0000	1.0000	1.0000	1.0000
V_3	0.9570	0.9496	0.7532	0.7332	0.7132
λ	-0.0000	0.1000	1.2000	1.2286	1.2481

Table 4.2 State Variables during Predictor Step at some LFs of the Three-bus System

	Predictor Step				
δ_1	0.0000	0.0000	0.0000	0.0000	0.0000
δ_2	-0.2888	-0.3255	-0.3627	-0.4004	-0.4386
δ_3	-0.5223	-0.5829	-0.6448	-0.7082	-0.7734
V_1	1.0000	1.0000	1.0000	1.0000	1.0000
V_2	1.0000	1.0000	1.0000	1.0000	1.0000
V_3	0.9500	0.9419	0.9329	0.9230	0.9119
λ	0.1000	0.2000	0.3000	0.4000	0.5000

4.3.2 The Modified IEEE 14-bus Test System

The proposed simulation approach is tested in the modified IEEE 14-bus test system. PV curve at the weakest bus of the system is illustrated in Fig. 4.2. From Fig. 4.2, LM of the system is 0.9278 p.u.

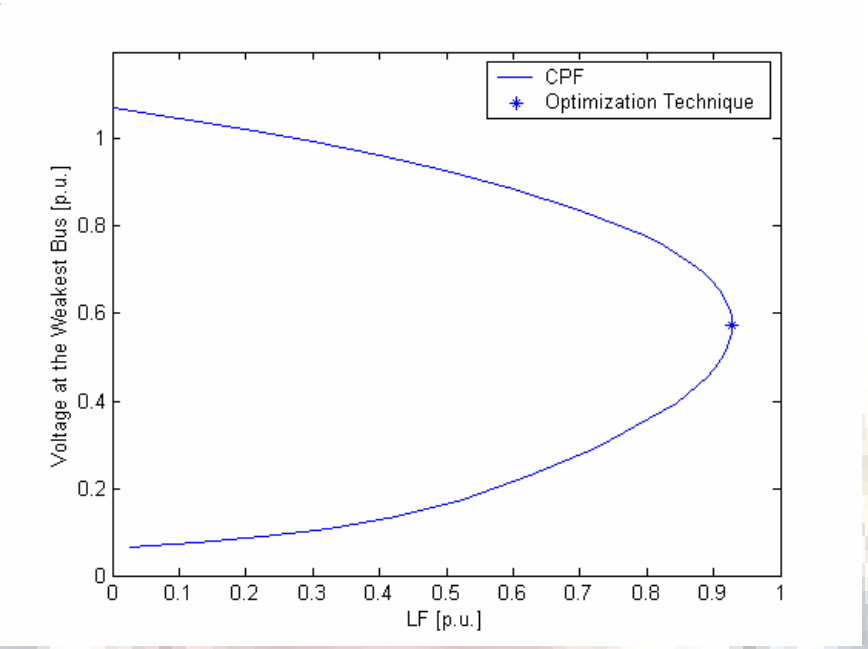

Figure. 4.2 PV curve of 14-bus test system.

4.4 Optimization Technique

4.4.1 The Three-bus Test System

Symbolic and Optimization toolboxes can be used to find loading margin of the system based on optimization technique. All state variables and LM at the collapse point of the 3-bus test systems are $x = [\delta_1, \delta_2, \delta_3, V_1, V_2, V_3, \lambda]^T$=[0.0000, -0.6334, -1.3689, 1.0000, 1.0000, 0.6744, 1.2625]^T. The result is compared with CPF in Fig. 4.1. From Fig. 4.1, it is noticed that optimization technique provides only single solution, the maximum point. CPF, on the other hand, provides a complete PV curve and voltages at various loading factors. Moreover, CPF can provide the information about the weakest location in the system.

4.4.2 The Modified IEEE 14-bus Test System

Symbolic and Optimization toolboxes is further applied to the modified IEEE 14-bus test system. LM of the system is 0.9278 p.u. and the voltage at the weakest bus, bus 14, is 0.5749 p.u. The LM obtained from the optimization technique is plotted with the complete PV curve obtained from CPF method in Fig. 4.2. Again, the optimization technique provides only single solution, the maximum solution.

The necessary equation of the optimization process is shown as follows:

$$\delta_1 = 0$$
$$P_{G2} - (1+\lambda) P_{D2} + 10V_1V_2 \sin(\delta_1 - \delta_2) - 10V_2V_3 \sin(\delta_2 - \delta_3) = 0$$
$$-(1+\lambda) P_{D3} + 10V_2V_3 \sin(\delta_2 - \delta_3) = 0$$
$$V_1 = 1$$
$$V_2 = 1$$
$$-(1+\lambda) Q_{D3} + 10V_2V_3 \cos(\delta_2 - \delta_3) - 10V_3^2 = 0$$
$$w_1 + 10w_2V_1V_2 \cos(\delta_1 - \delta_2) = 0$$
$$w_2\left[-10V_1V_2 \cos(\delta_1 - \delta_2) - 10V_2V_3 \cos(\delta_2 - \delta_3)\right]$$
$$+10w_3V_2V_3 \cos(\delta_2 - \delta_3) - 10w_6V_2V_3 \sin(\delta_2 - \delta_3) = 0$$
$$10w_2V_2V_3 \cos(\delta_2 - \delta_3) - 10w_3V_2V_3 \cos(\delta_2 - \delta_3)$$
$$+10w_6V_2V_3 \sin(\delta_2 - \delta_3) = 0$$
$$10w_2V_2 \sin(\delta_1 - \delta_2) + w_4 = 0$$
$$w_2\left[10V_1 \sin(\delta_1 - \delta_2)\right] - 10V_3 \sin(\delta_2 - \delta_3)$$
$$+10w_3V_3 \sin(\delta_2 - \delta_3) + w5 + 10w_6V_3 \cos(\delta_2 - \delta_3) = 0$$
$$-10w_2V_2 \sin(\delta_2 - \delta_3) + 10w_3V_2 \sin(\delta_2 - \delta_3)$$
$$+w_6\left[10V_2 \cos(\delta_2 - \delta_3) - 20V_3\right] = 0$$
$$-1 - 1.5w_2 - 2w_3 - w_6Q_{D3} = 0$$

4.5 Simulation Times

Simulation times used to simulate load flow, CPF and optimization technique are shown in Table 4.3 for the test systems. From Table, it can be observed that the proposed approach takes about 6 and 32 seconds to find the load flow solutions for the 3-bus and 14-bus test systems, respectively. The proposed approach uses about 2 and 17 minutes to plot complete PV curves based on CPF process. Simulation time for optimization technique is close to that of load flow in the test systems. It is noticed that the proposed approach is simulated by using AMD 1.3 MHz notebook computer.

Table 4.3. Simulation time for the test systems

Case	Simulation Time for	
	Three Bus	Fourteen Bus
Load Flow	5.588 sec	32.056
CPF	2 min 0.634 sec	17 min 6.353 sec
Optimization	6.349 sec	26.478 sec

4.6 Voltage Stability with FACTS Devices

4.6.1 PV Curves and Voltage Profiles

In this section, various FACTS controllers are compared. Figure 4.3 shows PV curves of base case and system with FACTS devices for the modified IEEE 14-bus test system. LM of base case and various FACTS devices are shown in Table 4.4. From Figure 4.3 and Table 4.4, UPFC gives the highest LM improvement followed by shunt FACTS devices and series FACTS devices, respectively. The IEEE 14-bus test system requires reactive power compensation at the distribution level, thus installing shunt reactive devices could provide higher LM than series devices. UPFC, on the other hand, is composed of both shunt and series devices. Introducing UPFC can provide reactive power both at the distribution level and at the line, thus making the device the most effective one in the terms of LM improvement in this test system.

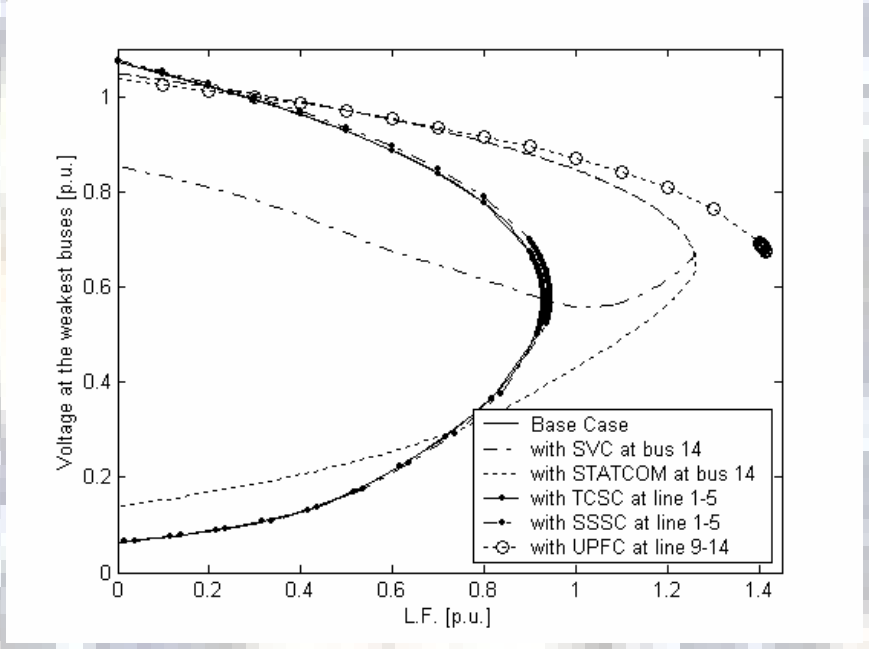

Figure 4.3: PV curves of base case, with FACTS devices.

Table 4.4: LM and % Increase of LM of base case, with FACTS devices

Case	Loading Margin [p.u]	% Increase of LM from base case
Base Case	0.9278	-
SVC	1.2606	35.9
STATCOM	1.2625	36.1
TCSC	0.9307	0.3
SSSC	0.9452	1.9
UPFC	1.4165	52.7

Voltage profiles at the LM of base case and various FACTS devices are illustrated in Figure 4.4. From Figure 4.4, it can be seen that UPFC provides better voltage profiles than other FACTS devices with higher LM. Compared to series FACTS devices, shunt devices give better voltage profiles since the reactive power is introduced at the weakest bus.

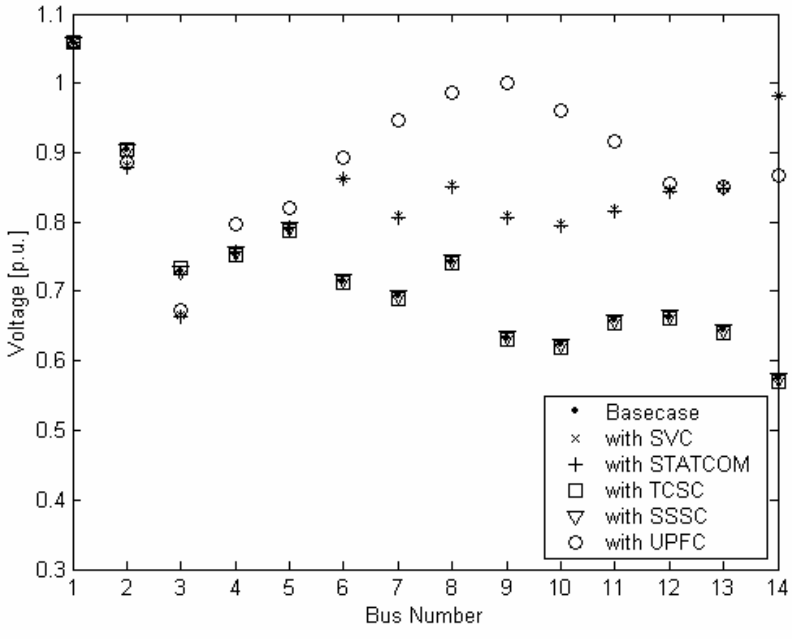

Figure 4.4: Voltage profile of base case, with FACTS devices.

4.6.2 Power Losses

Real and reactive power losses occurred in the system are plotted in Figures 4.5 and 4.6, respectively. From Figures 4.5 and 4.6, both real and reactive power losses follow the same pattern at various LFs. UPFC has lower losses as well as the incremental losses compared to other FACTS devices, thus giving highest LM and better voltage profile. Shunt FACT devices provide lower losses compared to series FACTS devices and base case.

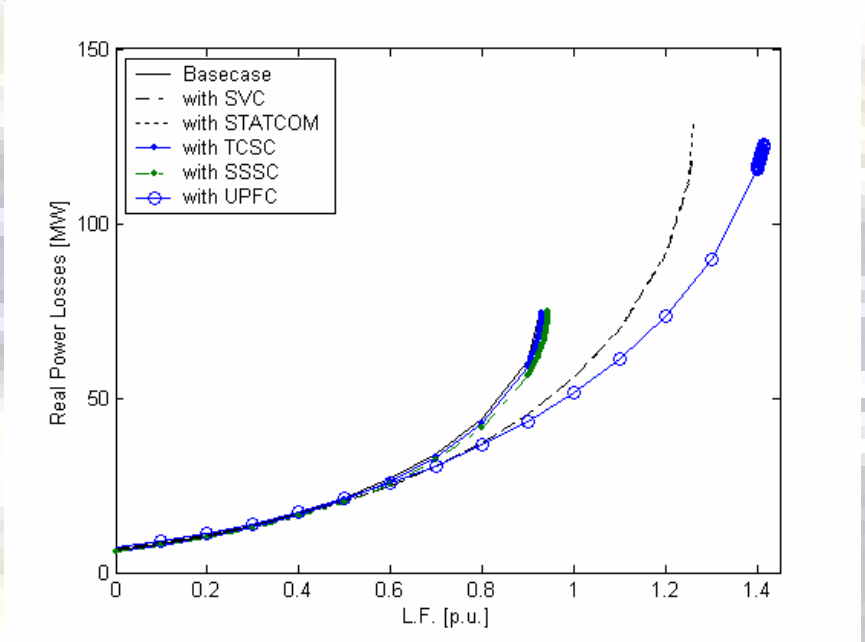

Figure 4.5: Real power losses of the system with FACTS devices.

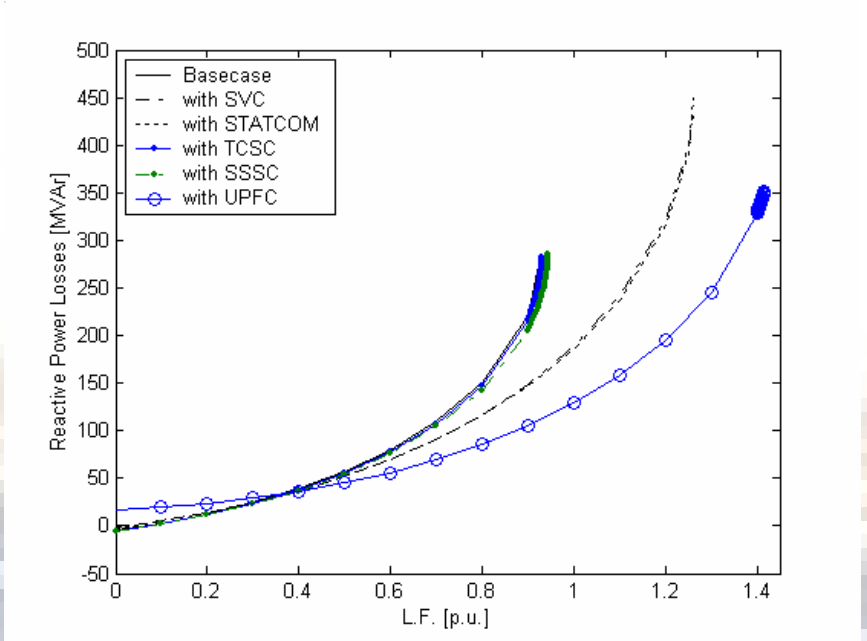

Figure 4.6: Reactive power losses of the system with FACTS devices.

4.6.3 Contingency

LMs for three worst contingency cases are shown in Table 4.5 for various FACTS devices. From Table 4.5, shunt FACTS devices provide higher LM than series FACTS devices for all contingency cases, as the system requires reactive power at the load location. UPFC is the device that gives the highest voltage stability margin improvement.

Table 4.5: Loading Margin for various line outages for base case and various FACTS controllers

Case	Loading Margins [p.u.] for line outages		
	1-2	2-3	1-5
Base Case	0.25184	0.38278	0.59605
SVC	0.40205	0.49212	0.87061
STATCOM	0.40097	0.49174	0.86916
TCSC	-	0.4033	-
SSSC	-	0.3964	-
UPFC	0.5003	0.5596	1.0161

The results are validated with UWPFLOW program for all the cases except SSSC and UPFC cases as they are not available in UWPFLOW. Voltage stability study with SSSC and UPFC are one of the contribution in this research. Another contribution is the comparison of all FACTS devices with full AC-DC representation in the same test system. Finally, the novel simulation approach based on Symbolic and Optimization toolboxes is proposed to help researchers do the simulation in an easy way.

4.7 Summary

In this chapter, simulation results of voltage stability study using Symbolic and Optimization toolboxes are presented through simple three bus system and the modified IEEE 14 bus test system including various FACTS controllers. Important issues associated with FACTS applications for voltage stability improvement are discussed in details. All the devices are compared for loading margin, voltage profile and losses. Finally the influence of these devices on static voltage stability margin under the worst contingency condition is also included.

Chapter 5

Conclusions

5.1 Concluding Observations

This research proposes a new simulation approach for static voltage stability study based on Symbolic and Optimization toolboxes. Load flow, CPF and optimization techniques are used to analyze the static voltage stability based on the proposed technique. Equations are created by using Symbolic toolbox and the solutions can be found by using a single command in Optimization toolbox. The proposed method is applied to the power system with FACTS devices. The simulation time is acceptable, not too high. This may be useful for utilities or researchers to find voltage stability assessment of medium size power systems in a simple way. The new ideas proposed are applied to the modified IEEE 14- bus test system to see the usefulness of the methods.

5.2 Main Contributions

The major contributions of this research can be summarized as follows:

(i) A new simulation approach for static voltage stability study based on Symbolic and Optimization toolboxes including load flow, CPF and optimization techniques.
(ii) Voltage stability assessments of various FACTS devices are studied and compared in the same test system. AC and DC representation of FACTS devices are used throughout the study.
(iii) Voltage stability study with SSSC and UPFC with AC-DC representation is presented.

5.3 Future Directions

There are numbers of issues that are still to be addressed in simple simulation approach and FACTS controllers in static voltage stability study:

(i) The proposed simulation approach should be applied to practical power systems. Appropriate simulation tool such as high performance computer may be used.
(ii) Due to the advantages of simple simulation, other issues on FACTS controllers may be exploted such as
    - Coordination and interaction of various FACTS devices related to static voltage stability can be studied to provide composite enhanced performance of these devices. Moreover, mathematical representation of capacities and locations may be investigated for the use of a full optimization technique to find the most appropriate size and location.
    - Due to the expensive nature of FACTS controllers, a thorough cost-benefit analysis can be carried out to justify the economic viability of these controllers by translating various benefits of the use of the controllers on system performance in terms of money. This would be a useful contribution in the framework of deregulated market environment.

BIBLIOGRAPHY

[1] B. Gao, G.K. Morison, P. Kundur, "Towards The Development of a Systematic Approach for Voltage Stability Assessment of Large-Scale Power Systems", *IEEE Transactions on Power System*, Vol. 11, No. 3, pp. 1314-1324, August 1996.

[2] T. Nagao, K. Tanaka and K. Takenaka, "Development of static and simulation programs for voltage stability studies of bulk power system", *IEEE Transactions on Power System*, Vol. 12, No. 1, pp. 273-281, February 1997.

[3] IEEE/PES Power System Stability Subcommittee, *Voltage Stability Assessment: Concepts, Practices and Tools*, special publication, August 2003.

[4] P. Kundur, *Power System Stability and Control*, McGrawHil, 1994.

[5] Blackout of 2003: Description and Responses, Available: http://www.pserc.wisc.edu/.

[6] C. A. Canizares, A. C. Z. DeSouza, and V. H. Quintana, "Comparison of performance indices for detection of proximity to voltage collapse", *IEEE Transactions on Power System*, Vol. 11, No. 3, pp. 1441-1447, August 1996.

[7] P-A. Lof, G. Andersson and D. J. Hill, "Voltage stability indices for stressed power systems", *IEEE Transactions on Power System*, Vol. 8, No. 1, pp. 326-331, February 1993.

[8] K. N. Srivastava, S. C. Srivastava and P. K. Kalra, "Prediction of voltage collapse in an integrated AC-DC network using the singular-value decomposition concept", *Electric Power System Research*, Vol. 28, pp. 111-122, 1993.

[9] B. H. Lee and K. Y. Lee, "A Study on Voltage Collapse Mechanism in Electric Power Systems," *IEEE Transactions Power System*, Vol. 6, pp. 966-974, August 1991.

[10] C.A. Canizares, A. C. Z. De Souza, and V. H. Quintana, "Comparison of performance indices for detection of proximity to voltage collapse," *IEEE Transactions Power System*, Vol. 11, No. 3, pp. 1441-1447, August 1996.

[11] A. Sode-Yome and N. Mithulananthan, "Comparison of shunt capacitor, SVC and STATCOM in static voltage stability margin enhancement," *International Journal of Electrical Engineering Education*, UMIST, Vol. 41, No. 3, July 2004.

[12] B. H. Lee and K. Y. Lee, "Dynamic and Static Voltage Stability Enhancement of Power Systems," *IEEE Transactions on Power Systems*, Vol. 8, No. 1, pp. 231-238, 1993.

[13] A. Sode-Yome and N. Mithulananthan, "Maximizing static voltage stability margin in power systems using a new generation pattern", *Australasian Journal of Electrical & Electronics Engineering*, Vol. 2, No 3, 2005.

[14] Cigre 95 TP108, FACTS Overview, IEEE Power Engineering Society, 1995.

[15] Canizares and Z. T. Faur, “Analysis of SVC and TCSC Controllers in Voltage Collapse”, IEEE Transactions on Power Systems, Vol. 14, No. 1, pp. 158-165, February 1999.

[16] C. A. Canizares, “Power flow and transient stability models of FACTS controllers for voltage and angle stability studies”, IEEE/PES WM on Modeling, Simulation and Applications of FACTS Controllers in Angle and Voltage Stability Studies, Singapore, January 2000.

[17] D. Thukaram and A. Lomi, “Selection of Static VAR Compensator Location and Size for System Voltage Stability Improvement”, Electrical Power Systems Research, Vol. 54, pp. 139-150, 2000.

[18] M. H. Haque, “Optimal location of shunt FACTS devices in long transmission lines”, IEE Proceeding-Generation, Transmission , Distribution, Vol. 147, No. 4, pp. 218-222, July 2000.

[19] S. Ibrahim and A. Abusorrah, ,“Optimal allocation of SVCs for improvement of power system performance”, Electric Power Components and Systems, Vol. 31, pp. 27-46, 2003.

[20] S. Chang and J. S. Huang, “Optimal SVC placement for voltage stability reinforcement”, Electric Power System Research, Vol. 42, pp. 165-172, 1997.

[21] S. N. Singh and A. K. David, “A new approach for placement of FACTS devices in open power markets”, IEEE Power Engineering Review, September 2001.

[22] N. Amjady and M. Esmaili, “Improving voltage security assessment and ranking vulnerable buses with consideration of power system limit”, Electric Power System Research, Vol. 25, pp. 705-715, 2003.

[23] N. Amjady and M. Esmaili, “Voltage security assessment and vulnerable bus ranking of power systems”, Electric Power System Research, Vol. 64, pp. 227-237, 2003.

[24] Leita da Silva, I. P. Coutinho, A. C. Z. De Souza, R. B. Prada and A. M. Rei ,“Voltage collapse risk assessment”, Electric Power System Research, Vol. 54, pp. 221-227, 2000.

[25] K. Y. Lee, A. Sode-Yome, and J. H. Park, “Adaptive Hopfield neural networks for economic load dispatch”, IEEE Transaction on Power System Apparatus and Systems, Vol. 13, No. 2, pp. 519-526, August 1995.

[26] K. Y. Lee, F. M. Nuroglu, and A. Sode-Yome, “Real power optimization with load flow using adaptive Hopfield neural networks”, Journal of Engineering Intelligent Systems, Vol. 8, No. 1, pp. 53-58, March 2000.

[27] J. Wood and B. F. Wollenberg, Power Generation Operation & Control, John Wiley & Sons, 1984.

[28] Z. Fend, V. Ajjarpu and D. J. Maratukulam, “A practical minimum load shedding strategy to mitigate voltage collapse”, IEEE Transactions on Power Systems, Vol. 13, No. 4, pp. 1285-1291, November 1998.

[29] Bompard, E. Carpaneto, G. Chicco and R. Napoli, “Evaluation of the critical load increase direction in voltage collapse studies”, Electric Power System Research, Vol. 43, pp. 61-67, 1997.

[30] G. M. Huang and N. K. C. Nair, “Voltage stability constrained load curtailment procedure to evaluate power system reliability measures”, Proceeding of IEEE Power Engineering Society-Winter Meeting, New York, January 2002, pp. 761-765.

[31] C. L. DeMarco and T. J. Overbye, “An energy based security measure for assessing vulnerability to voltage collapse”, IEEE Transactions on Power System, Vol. 5, No. 2, pp. 419-425, May 1990.

[32] C. A. Canizares, F. L. Alvarado, C. L. Demarco, I. Dobson and W. F. Long, “Point of collapse methods applied to AC/DC power systems”, IEEE Transactions on Power System, Vol. 7, No. 2, pp. 673-683, May 1992.

[33] C. A. Canizares and F. L. Alvarado, “Point of collapse and continuation methods for large AC/DC systems”, IEEE Transactions on Power System, Vol. 8, No. 1, pp. 1-8, February 1993.

[34] C. Z. De Souza, “Tangent vector applied to voltage collapse and loss sensitivity studies”, Electric Power System Research, Vol. 47, pp. 65-70, 1998.

[35] C. Z. De Souza, “Discussion on some voltage collapse indices”, Electric Power System Research, Vol. 53, pp. 53-58, 2000.

[36] M. H. Haque, “Determination of steady-state voltage stability limit using P-Q curve”, IEEE Power Engineering Review, pp.71-72, April 2002.

[37] M. H. Haque, “Novel method of accessing voltage stability of a power system using stability boundary in P-Q plane, Electric Power System Research, Vol. 64, pp. 35-40, 2003.

[38] K. P. Basu, “Power transfer capability of transmission line limited by voltage stability: simple analytical expressions”, IEEE Power Engineering Review, pp. 46-47, September 2000.

[39] K. Vu, M. M. Begovic, D. Novosel and M. M. Saha, “Use of local measurement to estimate voltage-stability margin”, IEEE Transactions on Power System, Vol. 14, No. 3, pp. 1029-1035, August 1999.

[40] T. J Overbye, “Use of FACTS devices for power system stability enhancement,” Proceedings of the 36th Midwest Symposium on Circuits and Systems, Vol.2, 1993, pp.1019 – 1022.

[41] M. Z. El-Sadek, M. M. Dessouky, G. A. Mahmoud and W. I. Rashed, “Enhancement of steady-state voltage stability by static VAR compensator”, Electric Power System Research, Vol. 43, pp. 179-185, 1997.

[42] C. A. Canizares, E. Uzunovic and J. Reeve and B. K. Johnson, “Transient stability and power flow models of the unified power flow controller for various control strategies,” Technical Report 2004-9, University of Waterloo, Waterloo, March 2004.

[43] A. Del Rosso, C. A. Canizares, V. Quintana and V. Dona, “Stability improvement using TCSC in radial power systems,” Proceedings of the North American Power Symposium (NAPS), Waterloo, ON, October 2000, pp. 12-32 - 12-39.

[44] M. Rahman, M. Ahmed, R. Gutman, R. J. O’Keefe, R. J. Nelson and J. Bian, “UPFC application on the AEP system: planning consideration”, IEEE Transactions on Power System, Vol. 12, No. 4, pp. 1695-1701, November 1997.

[45] E. Uzunovic, C. A. Canizares and J. Reeve, “Fundamental frequency model of unified power flow controller,” Proceedings of the North American Power Symposium (NAPS), Cleveland, Ohio, October 1998, pp. 294-299.

[46] B. T. Ooi, M Kanzerani, R. Marceau, Z. Wolanski, F.D. Galiana, D. McGillis and G. Joos, “Mid-point siting of FACTS device in transmission lines”, IEEE Transactions on Power Delivery, Vol. 12, No. 4, pp. 1717-1722, October 1997.

[47] C. P. Gupta, S. C. Srivastava and R. K. Varma, , “Enhancement of static voltage stability margin with reactive power dispatch using FACTS devices”, 13th PSCC, Trondheim, June 28-July 2, 1999.

[48] N. K. Sharma, R. K. Varma, and A. Ghosh, “Placement strategy for FACTS devices,” 11st National Power Systems Conference, Bangalor, India, December 2000, pp. 57-62.

[49] S. Green, I. Dobson and F. L. Alvarado, “Sensitivity of Loading Margin to Voltage Collapse with respect to Arbitrary Parameters,” IEEE Transactions Power Syst, Vol. 12, No. 1, pp. 262-272, Feb. 1997.

[50] L.C.P. da Silva, Y. Wang, V.F. da Costa and W. Xu, "Assessment of Generator Impact on System Power Transfer Capability Using Modal Participation Factors", IEE Proceedings - Generation, Transmission and Distribution, Vol. 149, Issue 5, pp. 564-570, Sept. 2002.

[51] R. Wang and R. H. Lasseter, "Re-dispatching generation to increase power system security margin and support low voltage bus," IEEE Transactions Power System, Vol. 15, No. 2, pp. 496-501, May 2000.

[52] O. Ekwue, H. B. Wan, D. T. Y. Cheng and Y. H. Song, “Voltage stability analysis on the NGC system”, Electric Power System Research, Vol. 47, pp. 173-180, 1998.

[53] J. G. Calderon-Guizar, G. A. Inda-Ruiz, and G. E. Tovar, "Improving the steady-state loading margin to voltage collapse in the North-West control area of Mexican power system", Electric Power System Research, Vol. 25, pp. 643-649, 2003.

[54] T. V. Cutsem and R. Mailhot, "Validation of a fast voltage stability analysis method on the Hydro-Quebec system", IEEE Transactions on Power System, Vol. 12, No. 1, pp. 282-292, February 1997.

[55] M. Khiat, A. Chaker, A. G. Exposito, J. L. Martinez Ramo, "Reactive power optimization an voltage control in the western Algerian transmission system: a hybrid approach", Electric Power System Research, Vol. 64, pp. 3-10, 2003.

[56] Z. Khan, "A discussion and analysis of the voltage stability problems in Oman", Electric Power System Research, Vol. 49, pp. 31-36, 1999.

[57] Feng and W. Xu, "Fast computation of post-contingency system margins for voltage stability assessment of large-scale power systems", IEE Proceeding-Generation, Transmission , Distribution, Vol. 147, No. 3, pp. 76-80, March 2000.

[58] Z. De Souza, J. C. S. De Souza and A. M. L. De Silva, "On-line voltage stability monitoring", IEEE Transactions on Power Systems, Vol. 15, No. 4, pp. 1300-1305, November 2000.

[59] C. A. Cañizares, et al., UWPFLOW: Continuation and Direct Methods to Locate Fold Bifurcations in AC/DC/FACTS Power Systems, University of Waterloo, available at http://www.power.uwaterloo.ca, Sept. 2004.

[60] Matlab Functions, available at http://www.mathworks.com, June 2004.

[61] A. Sode-Yome, V. Pothiratana and N. Mithulananthan, "Roles of small power producers as part of peak serving scheme," invited paper, Power-Gen Asia 2004, Bangkok, Oct. 5-7, 2004.

[62] W. D. Rosehart, C. A. Canizares, and V. H. Quintana, "Effect of detailed power system models in traditional and voltage-stability-constrained optimal power-flow problems," IEEE Transactions Power System, Vol. 18, No. 1, pp. 27-35, February 2003.

[63] F. Cazals and M. Pouget, "Estimating differential quantities using polynomial fitting of osculating jets", *Proceedings of the Eurographics/ACM SIGGRAPH symposium on Geometry processing*, Aachen, Germany, 2003, pp. 177-187.

APPRENDIX A

IEEE 14-Bus Test System

```
C                14 BUS TEST SYSTEM:
C                    WSCC data file
C
C Case Title (3 A8 lines)
HDG
  14 BUS AC TEST SYSTEM
  WSCC/ETMSP DATA FORMAT
  NOVEMBER 2002
BAS
C
C
C System Data
C
C                          AC BUSES
C
C Bus Input Data:
C - Type (A2) -> "B " -> PQ load bus
C               "BQ" -> PV generator bus with Q limits
C               "BE" -> PV generator bus with no Q limits
C               "BV" -> PQ generator bus with V limits
C               "BG" -> PQ generator bus with Q limits controlling voltage on
C                    a remote PV load bus
C               "BC" -> PV load bus with remote voltage control
C               "BT" -> PQ load bus with voltage controlled by LTC transformer
C               "BS" -> Swing bus
C - Ow (A3)   -> Owner
C - Name (A8) -> Bus Name
C - kV (F4.0) -> Bus kV base
C - Z (2A)    -> Zone
C - PL (F5.0) -> P load in MW
C - QL (F5.0) -> Q load in MVars
C - SHUNT (2F4.0) -> MW and MVars shunts (+ for Capacitors)
C - PM (F4.0) -> Max. generator P power in MW
C - P (F5.0)  -> generator P power in MW
C - QM (F5.0) -> Max. generator Q power in MVars (not needed for "BE"
C               PV bus types)
C - Qm (F5.0) -> Min. generator Q power in MVars (not needed for "BE"
C               PV bus types)
C - Vpu (F4.3)-> PV desired voltage magnitude in p.u. (max. voltage for
C               "BV" PV bus type)
C - Vm (F4.3) -> Min. voltage for "BV" PV bus type.
C - Remote Name (A8) -> Remote controlled bus name for "BG" type bus.
C - Remote kV (F4.0) -> Remote controlled bus kV for "BG" type bus.
C - Remote %Q (I3)   -> Percentage of Q of remote bus control for "BG" type bus.
C
C      1       2       3       4       5       6       7       8
```

```
C 3456789012345678901234567890123456789012345678901234567890123456789012345678901234567890
C                        | SHUNT |                    |REMOTE BUS
C  |Ow|Name   |kV |Z|PL  |QL  |MW |Mva|PM |P   |QM  |Qm  |Vpu|Vm |Name   |kV |%Q
BQ    BUS_1   69.0IE.0000.0000.000.0009999232.6990.0 -9891060   0          0.0
BQ    BUS_2   69.0IE21.7012.70.000.000999940.0050.00-40.01045   0          0.0
BQ    BUS_3   69.0IE94.2019.00.000.0009999.000040.00.00001010   0          0.0
B     BUS_4   69.0IE47.804.000.000.000.0000.0000.0000   0   0          0.0
B     BUS_5   69.0IE7.6001.600.000.000.000.0000.0000.0000   0   0          0.0
BQ    BUS_6   13.8IE11.207.500.000.0009999.000024.00-6.001070   0          0.0
B     BUS_7   13.8IE.0000.0000.000.000.000.0000.0000.0000   0   0          0.0
BQ    BUS_8   18.0IE.0000.0000.000.0009999.000024.00-6.001090   0          0.0
B     BUS_9   13.8IE29.5016.60.000.000.000.0000.0000.0000   0   0          0.0
B     BUS_10  13.8IE9.0005.800.000.000.000.0000.0000.0000   0   0          0.0
B     BUS_11  13.8IE3.5001.800.000.000.000.0000.0000.0000   0   0          0.0
B     BUS_12  13.8IE6.1001.600.000.000.000.0000.0000.0000   0   0          0.0
B     BUS_13  13.8IE13.505.800.000.000.000.0000.0000.0000   0   0          0.0
B     BUS_14  13.8IE14.905.000.000.000.000.0000.0000.0000   0   0          0.0
C
C******************************************************************************
C
C                        AC LINES
C
C Line Input Data:
C - Type (A2)   -> "L "
C - Ow (A3)     -> Owner
C - Name_1 (A8) -> Name of sending bus
C - kV1 (F4.0)  -> kV base for sending bus
C - M (I1)      -> Metered bus for flow interchange
C - Name_2 (A8) -> Name of receiving bus
C - kV2 (F4.0)  -> kV base for receiving bus
C - C (I1)      -> Circuit ID
C - S (I1)      -> Section number
C - In (F4.0)   -> Rated Amps.
C - N (I1)      -> Circuit number
C - R (F6.5)    -> p.u. series R of PI equivalent
C - X (F6.5)    -> p.u. series X of PI equivalent
C - G/2 (F6.5)  -> p.u. shunt G/2 of PI equivalent
C - B/2 (F6.5)  -> p.u. shunt B/2 of PI equivalent
C - Mil (F4.1)  -> Length in miles
C
C       1       2       3       4       5       6       7       8
C 3456789012345678901234567890123456789012345678901234567890123456789012345678901234567890
C                M           CS    N
C  |Ow|Name_1 |kV1||Name_2 |kV2|||In || R   | X   | G/2 | B/2 |Mil|
L     BUS_1   69.01BUS_2   69.011.0001.01938.05917.00000.02640
L     BUS_1   69.01BUS_5   69.011.0001.05403.22304.00000.02460
L     BUS_2   69.01BUS_3   69.011.0001.04699.19797.00000.02190
L     BUS_2   69.01BUS_4   69.011.0001.05811.17632.00000.01870
L     BUS_2   69.01BUS_5   69.011.0001.05695.17388.00000.01700
L     BUS_3   69.01BUS_4   69.011.0001.06701.17103.00000.01730
L     BUS_4   69.01BUS_5   69.011.0001.01335.04211.00000.00640
L     BUS_6   13.81BUS_11  13.811.0001.09498.19890.00000.00000
```

```
L    BUS_6   13.81BUS_12  13.811.0001.12291.25581.00000.00000
L    BUS_6   13.81BUS_13  13.811.0001.06615.13027.00000.00000
L    BUS_7   13.81BUS_8   18.011.0001.00000.17615.00000.00000
L    BUS_7   13.81BUS_9   13.811.0001.00000.11001.00000.00000
L    BUS_9   13.81BUS_10  13.811.0001.03181.08450.00000.00000
L    BUS_9   13.81BUS_14  13.811.0001.12711.27038.00000.00000
L    BUS_10  13.81BUS_11  13.811.0001.08205.19207.00000.00000
L    BUS_12  13.81BUS_13  13.811.0001.22092.19988.00000.00000
L    BUS_13  13.81BUS_14  13.811.0001.17093.34802.00000.00000
C
C*************************************************************************
C
C                       TRANSFORMERS
C
C Transformer Input Data:
C - Type (A2)   -> "T "
C - Ow (A3)     -> Owner
C - Name_1 (A8) -> Name of sending bus
C - kV1 (F4.0)  -> kV base for sending bus
C - M (I1)      -> Metered bus for flow interchange
C - Name_2 (A8) -> Name of receiving bus
C - kV2 (F4.0)  -> kV base for receiving bus
C - C (I1)      -> Circuit ID
C - S (I1)      -> Section number
C - Sn (F4.0)   -> Rated MVA
C - N (I1)      -> Circuit number
C - R (F6.5)    -> p.u. series R of equivalent circuit
C - X (F6.5)    -> p.u. series X of equivalent circuit
C - G (F6.5)    -> p.u. shunt G of equivalent circuit
C - B (F6.5)    -> p.u. shunt B of equivalent circuit
C - Tap1 (F5.2) -> kV tap for sending bus
C - Tap2 (F5.2) -> kV tap for receiving bus
C
C       1       2       3       4       5       6       7       8
C 345678901234567890123456789012345678901234567890123456789012345678901234567890
C             M          CS
C  |Ow|Name_1 |kV1||Name_2 |kV2|||Sn  | R   | X   | G   | B   |Tap1|Tap2|
T    BUS_4   69.01BUS_7   13.811.0001.00000.20912.00000.0000067.4813.80
T    BUS_4   69.01BUS_9   13.811.0001.00000.55618.00000.0000066.8613.80
T    BUS_5   69.01BUS_6   13.811.0001.00000.25202.00000.0000064.3113.80
A  IEEE14    BUS_2   69.0     0.00 IE
ZZ
C
C*************************************************************************
C
C                       SOLUTION CONTROL CARD
C
C Solution control card:
C - Max Iter (I5) -> Maximum number of Newton-Raphson iteration
C - Name (A8)     -> Name of the slack bus
C - kV (F4.0)     -> kV base for slack bus
C - Angle (F10.4) -> Reference angle for slack bus in degrees
```

```
C
C     1       2       3       4       5       6       7       8
C 345678901234567890123456789012345678901234567890123456789012345678901234567890
C                 |Max|  |SLACK BUS |
C                 |Itr|  |Name   |kV|   |Angle    |
SOL1                  20  BUS_1   69.0      0.0000    1.1000    1    1.00
IND
END
```

APPENDIX B

FACTS CONTROLLER DATA

SVC Data

X_c *(p.u.)*	X_l *(p.u.)*	α_{min} *(deg.)*	α_{max} *(deg.)*	Slope *(%)*	S *(MVA)*	*kV*
1.1708	*0.4925*	*90*	*175*	*2*	*150*	*26*

STATCOM Data

R_c *(p.u.)*	R *(p.u.)*	X *(p.u.)*	S *(MVA)*	k	X_{sl} *(%)*
0.0017	*0*	*0.145*	*150*	*0.9*	*2*

TCSC Data

X_c *(p.u.)*	X_l *(p.u.)*	α_{min} *(deg.)*	α_{max} *(deg.)*	S *(MVA)*
10% of X_l	*50% of the line*	*144*	*175*	*100*

SSSC Data

R_c *(p.u.)*	R *(p.u.)*	X *(p.u.)*	S *(MVA)*	k
0.0017	*0*	*0.145*	*100*	*0.9*

UPFC Data

Shunt Part

R_c *(p.u.)*	R *(p.u.)*	X *(p.u.)*	S *(MVA)*	k	X_{sl} *(%)*
0.0017	*0*	*0.145*	*150*	*0.9*	*2*

Series Part

R_c *(p.u.)*	R *(p.u.)*	X *(p.u.)*	S *(MVA)*	k
0.0017	*0*	*0.145*	*100*	*0.9*

APPREDIX C

Author's Publication

International Conference

A. Sode-Yome and K. Y. Lee, "Applications of MATLAB Symbolic and Optimization Toolboxes in Static Voltage Stability in Power Systems", *IFAC Symposium on Power Plants and Power Systems Control*, Tampere, Finland, July 5-8, 2009.

A. Sode-Yome and K. Y. Lee, "Approximate Loading Margin Methods Using Artificial Neural Networks in Power Systems", *The 15th International Conference on Intelligent System Applications to Power Systems*, Curitiba, Brazil, Nov. 8-12, 2009 (Available at www.isap-power.org/PDFs/Paper_127.pdf).

Internation Journal

Rakibuzzaman Shah, Nadarajah Mithulananthan, Arthit Sode-Yome, and Kwang.Y.Lee, "Investigation of the Impact of Large-Scale PV on Power System Oscillatory Stability", *IEEE Transactions on Sustainable Energy*, under review, submitted in Sep 2010.

PREPRINTS

EDITOR: *Krjö Majanne, Tampere University of Technology*

IFAC

IFAC Symposium on PP&PS

Power Plants and Power Systems Control

5–8 July 2009, Tampere Hall, Finland

Sponsored by
IFAC TC on Power Plants and Power Systems

Co-sponsored by
IFAC TCs on Chemical Process Control, Safeprocess, Modelling & Control of Environmental Systems

Other Co-Sponsors TAMPERE UNIVERSITY OF TECHNOLOGY

Supported by
Academy of Finland • Areva T&D • Metso Automation • Metso Power • OSKE The Centre of Expertise Programme (OSKE) • Pöyry Energy • The City of Tampere

Organised by **Finnish Society of Automation**

Applications of MATLAB Symbolic and Optimization Toolboxes in Static Voltage Stability in Power Systems

Arthit Sode-Yome*. Kwang Y. Lee**

**Graduate Shool of Engineering, Siam University, Bangkok 10163 Thailand*
(e-mail: arthit@ieee.org).
***Department of Electrical & Computer Engineering, Baylor University, Waco, TX 76798-7356*
(e-mail:Kwang_Y_Lee@baylor.edu)

Abstract: This paper presents a simple simulation approach to study static voltage stability in power systems. Symbolic and Optimization toolboxes in MATLAB are used to simulate load flow, continuation power flow and optimization technique in static voltage stability study. Flexible AC Transmission System devices including SVC, TCSC, STATCOM, SSSC and UPFC are used to validate the proposed technique. Various voltage stability parameters including PV curves, loading margin and simulation times are investigated. Three-bus and IEEE fourteen-bus test systems are used to demonstrate the proposed technique. The proposed approach may be of interest to utilities and researchers who wish to study voltage stability of medium size power systems in a simple way.

Keywords: Symbolic toolbox, Optimization toolbox, static voltage stability, MATLAB, FACTS.

1. INTRODUCTION

Modern electric power utilities are facing many challenges due to ever-increasing complexity in their operation and structure. In the recent years, one of the problems that receive wide attention is the voltage instability. With an open-access market, poorly scheduled generation for the competitive bidding is one of many reasons for voltage instability problem in the deregulated electricity environment. Thus, in order to relieve or at least minimize the system from the voltage instability problem, many electric utilities and researchers have devoted a great deal of efforts in system studies related to static voltage stability.

In static voltage stability study, Continuation Power Flow (CPF) and optimization methods are the main analysis techniques that are used to find voltage stability margin or loading margin (LM) of the system (Sode-Yome, *at al.,* 2004, 2006). Based on these techniques, utilities and researchers may require developing and devoting a great deal of effort to create a program. Adding to this, they may face a difficulty to ensure the correct answers. Moreover, with the use of Flexible AC Transmission system (FACTS) to enhance static voltage stability, simulation effort may be increased.

According to above observation, attention is drawn in this paper to propose a new simulation approach for voltage stability study using Symbolic and Optimization toolboxes in MATLAB. The paper simulates load flow, CPF and optimization technique in static voltage stability study. The proposed technique is applied to system with FACTS devices. Moreover, simulation times are studied and compared in test systems. This may be useful for utilities to find voltage stability assessment of medium-size power systems without devoting a great deal of effort.

Rest of the paper is organized as follows: Section 2 presents static voltage stability. FACTS devices are introduced in Section 3. A new simulation approach is proposed in Section 4 for load flow, CPF and optimization technique. Test systems and analysis tools are briefly stated in Section 5. In Section 6, numerical results are presented. Finally, in Section 7, major contributions and conclusions are presented.

2. STATIC VOLTAGE STABILITY

Voltage stability is the ability of power system to maintain adequate voltage magnitude so that when the system nominal load is increased, the actual power transferred to that load will increase (IEEE/PES Power System Stability Subcommittee, 2003). It is mainly associated with reactive power imbalance. Slowly developing changes in the power system occur that eventually lead to a shortage of reactive power and, hence, declining voltage. Maximum load that the system can be supplied before entering to the collapse point is called loading margin (LM) or static voltage stability margin of the system. Continuation Power Flow and optimization technique (or direct) methods are two analysis techniques used for voltage stability study.

2.1 Continuation Power Flow Method

Continuation Power Flow (CPF) presents a way to plot complete PV curves by automatically changing the value of Loading Factor (LF or λ). It involves predictor and corrector

steps to guarantee a well behaved numerical solution of the related equations.

2.2 Optimization Technique Method

Static voltage stability study can be carried out by formulating the problem as an optimization problem. Thus, distance to collapse can be maximized as follows:

Minimize $-\lambda$

subject to $F(z,\lambda) = 0$

where F are load flow equations with state variables z. Necessary conditions are used to find state variables including bus angles, bus voltages and loading margin. Other power system limits such as voltage, thermal and generator limits can be easily introduced as inequality constraints.

The CPF method is the promising approach, since it is based on power flow calculation and provides completed PV curves as well as voltages at every bus at various loading factors. It can be used as an indicator to detect the proximity to voltage collapse and the weakest bus of the system. Optimization technique provides a more accurate solution and it is able to handle power system constraints in a simple way. However, it gives only the solution at the optimal point, which may not be useful in the operation of an intermediate loading point, between base case and collapse point.

Although CPF and optimization methods are promising methods, it may not be easy for utilities to implement. Moreover, if the FACTS devices are used in the power system, it may make the study more complicated. In the following section, FACTS devices are introduced. Then, a simple approach based on Symbolic and Optimization toolboxes is proposed for finding the solutions for load flow, CPF and optimization technique methods in a simple way.

3. FLEXIBLE AC TRANSMISSION SYSTEM DEVICES

The development of FACTS devices in power transmission system has led to many applications of these controllers not only improve various stability issues but also provide operating flexibility to power systems. There are various types of FACTS devices available for this purpose, namely, Static Var Compensator (SVC), Static Synchronous Compensator (STATCOM), Thyristor-Controlled Series Capacitor (TCSC), Static Synchronous Series Compensator (SSSC) and Unified Power Flow Controller (UPFC). In the following subsections, concept of these well-known FACTS devices is presented.

3.1 SVC

The SVC is a shunt connected static Var generator/load whose output is adjusted to exchange capacitive or inductive current so as to maintain or control specific power system variables. It is similar to a synchronous condenser in that it is used to supply or absorb reactive power but without rotating part. It contains the equivalent of automatic voltage regulator system to set and maintain a target voltage level.

3.2 STATCOM

The STATCOM is the voltage-source converter, which converts a DC input voltage into AC output voltage in order to compensate the active and reactive needed by the system. It could be viewed as superior to SVC, as STATCOM provides better terminal characteristics compared to diminishing characteristics at low terminal voltages by SVC.

3.3 TCSC

The TCSC controllers use Thyristor Control Reactor (TCR) in parallel with segments of series capacitor bank. The combination of TCR and capacitor allow the capacitive reactance to be smoothly controlled over a wide range and switched upon command to a condition where the bi-directional thyristor pairs conduct continuously and insert appropriate reactance into the line. The total susceptance of the line is controlled by controlling the firing angle of the thyristor.

3.4 SSSC

The SSSC can be used for series compensation of transmission lines. It is similar to the STATCOM, as it is based on a DC capacitor fed Voltage Source Inverter (VSI) that generates a three-phase voltage at fundamental frequency, which is then injected in a transmission line through a transformer connected in series with line.

3.5 UPFC

The UPFC consists of two identical voltage-source inverters, namely shunt inverter and series inverter which operate via a common DC link with a DC storage capacitor, allow UPFC to independently control active and reactive power flows on the line as well as the bus voltage. Active power can freely flow in either direction between the AC terminals of the two inverters through the DC link.

Appropriate model including AC and DC equations of FACTS devices can be incorporated in static voltage stability study by adding FACTS equations in the load flow equations.

4. PROPOSED SIMULATION APPROACH

The proposed simulation approach is applied to load flow, CPF and optimization techniques. Load flow is simulated first. Then, the method is applied to the CPF and optimization process.

4.1 Load Flow

Power flow or load flow consists of solving real and reactive power balance equations of all buses in power systems to obtain all state variables when control variables are specified. According to this, Symbolic toolbox in MATLAB can be used to create power flow equations when the system data and control variables are known. Then, a simple command called “lsqnonlin” in Optimization toolbox is used to find the

solution for all state variables. The steps behind the proposed method can be summarized as shown in the Fig. 1.

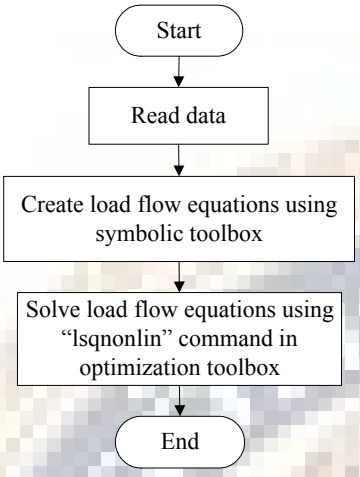

Fig. 1 Load flow calculation using Symbolic and Optimization toolboxes.

From Fig. 1, system parameters are read from input data to create power balance equations using Symbolic toolbox. The solution is then found by using a single "lsqnonlin" command. It can be noticed that Jacobian is not required to compute in the formulation process since it is already embedded in Optimization toolbox. The solution is found in a simple way, as only one command is used.

4.2 Continuation Power Flow

Continuation Power Flow is basically a series of load flow calculation with predictor and corrector steps. The formation of CPF is complicated and it requires good programming skill. However, with the help of Symbolic and Optimization toolboxes, the formulation is much easier. Figure 2 illustrates steps behind the CPF process with Symbolic and Optimization toolboxes. From Fig. 2, the system data is read first, then Symbolic toolbox is introduced to create power flow equations. The power flow calculation is performed to find the load flow Jacobian for the following predictor step.

In the predictor step, state variables are predicted from the current status of load flow Jacobian to predict the bus angles and voltages at higher LF. In the corrector step, the actual value of state variables are computed from load flow equations and initial condition obtained from the predictor step. Prior to the collapse point, parameterization step is performed to avoid convergence difficulty of CPF process by switching state variable from LF to the voltage at the weakest bus, which is found from a bus having highest voltage decrease. The process is repeated until the PV curve is completed. For simplicity, in the paper, parameterization is introduced after the last LF that allows load flow solution to converge.

4.3 Optimization Technique

Optimization technique can be solved with the help of Symbolic and Optimization toolboxes as well. Fig. 3 shows various steps of optimization technique including reading input data, creating power flow equations, creating necessary conditions and solving necessary conditions for optimal solutions. From the proposed method, Lagrangian function and necessary conditions are automatically created by using Symbolic toolbox. The optimal solution is then found from the necessary conditions by using a single command, "lsqnonlin".

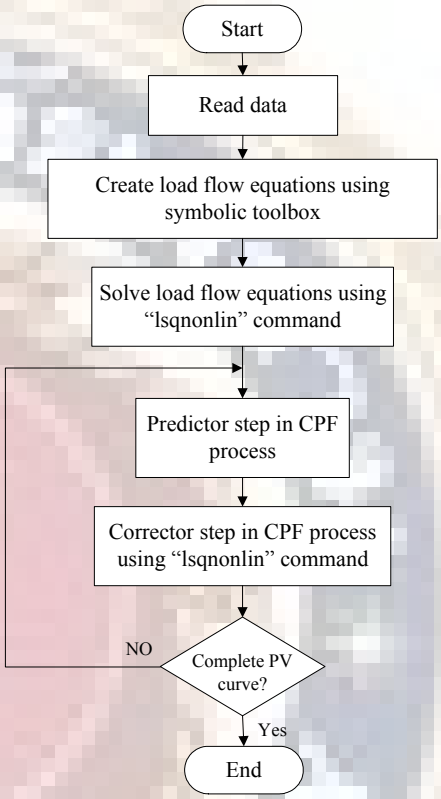

Fig. 2 CPF using Symbolic and Optimization Toolboxes.

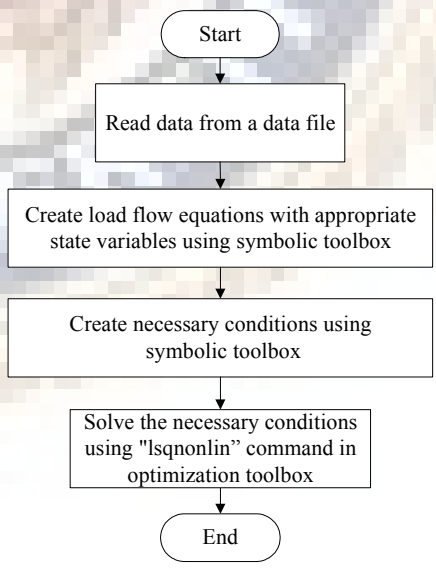

Fig. 3 Optimization technique using Symbolic and Optimization Toolboxes.

FACTS devices are applied in the process by adding equations including AC and DC representation in load flow equation. The proposed simulation method is validated in two test systems. In the following section, these test systems along with analysis tools are presented.

5. TEST SYSTEMS AND ANALYSIS TOOLS

The simple 3-bus test system and the modified IEEE 14-bus test systems are used to validate the proposed approach. Single line diagrams of the 3-bus and modified IEEE 14-bus test systems are illustrated in Figs. 4 and 5, respectively. The modification from the original IEEE 14-bus test system is that generators located at buses 6 and 8 were changed from synchronous compensators to generators.

The developed tool is tested and validated with the help of a standard CPF program, UWPFLOW. UWPLOW is a research tool that has been designed to calculate maximum loading margin of the power system.

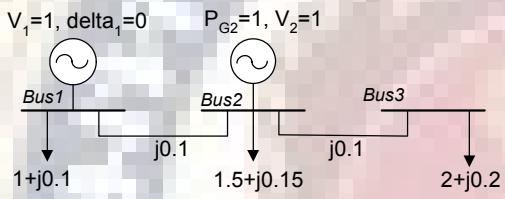

Fig. 4 Single line diagram of the 3-bus system.

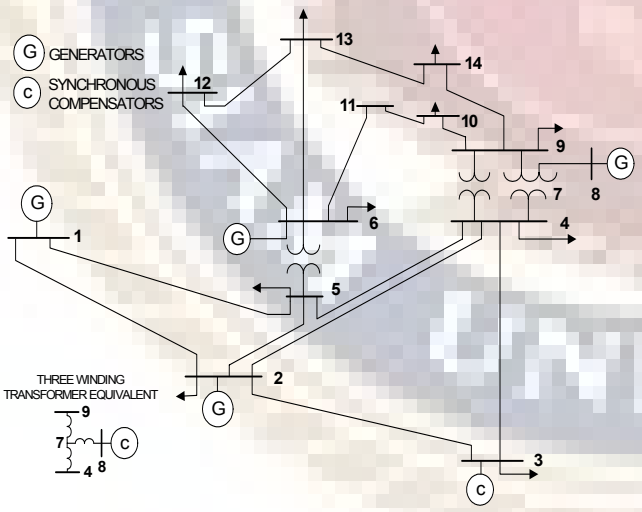

Fig. 5 Single line diagram of the modified IEEE 14-bus system.

6. NUMERICAL RESULTS

The proposed simulation approach is simulated for load flow, CPF and Optimization techniques. Load flow is tested in the first step, as it is the first part of CPF process. Optimization method is tested in the last step in order to compare the result with that of CPF method. Finally, FACTS devices are applied in the modified IEEE 14-bus test system.

6.1 Load Flow

a) The Three-bus Test System

In order to solve power flow equation in a simple way, state variables are selected to be equal to two times number of buses plus 1. The last state variable is LF, which is introduced in the load flow for CPF in the following step. In the three-bus test system, there are 7 state variables: 3 for bus angles, 3 for bus voltages and 1 for LF, which is zero for load flow. After reading the input data, Symbolic toolbox is introduced to create the following power flow equations:

$$\delta_1 = 0$$
$$P_{G2} - (1+\lambda)P_{D2} - 10V_2V_1\sin(\delta_2 - \delta_1) - 10V_2V_3\sin(\delta_2 - \delta_3) = 0$$
$$-(1+\lambda)P_{D3} - 10V_3V_2\sin(\delta_3 - \delta_2) = 0$$
$$V_1 = 1$$
$$V_2 = 1$$
$$-(1+\lambda)Q_{D3} + 10V_3V_2\cos(\delta_3 - \delta_2) - 10V_3^2 = 0$$
$$\lambda = 0$$

From the above equations, there are 7 equations with 7 state variables. State variables namely angle at bus 1, voltages at bus 1 and 2, and LF are control variables as they are specified. A single MATLAB command "lsqnonlin" is then used to obtain the solution in a simple way. The solution of load flow is therefore $x = [\delta_1, \delta_2, \delta_3, V_1, V_2, V_3, \lambda]^T$=[0.0000, -0.2527, -0.4632, 1.0000, 1.0000, 0.9570, 0.0000]^T.

b) The Modified IEEE 14-bus Test System

In the 14-bus test system, there are 28+1 state variables: 14 for bus angles, 14 for bus voltages and 1 for LF. There are 28 equations, which are created by using Symbolic toolbox. The solution is then found from the help of "lsqnonlin" command in Optimization toolbox. The solution of load flow is, therefore,

[0.0000, -0.0437, -0.1563, -0.0988, -0.0808, -0.1017, -0.0876, -0.0307, -0.1188, -0.1201,-0.1127, 0.1159, -0.1172, -0.1343, 1.0600, 1.0750, 1.0612, 1.0600, 1.0603, 1.1246, 1.0956, 1.1312, 1.0813, 1.0816, 1.0993, 1.1084, 1.1015, 1.0727, 0.0000] for state variables $[\delta_1, \ldots, \delta_{14}, V_1, \ldots, V_{14}, \lambda]$.

Load flow solution is used in CPF process, which is presented in the next subsection.

6.2 Continuation Power Flow

a) The Three-bus Test System

Jacobian of the first load flow is used in the predictor step to predict state variables for the next LF. At the next LF and predicted state variables, the corrected state variables can be found in the corrector step. When the load flow solution is diverged, parameterization step is activated at the last converged LF.

PV curves of the test systems based on CPF with the help of Symbolic and Optimization toolboxes are shown in Fig. 6. From PV curve, LM of the system is 1.2625 p.u. Numerical results of all state variables during predictor, corrector and parameterization steps are tabulated in Tables 1 and 2. In this study, step sizes of LF in the predictor step and voltage in parameterization step are specified at 0.1 and 0.02 p.u., respectively. These values are important and they should be carefully selected.

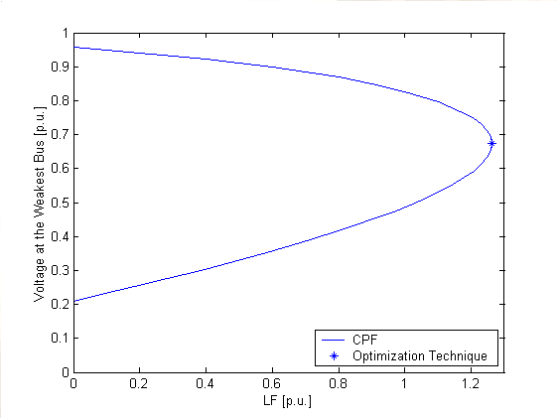

Fig. 6 PV curve of three bus test system.

Table 1 State Variables during Corrector and Parameterization Steps at some LFs of the Three-bus System

	Corrector Steps			Parameterization	
δ_1	0.0000	0.0000	0.0000	0.0000	0.0000
δ_2	-0.2527	-0.2890	-0.7342	-0.7478	-0.7571
δ_3	-0.4632	-0.5228	-1.3580	-1.4012	-1.4392
V_1	1.0000	1.0000	1.0000	1.0000	1.0000
V_2	1.0000	1.0000	1.0000	1.0000	1.0000
V_3	0.9570	0.9496	0.7532	0.7332	0.7132
λ	-0.0000	0.1000	1.2000	1.2286	1.2481

Table 2 State Variables during Predictor Step at some LFs of the Three-bus System

	Predictor Step				
δ_1	0.0000	0.0000	0.0000	0.0000	0.0000
δ_2	-0.2888	-0.3255	-0.3627	-0.4004	-0.4386
δ_3	-0.5223	-0.5829	-0.6448	-0.7082	-0.7734
V_1	1.0000	1.0000	1.0000	1.0000	1.0000
V_2	1.0000	1.0000	1.0000	1.0000	1.0000
V_3	0.9500	0.9419	0.9329	0.9230	0.9119
λ	0.1000	0.2000	0.3000	0.4000	0.5000

b) The Modified IEEE 14-bus Test System

The proposed simulation approach is tested in the modified IEEE 14-bus test system. PV curve at the weakest bus of the system is illustrated in Fig. 7. From Fig. 7, LM of the system is 0.9278 p.u.

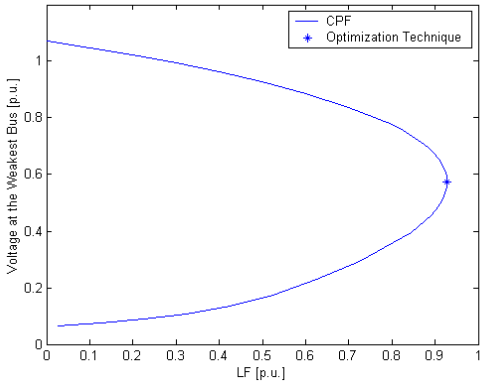

Fig. 7 PV curve of 14-bus test system.

Optimization Technique

a) The Three-bus Test System

Symbolic and Optimization toolboxes can be used to find loading margin of the system based on optimization technique. All state variables and LM at the collapse point of the 3-bus test systems are $x = [\delta_1, \delta_2, \delta_3, V_1, V_2, V_3, \lambda]^T = [0.0000, -0.6334, -1.3689, 1.0000, 1.0000, 0.6744, 1.2625]^T$.. The result is compared with CPF in Fig. 6. From Fig. 6, it is noticed that optimization technique provides only single solution, the maximum point. CPF, on the other hand, provides a complete PV curve and voltages at various loading factors. Moreover, CPF can provide the information about the weakest location in the system.

b) The Modified IEEE 14-bus Test System

Symbolic and Optimization toolboxes is further applied to the modified IEEE 14-bus test system. LM of the system is 0.9278 p.u. and the voltage at the weakest bus, bus 14, is 0.5749 p.u. The LM obtained from the optimization technique is plotted with the complete PV curve obtained from CPF method in Fig. 7. Again, the optimization technique provides only single solution, the maximum solution.

The necessary equation of the optimization process is shown as follows:

$$\delta_1 = 0$$
$$P_{G2} - (1+\lambda) P_{D2} + 10V_1V_2 \sin(\delta_1 - \delta_2) - 10V_2V_3 \sin(\delta_2 - \delta_3) = 0$$
$$-(1+\lambda) P_{D3} + 10V_2V_3 \sin(\delta_2 - \delta_3) = 0$$
$$V_1 = 1$$
$$V_2 = 1$$
$$-(1+\lambda) Q_{D3} + 10V_2V_3 \cos(\delta_2 - \delta_3) - 10V_3^2 = 0$$
$$w_1 + 10w_2V_1V_2 \cos(\delta_1 - \delta_2) = 0$$
$$w_2\left[-10V_1V_2 \cos(\delta_1 - \delta_2) - 10V_2V_3 \cos(\delta_2 - \delta_3)\right]$$
$$+10w_3V_2V_3 \cos(\delta_2 - \delta_3) - 10w_6V_2V_3 \sin(\delta_2 - \delta_3) = 0$$
$$10w_2V_2V_3 \cos(\delta_2 - \delta_3) - 10w_3V_2V_3 \cos(\delta_2 - \delta_3)$$
$$+10w_6V_2V_3 \sin(\delta_2 - \delta_3) = 0$$
$$10w_2V_2 \sin(\delta_1 - \delta_2) + w_4 = 0$$
$$w_2\left[10V_1 \sin(\delta_1 - \delta_2)\right] - 10V_3 \sin(\delta_2 - \delta_3)$$
$$+10w_3V_3 \sin(\delta_2 - \delta_3) + w5 + 10w_6V_3 \cos(\delta_2 - \delta_3) = 0$$
$$-10w_2V_2 \sin(\delta_2 - \delta_3) + 10w_3V_2 \sin(\delta_2 - \delta_3)$$
$$+w_6\left[10V_2 \cos(\delta_2 - \delta_3) - 20V_3\right] = 0$$
$$-1 - 1.5w_2 - 2w_3 - w_6Q_{D3} = 0$$

6.3 Simulation Times

Simulation times used to simulate load flow, CPF and optimization technique are shown in Table 3 for the test systems. From Table, it can be observed that the proposed approach takes about 6 and 32 seconds to find the load flow solutions for the 3-bus and 14-bus test systems, respectively. The proposed approach uses about 2 and 17 minutes to plot complete PV curves based on CPF process. Simulation time for optimization technique is close to that of load flow in the test systems. It is noticed that the proposed approach is simulated by using AMD 1.3 MHz notebook computer.

Table 3. Simulation time for the test systems

Case	Simulation Time for	
	Three Bus	Fourteen Bus
Load Flow	5.588 sec	32.056
CPF	2 min 0.634 sec	17 min 6.353 sec
Optimization	6.349 sec	26.478 sec

6.4 Voltage Stability with FACTS Devices

Voltage stability with various FACTS controllers are compared in the same system. Figure 8 shows PV curves of base case and system with FACTS devices for the modified IEEE 14-bus test system. From the figure, UPFC gives the highest LM improvement followed by shunt and series FACTS devices. The IEEE 14-bus test system requires reactive power compensation at the distribution level, thus installing shunt reactive devices could provide higher LM than series devices. On the other hand, UPFC is composed of both shunt and series devices. Introducing UPFC can provide reactive power both at the distribution level and at the line, thus making the device the most effective one in the terms of LM improvement in this test system.

From the simulation results, it may be concluded that the proposed method can be used to investigate voltage stability in an easy way. Simulation time used to find the solution is acceptable, less than 20 minutes for the whole process in the test system, not too high for the system study. However, it may be too long for some large systems. This may be useful for utilities, researchers and students to do simulation on voltage stability study of the small systems in an easy way.

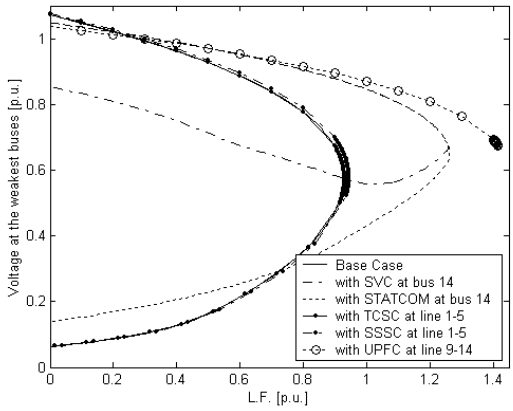

Fig. 8 PV curves of base case, and with FACTS devices.

6. CONCLUSIONS

This paper proposes a new simulation approach for static voltage stability study based on Symbolic and Optimization toolboxes. Load flow, CPF and optimization techniques are used to analyze the static voltage stability study based on the proposed technique. Equations are created by using Symbolic toolbox and the solutions can be found by using a single command in Optimization toolbox. The proposed method is applied in the power system with FACTS devices. The simulation time is acceptable, not too high. This may be useful for utilities or researchers to find voltage stability assessment of medium size power systems in a simple way.

ACKNOWLEDGEMENT

This paper is supported by Commission on Higher Education of Thailand, Thailand Research Fund under grant MRG5080412.

REFERENCES

Sode-Yome A., and Mithulananthan N. (2004). Comparison of shunt capacitor, SVC and STATCOM in static voltage stability margin enhancement. *IJEEE*, Vol. 41, No. 3. pp.158-171.

Sode-Yome A., Mithulananthan N., and Lee K. Y. (2006). A Maximum Loading Margin Method for Static Voltage Stability in Power Systems. *IEEE Trans. Power Syst.*, Vol. 21, pp. 799-808.

Blackout of 2003: Description and Responses, Available: http://www.pserc.wisc.edu/.

IEEE/PES Power System Stability Subcommittee, *Voltage Stability Assessment:* Concepts, *Practices and Tools*, special publication, final draft, Aug. 2003.

Lee, B. H. and K. Y. Lee (1993). "Dynamic and Static Voltage *Stability* Enhancement of Power Systems," *IEEE Transactions on Power Systems*, Vol. 8, No. 1, pp. 231-238.

Approximate Loading Margin Methods Using Artificial Neural Networks in Power Systems

Arthit Sode-Yome, *Member, IEEE* and Kwang Y. Lee, *Fellow, IEEE*

***Abstract*—This paper proposes approximate loading margin methods using Artificial Neural Networks (NN) for static voltage stability in power systems. Two methodologies, namely Actual LM with NN (ALM-NN) and Maximum Loading Margin with NN (MLM-NN), are proposed for finding NN training data sets. Artificial Neural Network is used to approximate the loading margin at particular generation direction. The proposed methods are validated and compared with the Maximum Loading Margin method in the modified IEEE 14-bus test system. The methods will help system operators to approximate voltage stability margin or loading margin of the system in a short period of time.**

***Index Terms*—Loading margin, maximum loading margin method, neural networks, generation direction.**

I. Introduction

Voltage instability has been a major concern in power systems, especially in planning and operation, as there have been several major power interruptions associated with this phenomenon, in the past [1]-[2]. Voltage instability due to the lack of the ability to foresee the impact of contingencies is one of the main reasons for the worst North American power interruptions on August 14th, 2003 [2]. Hence, many electric power utilities have been devoting a great deal of efforts in voltage stability assessment and margin enhancement.

Major contributory factors to voltage instability are power system configuration, generation pattern and load pattern [1], [3]-[6]. Generation pattern is easier to control by system operators compared to other factors, as long as there is enough margin left in the generators [4]-[5]. Conventionally, in typical voltage stability studies, generation of participating generators are raised at the same rate or predefined rate. Increasing generation at this rate may not lead to highest voltage stability margin.

Maximum Loading Margin (MLM) approach, which provides the maximum Loading Margin (LM) or static voltage stability margin is proposed in reference [5]. An approximate and simple model representing the relationship between the generation direction (GD) and the loading margin is used to obtain the maximum loading-margin point. Although, MLM method can provide maximum LM in the generation direction space, it approximate LM based on curve fitting methods. In addition, reactive power of all generators except the swing generator is at the limits for all cases at the LM point [5]. Alternatively, one may be interested in approximating the LM directly from the actual LM with corresponding generation direction from exhaustive simulation. This can be done by using a heuristic approach such as Artificial Neural Networks (NN) [7].

Based on the above observation, attention drawn in this paper is to propose a simple simulation approach that provides an approximation of LM in the generation direction space using Artificial Neural Networks. If the LMs at various generation directions are trained using Neural Networks, operator can approximate LM of the system at a particular generation direction in a fast and simple way. It may be useful in the real-time Energy Management System at the load dispatching center or System Operator.

The rest of the paper is organized as follows: Section II presents static voltage stability. Existing Generation Direction methods are summarized in Section III. New simulation approaches are proposed in Section IV. In Section V, numerical results are presented. Finally, in Section VI, major contributions and conclusions are given.

II. Static Voltage Stability

Voltage stability is the ability of power system to maintain adequate voltage magnitude so that when the system nominal load is increased, the actual power transferred to that load will increase [1]. It is mainly associated with reactive power imbalance. In static voltage stability study, Continuation Power Flow (CPF) and optimization methods are the main analysis techniques that are used to find voltage stability margin or loading margin of the system [1], [4]-[6], [8].

Major contributory factors to voltage instability are power system configuration, generation pattern, and load pattern. The generation pattern is easier to control by system operators compared to load pattern. Customarily, the generation of each participating generator is raised at the same rate, at a pre-defined rate, or according to their spinning reserves. In the following section, existing methods of generation directions are summarized.

III. Generation Direction

Generation pattern or “direction” is defined as the portions of generation increase in each participating generator to serve

This work was supported by Thailand Research Fund, office of the higher Education Commission of Thailand and the Siam University, Thailand under grant No. MRG5080412.

A. Sode-Yome is with Siam University, Bangkok, Thailand (e-mail: arthit@ieee.org).

K. Y. Lee is with Department of Electrical & Computer Engineering, Baylor University, Waco, TX 76798-7356, USA (e-mail: Kwang_Y_Lee@baylor.edu).

the desired load increase and losses in the system. Let K_{Gi} be the factor for active power increase at generator i and $P_{Gi,o}$ be the generation at the base case, then, the generation P_{Gi} at a higher loading point can be written as

$$P_{Gi} = P_{Gi,o}\left(1+K_{Gi}\right) \tag{1}$$

where i = 1, 2, …n, for all participating generators.

The factor K_{Gi} can be viewed as the generation direction (GD_i) and is very crucial to voltage stability. Generation Direction can be worked out by finding the slope of generation increase for individual generator. Existing methods to identify generation directions in voltage stability study are summarized below.

A. Conventional Approach

Conventionally, the generation for a system is increased by fixed percentage as pre-specified in the planning stage, e.g., according to the spinning reserve [1], [4]. The power generation of generator i after the load increase can be written as

$$P_{Gi} = P_{Gi,o}\left(1+K_{Gi}\right) = P_{Gi,o} + \Delta P_{Gi} \tag{2}$$

and

$$\sum_{NG} \Delta P_{Gi} = \Delta P_D + \Delta P_{loss} \tag{3}$$

where

P_{Gi} is the power generation of generator i,
$P_{Gi,o}$ is the generation of generator i at base load,
ΔP_{Gi} is the increase of power generation at generator i,
ΔP_D is the total load increase,
ΔP_{Loss} is the total loss increase,
NG is the number of generators.

B. Optimal Power Flow Approach

Traditional Optimal Power Flow (OPF) can be formulated to include voltage stability criteria as follows [8]:

Minimize
$$C\left(P_{Gi}\right) = \sum_{NG}\left(a_{Gi}P_{Gi}^2 + b_{Gi}P_{Gi} + c_{Gi}\right) \tag{4}$$

subject to

$$P_{Gi} - \left(1+\lambda\right)P_{Di,o} - \sum_{j=1}^{n}|U_i||U_j|\left(G_{ij}\cos\delta_{ij} + B_{ij}\sin\delta_{ij}\right) = 0 \tag{5}$$

$$Q_{Gi} - \left(1+\lambda\right)Q_{Di,o} - \sum_{j=1}^{n}|U_i||U_j|\left(G_{ij}\sin\delta_{ij} - B_{ij}\cos\delta_{ij}\right) = 0 \tag{6}$$

$$\left|P_{Gi}\right|_{\min} \le \left|P_{Gi}\right| \le \left|P_{Gi}\right|_{\max} \tag{7}$$

$$\left|U_i\right|_{\min} \le \left|U_i\right| \le \left|U_i\right|_{\max} \tag{8}$$

$$S_{ij} = \sqrt{P_{ij}^2 + Q_{ij}^2} \le S_{ij,\max} \tag{9}$$

Where

C is total operating cost of the system,
a_{Gi}, b_{Gi}, c_{Gi} are cost coefficients of generator i,
λ is load incremental parameter or loading factor (L.F.),
P_{Gi}, Q_{Gi} are real and reactive power generation at bus i,
$P_{Di,o}$, $Q_{Di,o}$ are real and reactive power demand at bus i at base load,
n is number of buses in the system,
$|P_{Gi}|_{min}$, $|P_{Gi}|_{max}$ are lower and upper power limits of generator i,
$|U_i|_{min}$, $|U_i|_{max}$ are lower and upper limits of voltage magnitude at bus i,
P_{ij} , $Q_{ij,}$, S_{ij} are the real, reactive and apparent power in line ij,
$S_{ij,max}$ is the MVA (Thermal) limit of line ij.

Generation direction, in this approach, can be worked out by subtracting the new dispatch from the old dispatch for individual generators.

C. Cost Participation Factor Approach

Cost participation factor is viewed as the easiest method to identify amount of power generation with economic load dispatch consideration. It is calculated based on generators' incremental cost [8]:

$$\Delta P_{Gi} = \frac{\left(1/C_i^{''}\right)}{\sum_{j=1}^{NG}\left(1/C_j^{''}\right)}\Delta P_D \tag{10}$$

where

C_i is the cost function of generator i,
$C_i^{''}$ is the second derivative of the cost function i,
ΔP_{Gi} is the increase in power generation for generator i,
ΔP_D is the total load increase.

Among the existing methods, very few of them can provide the highest LM of the system. Hence, in the following section, the Maximum Loading Margin method is presented to maximize the LM by searching in the "generation direction space."

D. Maximum Loading Margin Method

The MLM method identifies a vector of the GDs of generators that gives maximum LM by approximating the surface of the LM as a function of the generation directions. If one can approximate the LM surface as a function of all generation direction variables (K_{Gi}), optimization technique can be used to provide the highest LM point. Mathematically, the method can be formulated as follows:

$$LM = B_0 + \sum\left(\sum_{p=1}^{n} B_{i,p}K_{Gi}^{p}\right) \tag{11}$$

subject to

$$\sum_{i=1}^{NG} K_{Gi} = 1 \tag{12}$$

$$0 \le K_{Gi} \le 1 \tag{13}$$

where K_{Gi} is the generation direction for generator i, $B_{i,p}$ are the coefficients terms, B_o is a constant term, p is the power term and n is the number of terms of the polynomial

approximation. If generation is increased according to this direction, the system will have the maximum loading margin.

The MLM method provides a good approximation of the GD, which would give the maximum LM for a given case. Since LM surface may have multiple maximum, as it can be approximated by polynomial equations, MLM method may be required to find the global maximum.

E. Other Existing Methods

Linear and quadratic estimates of the LM with respect to system parameters, including power generation, are computed by using sensitivity method to locally predict the new location of the maximum loading margin points [9].

From the existing methods, only MLM method can provide maximum loading margin in the generation direction space. This method requires an approximated LM surface equation based on the two-dimensional LM curves in each generation direction. This may be useful when one would like to find the maximum LM point based on an optimization technique.

At the load dispatching center or System operator, however, one may be interested in finding the LM of the system in a short period of time when some generation directions are considered. Instead of approximating LM in an equation as proposed in the MLM method, one may suggest to use some heuristic methods such as Artificial Neural Networks to approximate the LM surface. In the following, new LM approximation methods are proposed based on the actual LM, MLM method and Neural Networks.

IV. Proposed Methodologies

A. Artificial Neural Networks [7]

Neural network is a collection of interconnected neurons that incrementally learn from their data to capture essential linear and nonlinear trends in complex data. Neuron networks perform a variety of tasks such as approximation, prediction, etc.

There are several NNs suitable for nonlinear analysis, including multilayer perceptron (MLP) networks, radial basis function (RBF) networks, etc. MLP is the most popular and widely used nonlinear networks for solving many practical problems. The reason for the popularity is that it is flexible and can be trained to assume the shape of the patterns. The MLP can be called universal approximators due to their ability to approximate any nonlinear relationship between inputs and outputs to any degree of accuracy. The power comes from the hidden layer of neuron located between the input layer and output layer of neurons. The hidden layer may consist of one or many nonlinear neurons and it performs continuous, nonlinear transformations of the weighted input. Nonlinear activation function transforms the weighted input of a neuron nonlinearly to an output. Sigmoid activation function is the popular one. The most widely used sigmoid activation functions are logistic function and hyperbolic tangent function. Output of each neuron is given in Equation (14), where the weighted sum of inputs is passed through a sigmoid function as

$$\sigma\left(\sum_{j=1}^{n}\omega_j x_j + b\right) \tag{14}$$

B. Proposed Methodologies

The simulation method is presented in two steps: *Step I-Obtaining Training Data Set* and *Step II-Approximation of LM Using NN*.

Step 1: Obtaining Training Data Set

Two methodologies for finding training data set, namely Actual LM Method with NN (ALM-NN) and Maximum LM Method with NN (MLM-NN) are proposed. The methodologies are described as follows:

- *Actual LM Method with NN (ALM-NN):* The actual loading margins and corresponding generation directions are found from exhaustive simulation using any voltage stability software to calculate loading margin of the power system for a given generation direction [5]. The actual LM and corresponding GD are used as a training data set.

- *Maximum LM Method with NN (MLM-NN):* The relationship of LM with respect to GD of each generator is found from a single dimensional space as only one generator is considered, except the swing bus. The LM surface is approximated for multi-dimensional case based on the separability condition and MLM method presented in Section III.D.

Step 2: Approximation of LM using NN

After LM and all possible GDs are found, the training data set is then used to train the NN. From the NN, the approximated LM can be found from any generation direction value.

Fig. 1 summarizes the process of the proposed approximated LM methods. In the beginning, generation direction is firstly set for the CPF process. Then the training data set is found. For ALM-NN method, the completed PV curve is plotted to obtain the LM of the particular generation direction. The process is then repeated until enough training data are obtained. For MLM-NN, the LM surface is approximated for all possible GDs. The training data is then used in NN process by introducing GDs as inputs and LM as an output. After the NN is trained to find the appropriate weights and other NN parameters, one can use the trained NN to approximate the LM at the GDs of interest. The proposed method is validated in the following section.

V. Numerical Results

A. Test Power Systems

The modified IEEE 14-bus test system [5] is used to validate the proposed method. Its single line diagram is depicted in Fig. 2, which consists of five synchronous machines, including one synchronous compensator used only

for reactive power support and four generators located at buses 1, 2, 6 and 8. The modification from the original IEEE 14-bus test system is that generators located at buses 6 and 8 were changed from synchronous compensators to generators. In the system, there are twenty branches and fourteen buses with eleven loads totaling 259 MW and 81.4 Mvar. The value of 259 MW is used for the base MVA of the IEEE 14-bus system.

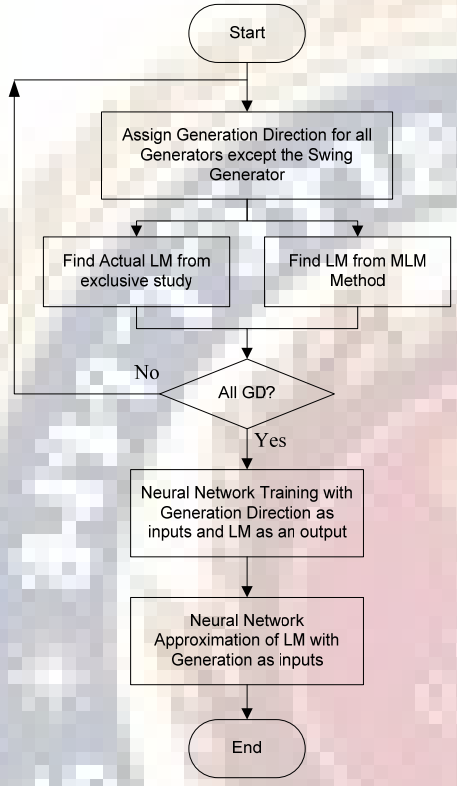

Fig. 1. LM Approximation Using Artificial Neural Networks.

Results presented in the paper were produced with the help of UWPFLOW [10] and another Neural Network Software. The UWPFLOW is a research tool that has been designed to calculate loading margin of the power system for a given load and generation direction. In the following section, simulation results are presented.

B. Training Data Set

The size of generation direction space is in proportion to the number of dispatchable generators considered in the study. To limit the number of generators in this study, a total of four generators are used for the IEEE 14-bus test system. Three cases of three generators are used throughout the paper.

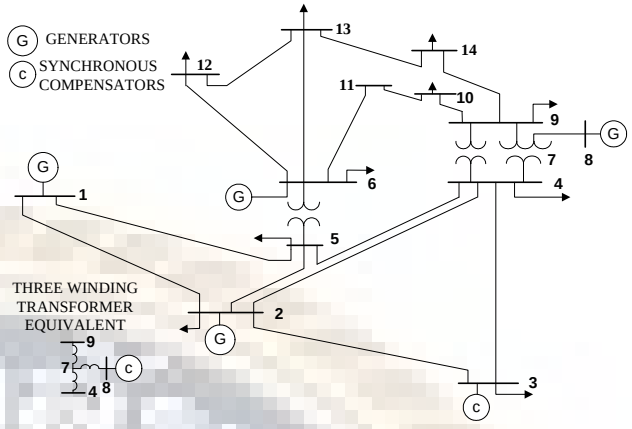

Fig. 2. Single line diagram of the modified IEEE 14-bus test system.

1. ALM-NN

Three cases of generator locations are considered: generators are located at buses 1, 2 and 6 (Case G126); at buses 1, 2 and 8 (Case G128); and at buses 1, 6 and 8 (Case G168). The actual LM is found with the help of UWPLOW program based on the methodology presented in Section IV. The actual data of LM and GDs are plotted in Figs. 3, 4 and 5 for the G126, G128 and G168 cases, respectively. These LM plots are obtained from PV at all possible GDs in the GD space with 0.1 GD step. The maximum LM and corresponding GD of each case are shown in Table I. From Table I, the maximum LM of G126, G128 and G168 cases are 1.1655, 1.0286 and 1.0686, respectively.

2. MLM-NN

The MLM method is based on the loading margin of the system at various possible generation directions in the generation direction space. The approximate plots obtained from MLM method for G126, G128 and G168 cases are shown in Figs. 6, 7 and 8, respectively. Clearly, the plots obtained from the MLM approach are almost the same as those obtained from the actual LM plot.

The LM obtained from actual LM and MLM methods are used to train NN in the following subsection.

C. Approximation of LM using NN

From LM and GD data obtained in previous subsection, one may use GDs as inputs and LM as an output to train the NN. Multilayer perceptron with activation functions and black propagation are used to capture nonlinearity of the training data. There are 66 training data used in the training process. Table II shows the summary of the training data and results for each case. The result is obtained from the best solution of 30 training results that provide the minimum training error. From the table, about 7-47 neurons are used in the hidden layer. Number of neurons and types of activation function are obtained from the best solution using NN software. The training times are only few minutes and testing time for each Gxyz case is less than 1 second.

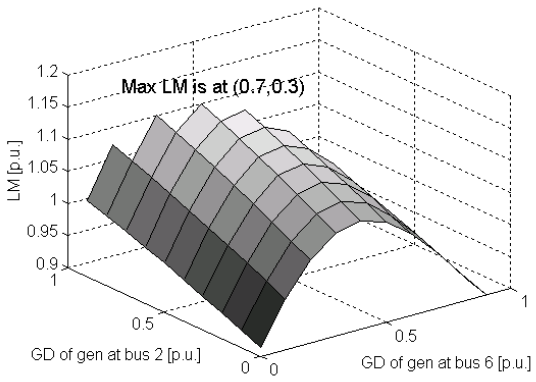

Fig. 3. Actual LMs in case G126.

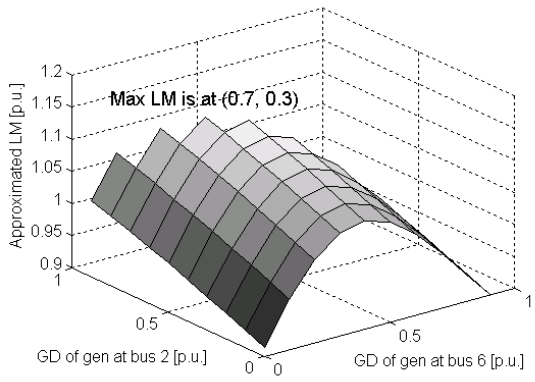

Fig. 6. Approximated LMs in case G126 using the MLM approach.

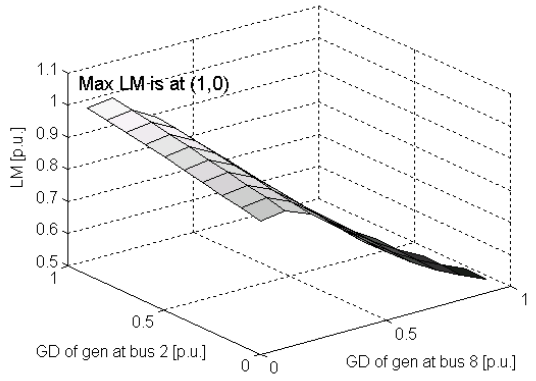

Fig. 4. Actual LMs in case G128.

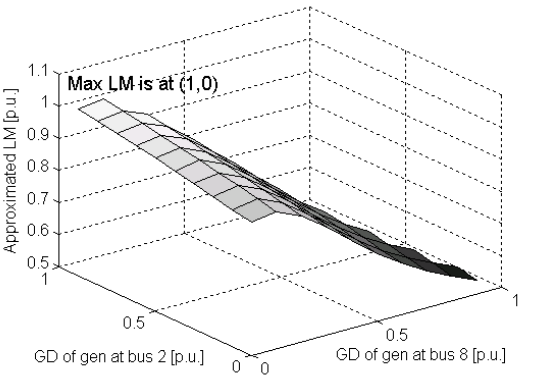

Fig. 7. Approximated LMs in case G128 using the MLM approach.

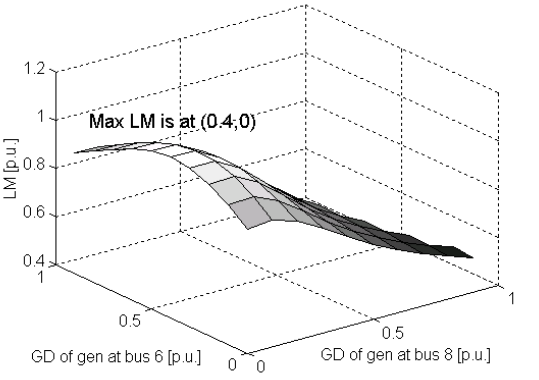

Fig. 5. Actual LMs in case G168.

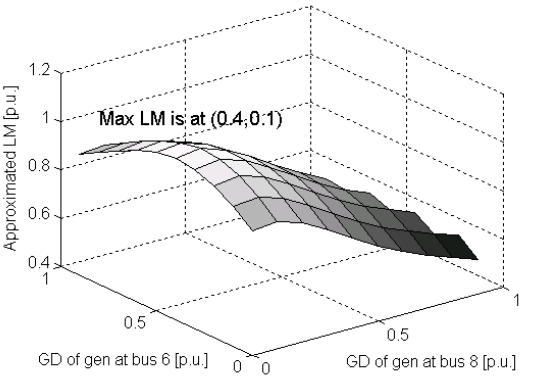

Fig. 8. Approximated LMs in case G168 using the MLM approach.

TABLE I. COMPARISON OF GENERATION DIRECTIONS AND LM.

Cases	Solutions obtained from the Actual LM plot	
	LM (p.u.)	GDs
G126	1.1655	(0,0.7,0.3)
G128	1.0286	(0,1,0)
G168	1.0686	(0.6,0.4,0)

The numerical solutions of each method are given in Table III for all the cases. The GD data used for testing has 0.25 interval where those for learning has 0.1 interval. From the table it can be seen that neural networks can capture nonlinearity of LM surface. The approximated LM solutions are very close to the actual LM value as shown in Figs. 3-5 and to approximated LM from MLM method [5]. The proposed method provides a good approximation of LM, which may help System Operator to obtain LM at some generation direction points in a short time. The methodology

may be applied to EMS system at load dispatching center or System Operator.

TABLE II. TRAINING RESULT INCLUDING HIDDEN LAYER, OUTPUT LAYER, ACTIVATION FUNCTION AND NUMBER OF NEURONS.

Case	Hidden Layer		Output Layer	
	Activation Function	No. of Neurons	Activation Function	No. of Neurons
	For ALM-NN/ MLM-NN			
G126	Tanh/Tanh	15/7	Sine/Sine	1/1
G128	Tanh/Sine	15/37	Tanh/Logistic	1/1
G168	Tanh/Exp	12/47	Exp/Identity	1/1

TABLE III. NEURAL NETWORK OUTPUT AT DIFFERENT GDS

GD for Gxyz case			ALM-NN for Gxyz			MLM-NN for Gxyz		
x	y	z	126	128	168	126	128	168
1.00	0.00	0.00	0.913	0.916	0.931	0.913	0.973	0.908
0.75	0.00	0.25	1.047	0.864	0.867	1.047	0.871	0.862
0.50	0	0.50	1.057	0.712	0.710	1.056	0.713	0.714
0.25	0	0.75	0.968	0.595	0.598	0.968	0.592	0.591
0.00	0	1.00	0.859	0.515	0.547	0.859	0.539	0.523
0.75	0.25	0.00	0.946	0.964	1.038	0.946	0.985	1.049
0.50	0.25	0.25	1.087	0.889	0.958	1.080	0.897	0.999
0.25	0.25	0.50	1.094	0.729	0.753	1.089	0.744	0.849
0.00	0.25	0.75	0.996	0.604	0.613	1.000	0.609	0.718
0.50	0.5	0.00	0.976	0.990	1.052	0.976	0.994	1.057
0.25	0.5	0.25	1.124	0.907	0.969	1.110	0.920	1.004
0.00	0.5	0.50	1.129	0.744	0.753	1.119	0.776	0.858
0.25	0.75	0.00	1.003	1.012	0.967	1.003	1.002	0.979
0.00	0.75	0.25	1.157	0.944	0.902	1.138	0.941	0.925
0.00	1	0.00	1.029	1.025	0.866	1.028	1.008	0.846

VI. CONCLUSION

This paper proposes new methods, namely ALM-NN and MLM-NN, for approximating loading margin or voltage stability margin of the system using Artificial Neural Networks. Loading margins in generation direction space are used to train neural networks. Multilayer perceptron with activation functions and black propagation are used to capture nonlinear relationship of the training data. The proposed methods are validated and compared with Actual LM and MLM methods in the three generator cases in the modified IEEE 14-bus test system. The results show that the proposed method is able to find the result in a short period of time. It can be used in the EMS system to help System Operator to approximate voltage stability margin based on generation directions in a simple and fast way.

REFERENCES

[1] IEEE/PES Power System Stability Subcommittee, *Voltage Stability Assessment:* Concepts, *Practices and Tools*, special publication, final draft, Aug. 2003.

[2] Blackout of 2003: Description and Responses, Available: http://www.pserc.wisc.edu/.

[3] B. H. Lee and K. Y. Lee, "Dynamic and Static Voltage *Stability* Enhancement of Power Systems," *IEEE Transactions on Power Systems*, Vol. 8, No. 1, pp. 231-238, 1993.

[4] A. Sode-Yome and N. Mithulananthan, "Comparison of shunt capacitor, SVC and STATCOM in static voltage stability margin enhancement," *International Journal of Electrical Engineering Education*, Vol. 41, No. 3. pp.158-171, 2004.

[5] A. Sode-Yome, N. Mithulananthan, and K. Y. Lee, "A Maximum Loading Margin Method for Static Voltage Stability in Power Systems," *IEEE Trans. Power Syst.*, Vol. 21, pp. 799-808, 2006.

[6] C. A. Canizares, A. C. Z. De Souza, and V. H. Quintana, "Comparison of performance indices for detection of proximity to voltage collapse," *IEEE Trans. Power Syst.*, Vol. 11, No. 3, pp. 1441-1447, Aug. 1996.

[7] S. Samarasinghe, *Neural Networks for Applied Sciences and Engineering*, Auerbach Publications, Tylors and Francis Group, New York, 2007.

[8] A. Sode-Yome and N. Mithulananthan, "Generation Direction Based on Optimization Technique for Power System Static Voltage Stability", *Australasian Universities Power Engineering Conference*, Hobart, Australia, Sep. 25-28, 2005.

[9] S. Green, I. Dobson and F. L. Alvarado, "Sensitivity of Loading Margin to Voltage Collapse with respect to Arbitrary Parameters," *IEEE Trans. Power Syst*, Vol. 12, No. 1, pp. 262-272, Feb. 1997.

[10] C. A. Cañizares, et al., *UWPFLOW: Continuation and Direct Methods to Locate Fold Bifurcations in AC/DC/FACTS Power Systems*, University of Waterloo, available at http://www.power.uwaterloo.ca, June. 2009.

Arthit Sode-Yome (M'04) received the B.Eng degree in Electrical Engineering from Prince of Songkla University, Thailand, in 1993, M.S. degree in Electrical Engineering from the Pennsylvania State University, USA, in 1996 and Doctoral Degree in Energy from Asian Institute of Technology, Thailand, in 2005. Dr. Arthit is a lecturer at Department of Electrical Engineering, Siam University, Thailand. His main research interests are voltage stability, FACTS, neural networks, optimization techniques and HVDC.

Kwang Y. Lee (F'01) received his B.S. degree in Electrical Engineering from Seoul National University, Korea, in 1964, M.S. degree in Electrical Engineering from North Dakota State University, Fargo, in 1968, and Ph.D. degree in system science from Michigan State University, East Lansing, in 1971. He has been on the faculties of Michigan State, Oregon State, Houston, the Pennsylvania State University, and Baylor University, where he is currently Professor and Chair of Electrical and Computer Engineering and Director of Power and Energy Systems Laboratory. His interests are power systems control, operation and planning, and intelligent systems applications to power plants and power systems control. Dr. Lee is a Fellow of IEEE, Editor of IEEE Transactions on Energy Conversion, and Associate Editor of IEEE Transactions on Neural Networks.

Investigation of the Impact of Large-Scale PV on Power System Oscillatory Stability

Journal:	*IEEE Transactions on Sustainable Energy*
Manuscript ID:	TSTE-00142-2010
Manuscript Type:	Transactions
Date Submitted by the Author:	19-Sep-2010
Complete List of Authors:	Mithulananthan, Nadarajah; The University of Queensland,, School of Information Technology and Electrical Engineering, Shah, Rakibuzzaman; The University of Queensland, School of Information Technology and Electrical Engineering Lee, Kwang; Baylor University, Electrical and Computer Engineering Sode-Yome, Arthit; Siam University, School of Information Technology and Electrical Engineering
Technical Topic Area :	Solar photovoltaics < Transactions on Sustainable Energy, Grid interaction of sustainable energy sources < Transactions on Sustainable Energy
Key Words:	Power system dynamic stability, Pulse width modulated inverters, Solar energy

Investigation of the Impact of Large-Scale PV on Power System Oscillatory Stability

Rakibuzzaman Shah, *Student Member*, *IEEE*, Nadarajah Mithulananthan, *Member, IEEE*, Arthit-Sode-Yome, *Member, IEEE,* and Kwang.Y.Lee, *Fellow, IEEE*

***Abstract*—Grid connected photovoltaic (PV) generators are being developed in recent years due to many associated economic and environmental factors, triggering control and operational challenges to power utilities. Most of all, it touches the essence of power system mechanism, concerned with power system oscillatory stability. This paper investigates the impact of large-scale PV generators on local and global or inter-area modes of oscillatory behavior of complex power system. The IEEE-14 bus system and a two-area test system are used for investigating the PV generator impact on oscillatory stability with different load levels and penetration.**

***Index Terms* — Eigenvalue analysis, large-scale integration, local mode, global mode, PV integration, PV dynamic model.**

I. Introduction

RECENT studies suggest that in the medium and long term PV generators will become commercially so attractive that large-scale implementation of this type will be seen in many parts of developed and developing world [1], [2]. Photovoltaic generation, although the initial investment is high, has several advantages over other generations. In addition to no emissions, primary fuel is free and their deliveries are at no cost; other advantages are easy installation and low operation and maintenance costs. The cost of PV module has decreased almost 90% since early 1980s; improved technology and higher efficiency cell have played critical roles in driving the cost down [2]. According to studies done by European PV Industries Association (EPIA), the fastest growing PV market is the grid-connected PV system rather than stand-alone modules.

One of the most important issues related to large-scale penetration of PV generation is its impact on power system stability, which must be examined carefully [3]. The dynamics of the PV generator is completely different from conventional generators with rotating parts, though both of them have almost identical terminal characteristics. Hence, a thorough study on PV generator interaction with conventional power generation and transmission system is an urgent task to be pursued [4], as the results of case studies on large-scale PV generation impact on power system stability have been reported in [5] and [6].

The objective of this paper is to examine the effect of PV generation on power system local and global modes of oscillation, in conjunction with that of the conventional generators and transmission system. The rest of the paper begins with the basic idea and concepts of power system oscillatory stability in Section II. Then the eigenvalue analysis method and model for PV generator is presented in Sections III and IV, respectively. Test system along with analysis tools used throughout the paper is given in Section V. Numerical results and discussion are presented in Section VI. Finally, in Section VII, conclusions and contributions of the paper are presented.

II. Oscillatory Stability

Oscillatory instability problems can be either local or global in nature. Local oscillation is one of the common instability problems in power systems and it can be easily dealt with. Local problems involve a small area of power system, and are usually associated with rotor angle oscillation of a single generator or single power plant, or controllers against the rest of power system. Such oscillations are called local plant mode oscillations [7]. These problems are widely seen in typical power systems. This problem may also be associated with oscillation between the rotors of few generators close to each other. Such oscillations are called inter-machine or interplant-mode oscillation. Poor tuning of controllers such as HVDC converter, generator excitation, FACTS devices, and PV and fuel cell inverters can also cause the local oscillation.

Global oscillation, on the other hand, is caused by interaction among large groups of generators, which are spread out throughout a large geographical area. This type of oscillations has widespread impact and can lead to partial or full outage. In this case, a group of generators in one area oscillates against another group of generators in other area. This type of problem is known as inter-area or global mode of oscillation. In a large interconnected system, there are two types of inter-area oscillations; one is with very low frequency

R. Shah is with the School of Information Technology and Electrical Engineering, University of Queensland, Australia (e-mail: md.shah@uq.edu.au)

N. Mithulananthan is with the School of Information Technology and Electrical Engineering, University of Queensland, Australia (e-mail: mithulan@itee.uq.edu.au,).

A. Sode-Yome is with Siam University, Bangkok, Thailand (e-mail: arthit@ieee.org).

K. Y. Lee is with Department of Electrical and Computer Engineering, Baylor University, Waco, TX 76798-7356, USA
(e-mail: Kwang_Y_Lee@baylor.edu)

where all the generators in the system are involved, in which case, the whole system is essentially split into two parts and one part of the system swinging against another part with typical frequency range of 0.1-0.3 Hz. Another is with higher frequency, where a subgroup of generators swinging against one another with typically frequency range of 0.4 -1 Hz [7].

Oscillatory instability problems of power systems, both local and global problems, can be studied using eigenvalue analysis and verified often by time domain simulation.

III. Methodology

In a large interconnected system, weak modes may be triggered due to small and sudden disturbances. The weak modes show oscillatory behavior growing in amplitude if there is a lack of damping on the mode. Estimation of the rate of rise and decay of the oscillation is important, so that the poorly damped modes that put the system into risk can be identified. There are different methods for capturing the oscillatory modes. Some of the methods used by utilities and researchers are Prony analysis and a method based on Fourier transform and eigenvalue analysis [7]. Among them, eigenvalue analysis is more common and far superior compared with other methods as it provides additional useful information to help identifying the location for controllers for damping the oscillation.

A. Eigenvalue Analysis Method

The behavior of a dynamic system, such as a power system, can be described by a set of *n* first-order nonlinear differential and a set of algebraic equations as given in (1).

$$\begin{aligned} \dot{x}_i &= f_i(x, y, l, p) \\ 0 &= g_i(x, y, l, p) \end{aligned} \tag{1}$$

where x is a vector of state variables, y a vector of algebraic variables, and l and p are uncontrollable and controllable parameters, respectively. As disturbance considered here is small the above set of equations can be linearized to study the system oscillatory behavior. Hence, the linearized system can be written as

$$\begin{aligned} \Delta\dot{x} &= A\Delta x + B\Delta u \\ \Delta y &= C\Delta x + D\Delta u \end{aligned} \tag{2}$$

Some properties of the eigenvalues of linearized system in relation to stability are:

- If all the eigenvalues have negative real parts then the system is called asymptotically stable; in other words the system returns to its stable condition after being subjected to small disturbance.
- If one of the eigenvalue has positive real part, then the system is unable to retain its original position following some disturbance; which means the system is unstable.
- If the system has all the eigenvalues with negative real part but one with purely imaginary part, then the system shows oscillatory behavior; called critically stable or marginally stable [8].

B. Time Domain Simulation

Time domain simulation based on numerical integration techniques that are computationally demanding compared to other methods can often be used in collaboration with eigenvalue analysis. In this paper time domain simulation is used along with eigenvalue analysis to verify the results.

IV. Photovoltaic Generator

PV generator is based on semiconductor device and solid-state synchronous voltage source converter (VSC) that is analogous to a synchronous machine except the rotating part. It generates a balanced set of sinusoidal voltage at fundamental frequency with rapidly controllable amplitude and phase angle. VSC converts a DC input voltage into AC output voltage and supply active and reactive power to the system. A block diagram of typical grid connected photovoltaic generator is shown in Fig. 1. For this paper simplified PV generator as shown in Fig. 2 is used. The following section illustrates the modeling of different sections of PV generator.

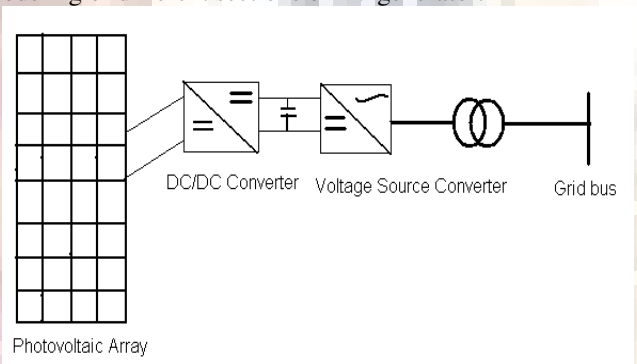

Fig. 1. Block diagram of typical grid connected PV-based generator.

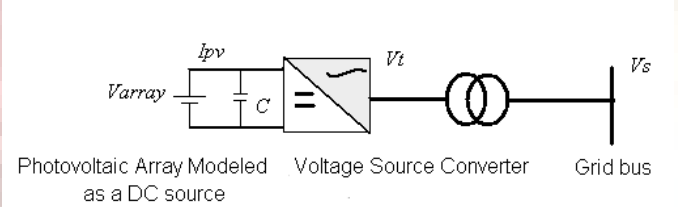

Fig.2. Simplified model of photovoltaic generator.

A. Photovoltaic Array

Solar cell is the basic building block of the photovoltaic array, which is a semiconductor device capable of generating electric power from solar radiations. Ideal solar cell at no illumination shows the same characteristic as ideal diode. Characteristic of the solar cell can be expressed by the following equation,

$$I_D = I_o(e^{\frac{V_c Q}{KT}} - 1) \tag{3}$$

where, I_D = dark current (A), I_o=saturation current of the diode (A), V_C= cell voltage (V), T= cell temperature, Q represents the charge of electron and K is the Boltzmann constant.

The performance of solar cell is strongly depends on radiation and environmental conditions. Here, in this paper only radiation sensitive model of photovoltaic cell is

considered. Commercially available solar cell never exhibits ideal characteristic as described in (3). The characteristic equation of non-ideal solar cell is given as

$$I_c = I_l(G) - I_o[e^{\frac{(v_C + I_C R_s)Q}{nKT}} - 1] - \frac{V_c + I_c R_s}{R_{sh}} \quad (4)$$

where, I_{SC}= cell short circuit current, I_l (G) = $I_{SC,}$ n= non-ideality constant of the diode, R_S=series resistance and R_{sh}= shunt resistance.

Normally, commercially available cell has very high value of shunt resistance, which can be ignored in modeling. Thus, the characteristic equation of the solar cell can be expressed as

$$I_C = I_l(G) - I_0\left[e^{\frac{(V_C + I_C R_S)Q}{nKT}} - 1\right] \quad (5)$$

Photovoltaic modules are developed by connecting these cells in parallel and series, which is capable of generating power in watts range. Large application requires parallel and series connection of these modules which is known as photovoltaic array. The characteristic equation of a photovoltaic array can be formed from the above solar cell equation. Now, the PV array terminal voltage can be found by the numerical analysis of the following equation

$$V_A = \frac{nN_S KT}{Q}\ln\left[\frac{I_{SCA}(G) - I_A}{N_p I_0} + 1\right] - I_A R_S \quad (6)$$

where, I_A= array current (A), V_A=array voltage (V), I_A= $N_P I_C$, I_{SCA} (G) = $N_p I_{SC}$ (G), N_S= $N_{CS}N_{SM,}$ N_P= N_{SP}. N_{SM} and N_{SP} represent the number of modules connected in series and parallel in the photovoltaic array, respectively. The alternative way of getting PV array terminal voltage is reported in [2],[20].

B. Power Conditioning Device

The power conditioning unit is used for the efficient interfacing between PV array and grid. All the system dynamics of PV generator are related to power conditioning unit. In this paper the multivariable state space model for power conditioning unit is obtained from line switching function and d-q transformation [14]. The differential equations related to VSC can be expressed as follows

$$\begin{aligned}
\frac{dI_d}{dt} &= -\frac{R}{L}I_d - \omega I_q + \frac{kmV_A\cos\alpha}{L} - \frac{V_s}{L} \\
\frac{dI_q}{dt} &= -\frac{R}{L}I_q + \omega I_d - \frac{kmV_A\sin\alpha}{L} \\
\frac{dV_{dc}}{dt} &= \frac{I_{PV}}{C} - \frac{km}{C}(I_d\cos\alpha + I_q\sin\alpha)
\end{aligned} \quad (7)$$

where, I_d and I_q represent d-q current components, V_{dc} = DC link voltage, C represent DC link capacitor value, R and L represent the resistance and inductance between VSC and grid, respectively, m= modulation index, α = phase angle, k = constant factor (depends on type of converter and coupling transformer) (0.6128), V_s = grid bus voltage, ω = angular frequency.

DC power generated from the PV array is considered to be the real power injected into the network. The real and reactive power absorbed and generated by VSC can be controlled by controlling α and m [10], [15]. Fig. 3, depicts the control block for real and reactive power control of VSC.

Now, the link with AC network can be expressed as follows:

$$P_s = \frac{V_t V_s}{X_t}\sin\alpha = P_{dc} \quad (8)$$

$$Q_s = \frac{V_t V_s}{X_t}\cos\alpha - \frac{V_s^2}{X_t} \quad (9)$$

where,

$V_t = mkV_A$, X_t = impedance between converter and grid bus, and V_t = Voltage at converter terminal.

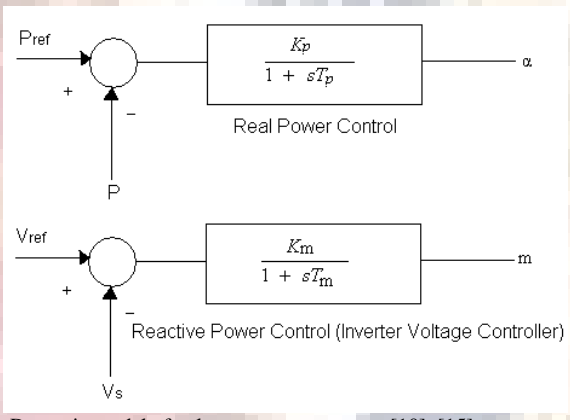

Fig. 3. Dynamic model of voltage source converter [10], [15].

V. Test System and Tool

The IEEE-14 bus and Two-area test systems are used in this paper to investigate the impact of PV generator on power system oscillatory stability. Single line diagram of IEEE-14 bus and two-area test systems are depicted in Fig.4 (a) and 4(b), respectively.

A. IEEE-14 Bus Test System

In the IEEE-14 bus system, there are five synchronous generators, including synchronous compensators. There are twenty branches and fourteen buses with eleven loads totaling 362.5 MW and 108.5 Mvar. PV generator is connected to the system to study the impact on system local mode of oscillation with increasing loading level, and penetration at different location.

B. Two-area Test System

Two area test system consists of four synchronous generators associated with four 20/230 kV step up transformers. There are twelve branches and eleven buses with two loads totaling 2734 MW and 250 Mvar. As in the IEEE-14 bus test system, PV generator is connected to this system to

study its impact on global mode of oscillation with increasing loading level, and penetration at different location.

C. Tools

Shell SQ-150-PC module data has been used in this paper for the basic building block of the PV array [20]. In the IEEE-14 bus test system , $5MW_P$ [MW peak] size of PV generator has been considered; while for the investigation of penetration effect of PV generator on power system oscillatory stability, PV generator size was increased by $5MW_P$ step size. On Two-area Test System, 50 MW_P size of PV generator has been considered with step size of 50 MW_p while investigating penetration effect.

Results presented in the paper were obtained by MATLAB and MATLAB-based software PSAT [18]. PSAT 1.3.4 version was used to develop the PV based generator function file.

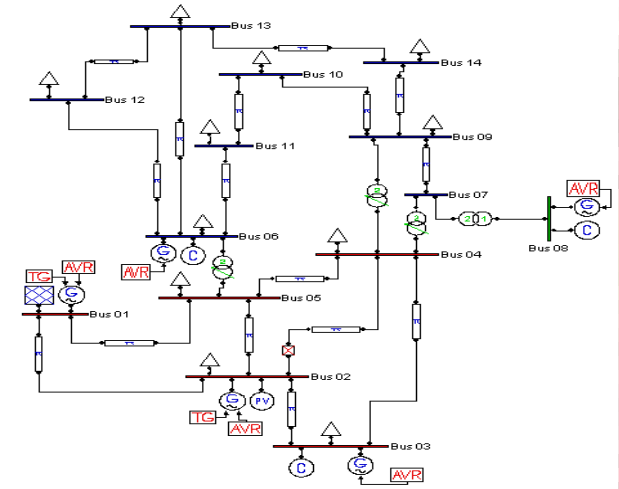

Fig. 4 (a). Single line diagram of the IEEE-14 bus test system.

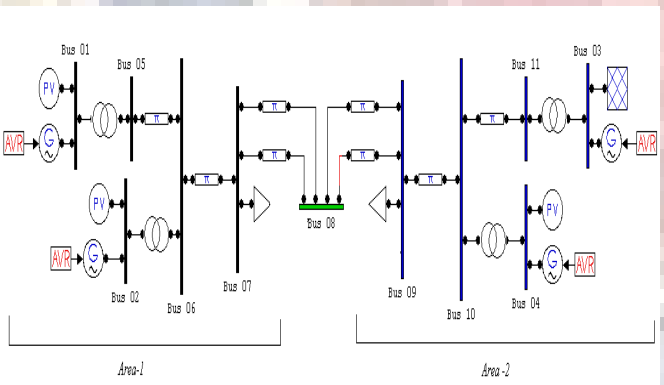

Fig.4(b). Single line diagram of two-area test system.

VI. Numerical Results

In order to see the impact of a large scale PV generation system on power system local and global modes of oscillation, IEEE-14 bus test system and two-area test system are used. In both cases, eigenvalue analyses have been performed first without PV systems which have been referred to as base cases.

A. PV Impact on Local Mode -IEEE-14 Bus Test System

Six order-model of a synchronous generator is considered in this work, assuming the presence of a field circuit and an additional circuit along the d-axis and two additional circuits along q-axis. The system has six-state variables: rotor angle, rotor speed, *q*-axis transient voltage, *d*-axis transient voltage, *q*-axis sub-transient voltage and *d*-axis sub-transient voltage. The machine includes a Type-II automatic voltage regulator (AVR), which is IEEE model-I. As it has been mentioned in [20], detailed and simplified PV generator models provide apparently the same effect on system oscillatory behavior; hence, in this paper simplified model which has already explained on the modeling section has been used.

Fig. 5 shows eigenvalue analysis results at the base case. From the figure, it can be observed that system is oscillatory unstable as a complex mode is located in the open left half plane. Participation factor revealed that the states most associated with the critical complex mode are generator 1 *q*-axis internal voltage (*Elq_syn_1*) and the exciter control voltage of the generator 1 (*Vf_Exc_1*). The frequency of oscillation and damping ratio associated with the critical modes are 1.45 Hz and -0.00341, respectively.

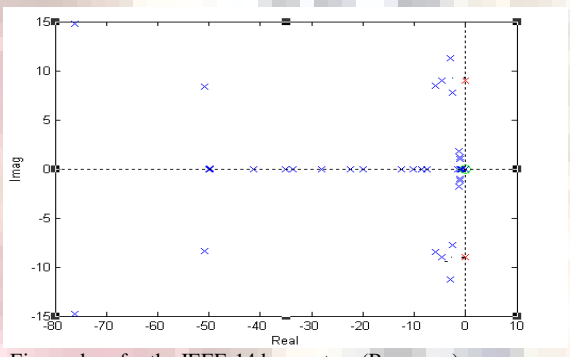

Fig. 5. Eigenvalues for the IEEE-14 bus system (Base case).

Next, PV generator has been installed at bus 14. Bus 14 is selected in this case, as it is the weakest bus of the system. Weakest bus of the system is selected here by Q-V sensitivity analysis. Fig. 6 shows eigenvalue results of IEEE-14 bus system with PV. It can be observed that all the eigenvalues are located at the open left half plane with PV integration. The damping ratio on the critical mode has been increased from -0.003 to 0.033. Fig. 7 depicts time domain simulation results of the state variable *Elq_syn_1* with and without PV generator. For time domain simulation a three phase faults is applied and cleared quickly to trigger the weak mode. It can be observed that PV generator damps out the oscillation by adding damping on critical mode as indicated by the eigenvalue analysis. Effect of PV generator on IEEE-14 bus test system's critical mode is illustrated in Table I. As the interests are for those eigenvalues which have damping less than 2.5%, the effects of PV generator on electromechanical modes are not shown as their damping is higher than the pre-defined critical value.

It can be observed that PV generator positively affect the system's critical mode by adding more damping on critical mode. Impact of radiation change has no significant impact on system's critical modes and the modes associated with PV generator, as reported in [20]. Therefore, all studies in this paper have been done on one particular radiation level. The radiation level of 550 W/m^2 is used here for all the studies.

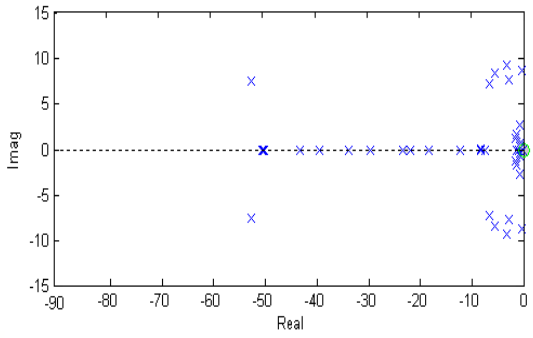

Fig. 6. Eigenvalues for the IEEE-14 bus system with a PV at Bus 14.

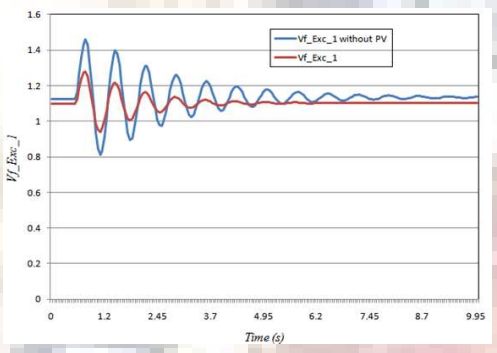

Fig. 7 . Time domain simulation results for *Vf_Exc_1* with and without PV at reduced load level than base case.

TABLE I
COMPARISON OF THE CRITICAL MODE FOR IEEE-14 BUS TEST SYSTEM WITHOUT AND WITH PV GENERATOR

State variables	Without PV	With PV
Elq_syn_1, Vf_Exc_1	0.030±j9.006	-0.300±j9.081

B. *Effect of PV Generator on IEEE-14 Bus System Loading*

The effect of loading on oscillatory stability of the system containing PV generator is studied next. The base case loading level corresponding to the test system is 362.52 MW. Uniform real and reactive power change for all load buses is considered for this study. Damping ratio of the critical mode on IEEE-14 bus test system with and without PV at different loading is shown in Fig. 8. In the base case, system is oscillatory unstable, and with higher loading values, damping of the critical mode become more negative which is clearly shown in Fig. 8. However, introduction of PV generator at bus 14 affects the local oscillatory behavior of the system positively. It brings those problematic eigenvalues from open right half plane to open left half plane and still remain well inside the open left half plane even in higher loading condition. From the figure it can be observed that with PV penetration system can be loaded more without subjected to any oscillatory behavior as compared to system without PV, and the critical loading point for the system with PV is 399.21 MW which is 12% higher than the critical loading of the system without PV.

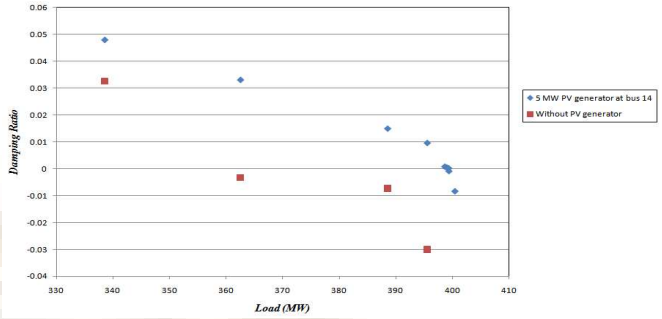

Fig. 8. Effect of PV on critical mode at IEEE-14 bus test system.

C. *Effect of PV Penetration in IEEE-14 Bus System*

The effect of penetration of PV generator on power system oscillation has been studied in the IEEE-14 bus system. The following scenarios are considered in penetration:

- PV generator at a single location.
- Scattered PV generator location.

Penetration from 5 MW_p to 20MW_p has been considered for the analysis in both scenarios. In single PV location, increment of the size has been considered at the same bus, whereas for the scattered case, different location has been considered to make the total penetration same as the single location scenario. Fig. 9 shows the effect of penetration. From the figure it can be observed that, scattered penetration provides higher damping ratio to the critical mode than the single location penetration in IEEE-14 bus test system.

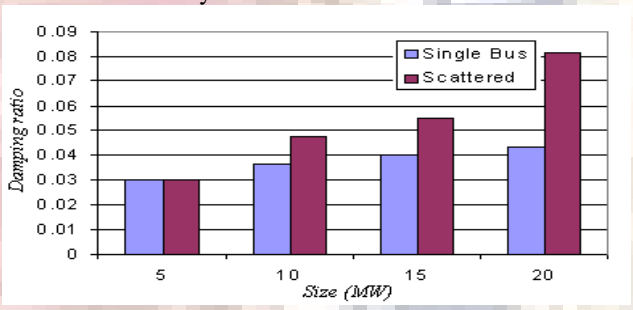

Fig. 9. Effect of PV penetration on critical mode for two scenarios.

Location of PV generator has a significant effect on system local oscillatory behavior. Fig. 10 shows the damping ratio of the critical mode in the IEEE-14 bus system at different PV generator location. From the figure, it can be observed that change of PV generator position has a significant impact on critical mode. When PV generator is placed closer to the problematic machine, it adds more damping to the critical mode than the location away from the machine.

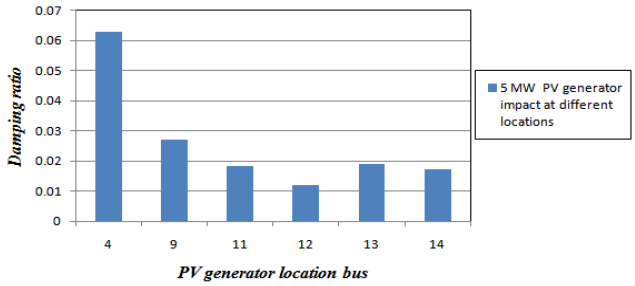

Fig. 10. Damping ratio of the critical mode in IEEE-14 bus system with PV at different locations.

D. PV impact on global mode -Two-area Test System

So far all the above analyses have shown the impact of PV generator on power system local mode of oscillation. To see the impact of PV generator on inter-area or global mode of oscillation, analyses have been carried out in two-area test system. As in the IEEE-14 bus system, six-order model of synchronous generator along with IEEE model-I exciter are considered for the study. From eigenvalue analysis it is found that all eigenvalues in the system are in the left half of the complex plane, among those, mode 2 is the most critical. All generators in the system are participating in this mode, among them participation of generator 3 is highest which associated with *delta_syn_3, omega_syn_3*. The frequency of oscillation and damping ratio of the mode are 0.482 Hz and 0.018, respectively. Next, PV generator has been installed at bus 8. Bus 8 is selected in this case, as it is the weakest bus in the system and near the load center of the system. Weakest bus of the system is selected by Q-V sensitivity analysis. Table II, shows the effect of PV generator on the critical mode of the system.

TABLE II
EFFECT OF PV GENERATOR ON COMPLEX MODE OF MACHINES IN TWO-AREA TEST SYSTEM

Electro-mechanical modes	Without PV generator	With PV generator
Mode 1	-0.497±j5.994	-0.478±j6.044
Mode 2	-0.056±j3.031	-0.053±j3.189
Mode 3	-0.508±j6.1672	-0.479±j6.256

From Table II, it can be observed that if a PV generator is placed at bus 8 of the system, then it has a negative effect on system's global mode of oscillation and the damping of the critical mode decreased from 0.01847 to 0.01668. Fig. 11 depicted the change of critical mode damping with the placement of the PV generator on different system bus. From the figure, it is clear that placement of PV generator in other area away from the most participating generator in the critical mode negatively affect global mode of oscillation.

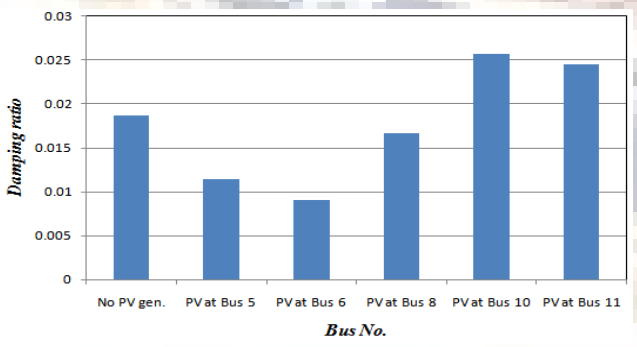

Fig 11. Damping ratio of critical mode in Two-area Test System with PV at different locations.

A time domain simulation of rotor angle of generator 3 is shown in Fig. 12. Disturbance is applied to the system in the form of three-phase faults at 0.5 sec and cleared at 0.505 sec. The figure clearly indicates that rotor angle has high magnitude and less damped oscillation in the absence of PV generator at bus 10; bus 10 is selected as in this position PV generator provides more damping to the critical mode.

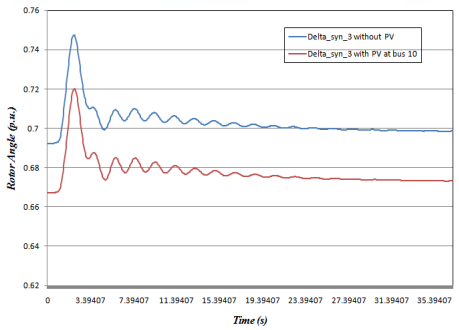

Fig. 12 . Time domain simulation results of rotor angle for Generator 3.

E. Effect of PV Generator on Two-area Test System Loading

The effect of loading on global mode of oscillation with PV generator is studied next. The base case load level to the two-area test system is 2734 MW and 250 Mvar and other three different loading levels are considered. Uniform real and reactive power changes for the load buses of the system are considered. For all cases, PV at bus 10 is considered. In all loading levels system is oscillatory stable. However, at higher loading level, damping of the critical modes decreases. But, at certain load level the damping of the critical mode increased and damping of other mode, which is so far higher than 3% damping, started to decrease. Table III clearly shows the eigenvalues of the critical mode without and with PV at different loading levels.

TABLE III
EFFECT OF LOADING ON CRITICAL MODE WITH AND WITHOUT PV IN TWO-AREA TEST SYSTEM

Load demand in MW	Eigenvalues of the critical modes	
	Without PV	With PV
2597.3	-0.074±j2.967	-0.083±j2.920
2734	-0.056±j3.031	-0.080±j3.112
2870.7	-0.054±j3.216	-0.068±j3.210
3007.4	-0.054±j3.169	-0.055±j3.215

F. Effect of PV Penetration in Two-area Test System

The effect of an increase in penetration of PV generator on power system global mode of oscillation has been studied in two-area test system. In both cases, PV generator shared total loads of the system with synchronous generators and slack generator. The following two scenarios are considered in penetration:

- PV generator at single location.
- Scattered PV generator location.

Penetration from 50 MW_P to 200 MW_P has been considered for the analysis in both cases. In single PV location increment

of the size has been considered at same bus, whereas for the scattered case different location has been considered to make the total size same as the single location. Fig. 13 shows the effect of the single location PV penetration on global mode of oscillation. From the figure it can be clearly observed that based on PV generator location, higher penetration can affect the critical mode of oscillation negatively.

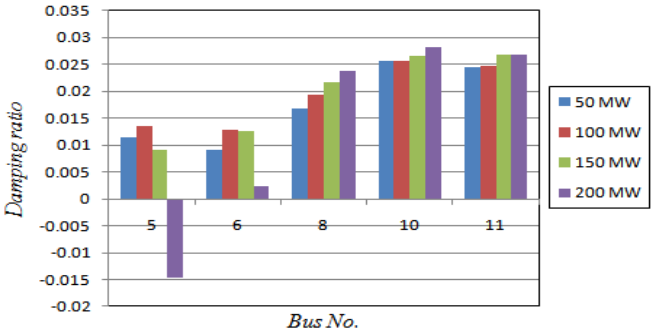

Fig. 13. Effect of PV penetration on critical mode for single location

Table IV, illustrates the effect of concentrated and scattered PV penetration in two-areas test system. From Table IV, it can be observed that for a given size, single location PV penetration is better for area-1 and scattered penetration is better for area-2. However, at area-1 incremental penetration at single location has negative impact on damping of the critical mode, whereas, incremental PV penetration both single and scattered location improve the damping of the critical mode. Overall, scattered penetration provides better damping than single location at area-2. It is worthwhile to note that participation factor analysis revealed that the most associated state variables of the critical mode are located at area -2.

TABLE IV
EFFECT OF CONCENTRATED AND SCATTERED PENETRATION ON CRITICAL MODE OF TWO-AREA TEST SYSTEM

Size MW_P	All PV in area 1		All PV in area 2	
	Concentrated	Scattered	Concentrated	Scattered
100	0.013	0.003	0.025	0.027
150	0.009	0.002	0.027	0.028
200	-0.015	0.0023	0.028	0.029

G. *Effect of PV on Two-area System's Local mode*

In two-area test system, most critical local modes of oscillation are associated with electromechanical modes of generator 2 and 4, respectively. In base case, damping of the both modes is 0.082. But, the integration of 50 MW_P PV generator at different bus negatively affects the damping of those modes of the system. Table V depicted the effect of PV generator on those modes in two-area system. From the table it can be observed that at all locations; PV generator has negative damping effect on those modes. Fig.14 shows the variation of damping ratio for electromechanical mode of generator 2 with different PV penetrations whereas; Fig. 15 shows the variation of damping ratio for generator 4. From Fig. 14 it can be observed that concentrated penetration of PV at area 1 provides better damping to the local mode of oscillation associated with generator 2.

For all penetration cases, with increasing PV size add damping to the local mode except scattered penetration in area 2. From Fig. 15 it can be clearly observed that for both concentrated and scattered penetration of PV, increasing PV size add damping to the electromechanical mode of oscillation.

TABLE V
EFFECT OF PV GENERATOR ON LOCAL MODE OF OSCILLATION IN TWO-AREA TEST SYSTEM

PV gen. Location	% Damping associated with Local mode 1			% Damping associated with Local mode 2		
	With out PV	With PV	Change of damping	With out PV	With PV	Change of damping
5	8.2	8.00	-0.20	8.2	7.76	-0.44
6		7.95	-0.25		7.75	-0.45
8		7.89	-0.31		7.65	-0.55
10		7.90	-0.30		7.70	-0.53
11		7.90	-0.30		7.71	-0.48

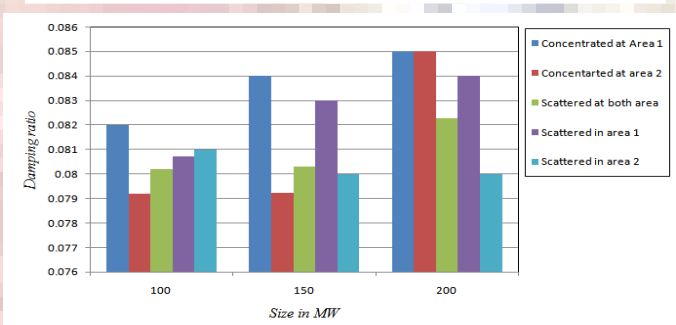

Fig. 14. Effect of PV penetration on EM mode of generator 2.

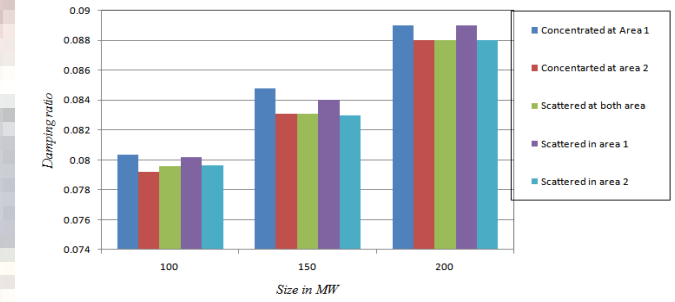

Fig. 15. Effect of PV penetration on EM mode of generator 4.

VII. CONCLUSIONS

In this paper, the impacts of large-scale PV generator on power system local and inter-area mode of oscillation are observed for two IEEE recommend test systems.

From the numerical results, it can be observed that random placement may positively or negatively influence the critical

mode and hence the oscillatory behavior of power system, suggesting a thorough investigation of the location for large scale PV integration. It also suggests that location and size of PV generation are crucial factors that influence the oscillatory behavior of power systems. A PV generation location closer to problematic machine seems to be favorable if there is no limitation on the resources or other constraints associated with locating PV generation. Moreover, based on numerical results a scattered penetration of PV system is better compared to a concentrated penetration at a single location as far as oscillatory stability of power systems are concerned.

REFERENCES

[1] M. A. Eltawil and Z. Zhao "Grid connected Photovoltaic Power Systems: Technical and Potential Problems- A review," *Elsevier Renewable and Sustainable Energy Reviews*, Vol. 14, pp. 112-129, 2010.

[2] M. R. Patel, *Wind and Solar Power Systems*, CRC press, Boca Raton, USA,1999.

[3] Y. T. Tan, D. S. Kirschen and N. Jenkins, "A model of PV generation suitable for stability analysis," *IEEE Trans. on Energy Conversion*, Vol. 19, No. 4, pp. 748-755, 2004.

[4] L. Wang and T. Lin, " Dynamic stability and transient response of multiple grid connected PV system", *Proc. of IEEE PES T&D conference*, 2008.

[5] Y. T. Tan and D. S. Kirschen, "Impact on power system of a large penetration of photovoltaic generator," *Proc. of IEEE PES General Meeting*, 2007.

[6] W. Du, H. F. Wang and R. Dunn, "Power system small-signal oscillation stability as affected by large-scale PV penetration," *Proc. of International Conference on Sustainable Power Generation and Supply*, 2009.

[7] P. Kunder, *Power System Stability and Control*: *Introduction to the Power System Stability Problem,* Electric Power Research Institute, New York, 1994.

[8] N. Mithulananthan, C. A. Canizares and J. Reeve, "Linear performance indices to predict oscillatory stability problems in power systems," *IEEE Trans. on Power Syst*., Vol. 19, No. 2, pp.1104-1114, May 2004.

[9] D.-J. Lee and L. Wang. "Small–signal stability analysis of an autonomous hybrid renewable energy power generation/energy storage Part I: Time domain simulations," *IEEE Trans. on Energy Conversion*, Vol. 23, No.1, pp.311-320, March 2008.

[10] S.-Y. Ruan, G.-J. Li, B.-T. Ooi and Y.-Z. Sun.. "Power system damping from real and reactive power modulations of voltage source converter station," *IET Generation, Transmission & Distribution Journal*, Vol. 2, No. 3, pp. 3311-320, 2008.

[11] L. Wang and Y.-H. Lin. "Random fluctuation on dynamic stability of a grid–connected photovoltaic Array," *IEEE Trans. on Power System*, Vol. 3 No. 2, pp. 985-989, 2001.

[12] C. Rodriguez and A. J. Amaratuga. "Dynamic Stability of Grid Connected Photovoltaic System," *IEEE Trans. on Power System*, Vol.2 .No.1 pp 3301-3309, March 2007.

[13] V. K. Sood, *HVDC and FACTS Controllers*: Application of Static Converter in Power Systems, Kluwer Academic Publishers, New York, USA 2004.

[14] C. Schauder and H. Mehta,"Vector Analysis and control of advanced Static Var compensator," *IEE Proceedings-C*, pp. 299-306,1993.

[15] C. Shen, Z. Yang, M. L.Crow and Stan. Atcitty, "Control of STATCOM with energy storage device," *IEEE Trans. on Power Systems*, Vol. 4, No. 2, pp. 2722-2728, Jan 2000.

[16] F. Blaabjerj, Z. Chen and S. B. Kiaer,"Power electronics as efficient interface in dispersed power generation systems," *IEEE Trans. on Power Electronics*, Vol. 19, No. 5, pp.1186-1194, Sep 2004.

[17] L. Wang and Y.-H. Lin,"Dynamic stability analysis of a photovoltaic array connected to a large utility grid," *IEEE Trans. on Power Systems*, Vol. 3, No. 2, pp. 476-481, 2000.

[18] F. Milano, *Power System Analysis Toolbox*, Documentation for PSAT version 1.3.4, July 14, 2005, available on www.power.unwaterloo.ca

[19] N. Mithulananthan, C. A. Cañizares, J. Reeve, and G. J. Rogers, "Comparison of PSS, SVC and STATCOM controllers for damping power system oscillation," *IEEE Trans. Power Systems,* Vol. 18, No. 2, pp. 786-792, May 2003.

[20] R. Shah, N. Mithulananthan, A. Sode-Yome and K. Y. Lee, "Impact of Large-Scale PV Penetration on Power System Oscillatory Stability," *IEEE-PES General Meeting*, Minneapolis, USA, 25-19, July 2010.

[21] G. J. Li, S. Y. Ruan and L. Peng, "A novel nonlinear control for stability improvement in HVDC light system," *IEEE Power Engineering Society General Meeting,* pp. 837-845, June 2005.

Rakibuzzaman Shah (S'10) received the B.Sc Eng in EEE from Khulna University of Engineering & Technology (KUET), Khulna, Bangladesh, and the M.Eng from Asian Institute of Technology, Bangkok, Thailand in 2005 and 2009, respectively. He has served as a lecture at Chittagong University of Engineering & Technology (CUET), Bangladesh. Mr. Shah is currently involves in Ph.D. research at University of Queensland, Australia. His main research interests are power system stability, energy security, power system interconnection and renewable energy technology.

Nadarajah Mithulananthan (M'02) received his Ph.D from University of Waterloo, Canada in Electrical and Computer Engineering in 2002. He has worked as an electrical engineer at Generation Planning Branch of Ceylon Electricity Board in Srilanka and as a researcher at Chulalongkorn University, Bangkok, Thailand. Dr. Mithulan is currently a senior lecturer at University of Queensland, Australia. He has also served as an associate professor at Asian Institute of Technology, Bangkok, Thailand. His main research interests are voltage stability and oscillation studies on practical power systems, application of FACTS controller and renewable energy technology.

Arthit Sode-Yome (M'04) received the B.Eng degree in Electrical Engineering from Prince of Songkla University, Thailand, in 1993, M.S. degree in Electrical Engineering from the Pennsylvania State University, USA, in 1996 and Doctoral Degree in Energy from Asian Institute of Technology, Thailand, in 2005. Dr. Arthit is a lecturer at Department of Electrical Engineering, Siam University, Thailand. His main research interests are voltage stability, FACTS, neural networks, optimization techniques and HVDC.

Kwang Y. Lee (F'01) received his B.S. degree in Electrical Engineering from Seoul National University, Korea, in 1964, M.S. degree in Electrical Engineering from North Dakota State University, Fargo, in 1968, and Ph.D. degree in System Science from Michigan State University, East Lansing, in 1971. He has been on the faculties of Michigan State, Oregon State, Houston, the Pennsylvania State University, and Baylor University, where he is currently Professor and Chair of Electrical and Computer Engineering and Director of Power and Energy Systems Laboratory. His interests are power systems control, operation and planning, and intelligent systems applications to power plants and power systems control. Dr. Lee is a Fellow of IEEE, Editor of IEEE Transactions on Energy Conversion, and former Associate Editor of IEEE Transactions on Neural Network

APPENDIX A

Author's CV

Name	Dr. Arthit Sode-Yome		
Birth date	August 30, 1970		
Birth Place	Bangkok, Thailand		
Education	D.Eng	Asian Institute of Technology	2003-2005
	MS.EE.	The Pennsylvania State University	1994-1996
	B.Eng.	Prince of Songkhla University	1989-1993
Affiliation	Siam University		
Designation	Assistant Professor		

Journal Articles

1. **A. Sode-Yome** and N. Mithulananthan, "An Economical Generation Direction for Power System Static Voltage Stability", *Electric Power System Research Journal*, Vol. 76, Issue 12, pp. 1075-1083, August 2006.
2. **A. Sode-Yome**, N. Mithulananthan and K. Y. Lee, "A Maximum Loading Margin Method for Static Voltage Stability in Power Systems", *IEEE Transactions on Power Systems*, Vol. 21, No. 2, pp. 799-808, May 2006.
3. **A. Sode-Yome** and N. Mithulananthan, "Maximizing Static Voltage Stability Margin in Power Systems using a New Generation Pattern", *Australian Journal of Electrical and Electronics Engineering*, Vol. 2, No. 3, 2005.
4. **A. Sode-Yome** and N. Mithulananthan, "Comparison of Shunt Capacitor, SVC and STATCOM in Static Voltage Stability Margin Enhancement", *Journal of Electrical Engineering Education*, Vol. 41, No. 2, pp 158-171, April 2004.
5. K. Y. Lee, F. M. Nuroglu and **A. Sode-Yome**, "Real Power Optimization with Load Flow using Adaptive Hopfield Neural Networks", *Journal of Engineering Intelligent Systems*, Vol. 8, No. 1, pp 53-58, March 2000.
6. K. Y. Lee, **A. Sode-Yome** and J. H. Park, "Adaptive Hopfield Neural Networks for Economic Load Dispatch", *IEEE Transaction on Power Systems*, Vol. 13, No. 2, pp 519-526, May 1998.